Neurotrophin mediated signaling pathways common to the immune and nervous system

Von der Fakultät für Lebenswissenschaften
der Technischen Universität Carolo-Wilhelmina zu Braunschweig
zur Erlangung des Grades
eines Doktors der Naturwissenschaften (Dr. rer. nat.)
genehmigte

D i s s e r t a t i o n

von Jan Alexander Kleveman
aus Bremerhaven

1. Referent: Professor Dr. Martin Korte
2. Referent: Professor Dr. Reinhard Köster
eingereicht am: 09.10.2017
mündliche Prüfung (Disputation) am: 12.01.2018

Druckjahr 2018

Veröffentlichungen

Teilergebnisse aus dieser Arbeit wurden mit Genehmigung der Fakultät für Lebenswissenschaften, vertreten durch den Mentor der Arbeit, in den folgenden Beiträgen vorab veröffentlicht:

Posterbeiträge:

Jan Kleveman, Marianna Weller*, Alexandru Parlog, Ildiko Dunay, Marta Zagrebelsky and Martin Korte: Effects on neuronal morphology by chronic murine toxoplasmosis *First N-RENNT Symposium on Neuroinfectiology, Hannover (2014)*

* Marianna Beyer, geb. Weller

Jan Kleveman, Marianna Beyer, Ildiko Dunay, Marta Zagrebelsky and Martin Korte: Effects of $p75^{NTR}$ on neuronal morphology in a model of chronic neuroinflammation, *Second N-RENNT Symposium on Neuroinfectiology, Hannover (2015)*

Jan Kleveman, Marianna Beyer, Ildiko Dunay, Marta Zagrebelsky and Martin Korte: Role of $p75^{NTR}$ on neuronal morphology in a model of chronic neuroinflammation, *SFB854 Symposium, Magdeburg (2015)*

Tagungsbeiträge:

Jan Kleveman, Marianna Weller*, Alexandru Parlog, Ildiko Dunay, Marta Zagrebelsky and Martin Korte: Effects on neuronal morphology by chronic murine *Toxoplasma gondii* infection *SFB854 Retreat, Quedlinburg (2014)*

* Marianna Beyer, geb. Weller

Jan Kleveman, Marianna Beyer, Alexandru Parlog, Ildiko Dunay, Marta Zagrebelsky and Martin Korte: Role of p75 neurotrophin receptor in mediating neuronal alterations of *Toxoplasma gondii* infected mice, *11th Göttingen Meeting of the German Neuroscience Society, Göttingen (2015)*

Jan Kleveman, Ildiko Dunay, Marta Zagrebelsky and Martin Korte: Toxoplasmis as a model of study of the p75 neurotrophin receptor in chronic neuroinflammation, *4th Venusberg Meeting on Neuroinflammation, Bonn (2015)*

Weil die Frage Warum immer einen zureichenden Grund will und die Verbindung der Erkenntnisse nach dem Satz vom zureichenden Grunde die Wissenschaft vom bloßen Aggregat von Erkenntnissen unterscheidet, ist gesagt worden, dass das Warum die Mutter der Wissenschaften sei. Auch findet sich, dass in jeder derselben Eine der Gestaltungen unsers Satzes, vor den übrigen, der Leitfaden ist; obgleich in derselben auch die andern, nur mehr untergeordnet, Anwendung finden. So ist in der reinen Mathematik der Seinsgrund Hauptleitfaden (obgleich die Darstellung in den Beweisen nur am Erkenntnisgrunde fortschreitet); in der angewandten tritt zugleich das Gesetz der Kausalität auf; und dieses gewinnt ganz die Oberherrschaft in der Physik, Chemie, Geologie u.a.m. Der Satz vom Grunde des Erkennens findet durchaus in allen Wissenschaften starke Anwendung, da in allen das Besondere aus dem Allgemeinen erkannt wird. Hauptleitfaden und fast allein herrschend aber ist er in der Botanik, Zoologie, Mineralogie und andern klassifizierenden Wissenschaften. Das Gesetz der Motivation ist, wenn man alle Motive und Maximen, welche sie auch seien, als Gegebenes betrachtet, aus dem man das Handeln erklärt, Hauptleitfaden der Geschichte, Politik, pragmatischen Psychologie u. a. — wenn man aber die Motive und Maximen selbst, ihrem Wert und Ursprung nach, zum Gegenstand der Untersuchung macht, Leitfaden der Ethik.

—Arthur Schopenhauer

Für meine Mutter Anja und meinen Sohn Paul Levi

Zusammenfassung

Neuroinflammation beschreibt Entzündungsprozesse im zentralen Nervensystem. Die Ursachen für Neuroinflammation sind vielfältig: von Infektionen über Schädel-Hirn-Traumata, Toxine und Autoimmunreaktionen. Während im restlichen Körper aktivierte Makrophagen und dendritische Zellen die erste Verteidigungsebene, die angeborene Immunantwort, darstellen, produzieren im Gehirn Astrozyten und Mikroglia pro-inflammatorische Zytokine und induzieren damit Neuroinflammation. In der Pathogenese unterschiedlicher neurodegenerativer Erkrankungen, beispielsweise der Alzheimer-Erkrankung, ist Neuroinflammation und eine anhaltende Immunaktivierung als Risikofaktor identifiziert worden.

In dieser Arbeit habe ich überprüft, welche Effekte andauernde Neuroinflammation durch den Parasiten *Toxoplasma gondii* auf das Gehirn von unterschiedlichen Mausstämmen hat. Außerdem habe ich in diesem Zuge überprüft, ob diese Effekte über den p75 Neurotrophinrezeptor vermittelt werden. Neurotrophine sind Signalstoffe, die weitreichende Wirkungen auf Neurone haben. Sie vermitteln die Aufrechterhaltung und den Abbau bestehender neuronaler Verbindungen, die Differenzierung von Nervenzellen. Da sie außerdem von Mikroglia und anderen Zelltypen des Immunsystems produziert werden, stellen sie eine direkte Verbindungen zwischen dem zentralen Nervensystem und dem Immunsystem dar.

Die Daten zeigen, dass der C57BL/6 (B6) Mausstamm empfindlicher auf den Parasiten reagiert als BALB/c Mäuse. Neben einem deutlichen Gewichtsverlust in den infizierten B6 Tieren, zeigen sie außerdem deutlichere Veränderungen in der Architektur der Neurone. Während beide Mausstämme mit einer starken Aktivierung der Mikroglia auf *Toxoplasma gondii* reagieren, zeigt sich jedoch, dass die Morphologie der Mikroglia stammspezifisch auf die Infektion reagiert und unterschiedliche Phenotypen aufweist.

Der zweite Teil der Daten zeigt, dass in B6 Mäuse, denen der p75 Neurotrophinrezeptor fehlt (knock out), die Neuronenarchitektur weniger stark durch die Infektion verändert werden, als das im Wildtyp der Fall ist.

Abstract

Neuroinflammation subsumes inflammatory processes in the central nervous system(CNS). The insults causing for neuroinflammation are diverse: infections, traumatic brain injury, toxins, and autoimmunity are among these. In the periphery activated macrophages and dendritic cells represent the first line of defense - the innate immunity. In the central nervous system pro-inflammatory cytokines are released by microglia, the brain resident macrophages, and astrocytes. This induces neuroinflammation. For the progression of various neurodegenerative diseases, including, e.g., Alzheimer's Disease, neuroinflammation, and prolonged immune activity have been identified as a risk factor.

In this thesis, I investigated which effects the chronic infection with the parasite *Toxoplasma gondii* (*T. gondii*) and thereby prolonged neuroinflammation take on the brains of different laboratory mouse strains. Additionally, I investigated whether these effects are in part mediated by the p75 neurotrophin receptor. Neurotrophins are secreted proteins that belong to a class of growth factors. They have shown to be capable of regulating neuronal survival, differentiation, growth, and maintenance among other. Intriguingly neurotrophins are also expressed and secreted by microglia and other cell populations of the immune systems and thereby represent a direct signaling connection between the CNS and the immune system.

My data shows that the C57BL/6 (B6) mouse strain is more susceptible to the parasite than BALB/c mice. Additionally to a significant weight loss upon infection B6 mice also show more drastic changes in neuronal morphology than BALB/c mice. Both strains react strongly microglial activation to *T. gondii* infection. Interestingly microglial morphology upon infection is strain specific and display different phenotypes.

The second part of the data shows that B6 mice lacking the p75 neurotrophin receptor (knock out) show a milder reaction to the *T. gondii* infection on their neuronal architecture compared to the wild type.

Contents

List of Figures

List of Tables

Lists of abbreviations

AD	Alzheimer's Disease
AEBSF	4-(2-aminoethyl)benzenesulfonyl fluoride hydrochloride
AIDS	Acquired immune deficiency syndrome
Akt	Protein kinase B (PKB)
ALS	Amyotrophic Lateral Sclerosis
AMPA	α-amino-3-hydroxy-5-methyl-4-isoxazol propionic acid
APS	Ammonium persulfate
B6	C57BL/6
BBB	Blood-brain barrier
BDNF	Brain Derived Neurotrophic Factor
bFGF	Basic fibroblast growth factor
BSA	Bovine serum albumine
CA	*cornu ammonis*
CamKII	Calmodulin-dependent protein kinase II
cAMP	Cyclic adenosine monophosphate
Caspase	Cysteine-aspartic proteases, cysteine aspartases or cysteine-dependent aspartate-directed proteases
CD	Cluster of Differentiation
CD11b	Integrin alpha M
CNS	Central Nervous System
COX-2	Cyclooxinase2
CRMP2	Collapsin response mediator protein 2

CX_3CR1	CX3C chemokine receptor 1
CX3CL1	Fractalkine, chemokine (C-X3-C motif) ligand 1
Cy2, 3, 5	Cyanine 2, 3, 5
DAPI	4´,6-diamidino-2-phenylindole
DC	Dendritic Cell
DiI	1,1'-dioctadecyl-3,3,3'3'-tetramethylindocarbocyanine perchlorate
EGF	Epidermal Growth Factor
eGFP	Enhanced green flourescent protein
EGFR	Epidermal Growth Factor Receptor
EGTA	Ethylene glycol-bis(β-aminoethyl ether)-N,N,N',N'-tetraacetic acid
ELISA	Enzyme-linked immunosorbent assay
EM	Electron Microscopy
ERK	Extracellular signal–regulated kinases
eYFP	Enhanced yellow flourescent protein
F4/80	EGF-like module-containing mucin-like hormone receptor-like 1
GABA	Gamma-Aminobutyric acid
GAPDH	Glyceraldehyde 3-phosphate dehydrogenase
GDNF	Glial cell-derived neurotrophic factor
HC	Hippocampus
HD	Huntington's Disease
HEPES	4-(2-hydroxyethyl)-1-piperazineethanesulfonic acid
HIV	Human immunodeficiency virus
HRP	Horseradish peroxidase
Iba1	Ionized calcium-binding adapter molecule 1
ICAM	Intercellular Adhesion Molecules

IFN-γ	Interferon-γ
IgG	Immunoglobulin G
IgM	Immunoglobulin M
IHC	Immunohistochemistry
IL	Interleukin
JNK	c-Jun N-terminal kinases
kDa	Kilo Dalton
Ko	Knock out
LIMK	LIM domain kinase
LINGO-1	Leucine rich repeat and Immunoglobin-like domain-containing protein 1
LTD	Long-term Depression
LTP	Long-term Potentiation
MAG	Myelin-associated glycoprotein
MAPK	Mitogen-activated protein kinase
MCP-1	Monocyte chemotactic protein 1
MHC-I/II	Major Histocompatibility Complex I/II
MICs	Micronemal proteins
MLC2	Myosin light chain 2
MOG	Myelin oligodendrocyte glycoprotein
NCAM	Neural cell adhesion molecule
NF-KB	Nuclear factor 'kappa-light-chain-enhancer' of activated B-cells
NGF	Nerve Growth Factor
NgR1	Nogo receptor 1
NK cell	Natural killer cell
Nogo-A	Neurite outgrowth inhibitor
NT-3	Neurotrophin 3

NT-4	Neurotrophin 4
P2X4R	ATP-gated P2X Receptor Cation Channel
p75^{NTR}	p75 neurotrophin receptor
PBS	Phosphate buffered saline
PBS	Phosphate-buffered saline
PC12	Pheochromocytoma cell line 12
PCR	Polymerase Chain Reaction
PFA	Paraformaldehyde
PGE2	Prostaglandin E2
PI3K	Phosphatidylinositol-4,5-bisphosphate 3-kinase
PLCγ	Phospholipase C– γ
PSGL-1	P-selectin glycoprotein ligand 1
PVDF	Polyvinylidene fluoride
Rho-GDI	RHO protein GDP dissociation inhibitor of Rho proteins
RhoA	Ras homolog gene family, member A
ROCK	Rho-associated protein kinase
ROI	Region of interest
ROS	Reactive oxygen species
RT	Room temperature
SDS-PAGE	Sodium dodecyl sulfate – polyacrylamide gel electrophoresis
TBST	Mixture of tris-buffered saline (TBS) and Polysorbate 20
TEMED	Tetramethylethylenediamine
TGF-β	transforming growth factor-beta
TLR	Toll-like receptor
TNFα	Tumor necrosis factor α
Trk(A, B, C)	Tropomyosin receptor kinase (A, B, C)
WT	Wildtype

1 Introduction

1.1 Neuroinflammation

Neuroinflammation is commonly named as one major contributor to multiple neurological diseases. An acute neuroinflammation is most often considered neuroprotective by default while a long lasting or even chronic neuroinflammation triggers signal cascades causing neurodegeneration. This damaging effect has been subject to studies in the context of neurodegenerative disorders like Huntington's disease (HD), amyotrophic lateral sclerosis (ALS) and Alzheimer's disease (AD) among others.

Any alteration in the CNS' functional and cellular integrity induces neuroinflammation. The process of neuroinflammation aims to reinstate the tissue homeostasis by inducing different repair mechanisms (Goldszmid and Trincheri, 2012). However, if the precise regulation of this processes evades controlled conditions, the initial inflammatory response can amplify exceedingly, and as a result, the protective effect transforms into a neurotoxic effect, causing collateral destruction and resulting in a possibly severe progression of a pre-existing disease.

Neuroinflammation is a highly dynamic set of processes in which different cell types participate (Microglia, section 1.1.2.1; Astrocytes, section 1.1.2.2; Neurons, section 1.1.2.3), by proliferating, migrating, releasing immune active factors (e.g. reactive oxygen species and cytokines, section 1.1.3), displaying surface proteins (e.g. MHC-I/II) and participate in phagocytosis and antigen presentation as a response to protein aggregates, glial products (e.g. cytokines) and neuronal degeneration.

Intriguingly cytokine signalling upon neuroinflammation actively mediates the regulation of several CNS functions like neuroendocrine release, neurotransmission, synaptic plasticity, neural circuitry, behaviour, memory function and cognition (Camacho-Arroyo *et al.*, 2009; del Rey *et al.*, 2013; Aprile-Garcia *et al.*, 2013; Cuartas and Jorge 2014; Liu *et al.*, 2017).

Altered cognitive or behavioral capacities are therefore presumably a possible consequence of misregulated cytokine signaling which in turn can result in previously mentioned neurodegenerative diseases or mental disorders (Lynch 2002; Magaki *et al.*, 2007; Holmes *et al.*, 2009; McAfoose and Baune 2009, Brosseron *et al.*, 2014).

1.1.1 Neuroinflammatory makers

Neuroinflammation is not recognized on the same hall marks as inflammation in general, as defined by Celsus (25 BC), being dolor, tumor, rubor, and calor. Instead, neuroinflammation is recognized by the expression of cytological makers of innate immune response, e.g., pro-inflammatory cytokines and chemokines. Additionally, morphological changes of microglia and astrocytes are characteristics of neuroinflammatory processes. The infiltration of circulating leucocytes or macrophages as part of the adaptive immune response are involved depending on the nature of the pathological event (Eikelenboom *et al.*, 2002; Amor *et al.*, 2010). While the CNS was previously thought to be an immune privileged organ, it is nowadays generally accepted that adaptive immune response and innate immune responses occur in the CNS and are coming into play to a varying extent during neuroinflammatory processes.

1.1.2 Cell types playing a critical role

1.1.2.1 Microglia

In contrast to the periphery, the central nervous system does lack the standard lymphatic systems. It contains a limited range of different immune cells and has, therefore, in former times, been considered to be immune privileged in former times. These days it is established that resident microglia, recruited macrophages and dendritic cells (DCs) in the CNS can prompt an all over immune reaction to pathological conditions; injury and disease.

Microglia were first recognized by Nissl in 1880 and later studied by Pío del Río Hortega. The Spanish neuroanatomist described them as resting ramified cells using silver carbonate staining methods (del Río Hortega 1932). Nowadays our understanding of microglia has shifted completely from them being a 'silent' cell in healthy brain to an actively involved component in cognition, behavioral functions, CNS physiology, and neurogenesis.

These microglial cells are now well accredited as elementary contributors in the pathogenic progression of several neurological disorders and diseases (Heneka *et al.*, 2010; Parpura *et al.*, 2012; Verkhratsky *et al.*, 2014).

Microglia are the surveyors of the CNS, actively extending and retracting their processes and by these means maintaining the post- and pre-synaptic elements and fine tuning of neuronal circuitry. Thus, a disruption of this homeostatic functions possibly contributes to the progression of neuronal disorders. Microglia are migratory cells of the CNS that continuously survey their surroundings with their highly motile processes for any kind pathogenic event (Gehrmann *et al.*, 1995) and represent ~15–20% of the total glial population (Carson *et al.*, 2006). Microglia are referred to as the CNS' resident macrophages and they are fully immunocompetent phagocytic cells and constitute the innate immunity, the first line of defense, against any CNS damage or insult and exhibit functional and structural plasticity. They are considered responsible for maintenance and homeostasis within the CNS and undergo substantial structural transformations to appropriately perform several immunological functions. While under normal conditions, the microglia cell bodies stay nearly stationary and the microglial processes scan the environment (extracellular space, blood vessels) and directly communicate with neurons and astrocytes. Uniquely microglia derive from yolk sac myeloid progenitors that are distinct from those which yield monocytes or macrophages. These progenitors migrate to the central nervous system before its vasculogenesis (Ginhoux *et al.*, 2010). In their resting state microglia is characterized by a small cell body with highly ramified processes - and can thereby easily be distinguished morphologically from dendritic cells and macrophages.

Activation of microglia upon and CNS insult or immune breaching has been widely observed (Saxena *et al.*, 2007; Patro *et al.*, 2010a, 2013; Nagayach *et al.*, 2014a, b, 2015; Sharma *et al.*, 2015). A rapid transformation of these activated immune cells into a reactive phenotype is characterized by a highly ramified morphology. Activated microglia repair damaged tissue by phagocytizing cell debris and sustain healing processes (Hanisch and Kettenmann 2007; Kettenmann *et al.*, 2011). More and more evidence shows that microglia activation is also liable in aggravating the neurodegeneration (Block and Hong 2005; Venero et al. 2011).

In their position as the carer for maintaining the general homeostasis of the central nervous system, they are equally important in health and disease. Follow sections will deal with their impact on neuronal maturation and learning as well as

their response to neuroinflammation.

1.1.2.1.1 Microglia shaping neurons - synaptic pruning Microglia have been studied mostly in the context of CNS disease, injury or similar pathological events (Hanisch and Kettenmann, 2007). Prevailing research shows a much more versatile array of functions for these cells. Besides their role in fighting off pathogens, microglia prune synapses during CNS development by actively engulfing synaptic material and phagocytizing excess structures (Paolicelli *et al.*, 2011). Also, microglia participate in the regulation of synaptic plasticity and function. While scanning their environment microglia make direct and transient connections with dendritic spines, synapses, axons, and somata. Further evidence for a more substantial role of microglia in cognitive functions was provided by showing activity depended neuron-microglia interaction (Tremblay *et al.*, 2010, Schafer *et al.*, 2012). Removing microglia from the adult mouse brain results in learning impairment and intriguingly genetically depleting the neurotrophin BDNF from microglia leads to a similar phenotype as the complete ablation of microglia, strongly indicating that microglial derived BDNF contributes to the synaptic remodeling associated with memory and learning (Parkhurst *et al.*, 2013).

The participating receptors and signaling pathways remain largely unknown.

1.1.2.2 Astrocytes

It is established for a very long time that upon damage, loss, and degeneration of neuronal tissue, among other glia, astrocytes proliferate and fill the resulting gaps, in some cases even leading to tissue scaring (astrogliosis). Their role in neuroinflammation has been the subject of study only recently. Similar to microglia CNS damage activates astrocytes, which contribute to neuroinflammation by cytokine and chemokine secretion (Miller 2005; Tandon 2007). Their inflammatory response is not as prominent as one of microglia cells (Streit *et al.*, 1999), although they get activated by pathological challenge (Aloisi 1999). It has been shown that in neurodegenerative disorders microglial response plays a bigger role than the astrocytic response (Teismann *et al.*, 2003; Vehmas *et al.*, 2003).

1.1.2.3 Neurons

The idea that neurons play a solely passive role in neuroinflammation has been thoroughly dismissed by findings indicating that neurons are actively contributing

to regulatory immune responses in the brain. Neurons express factors like membrane spanning proteins (CX3CLI; CD22; CD200; NCAM; ICAM) that regulate neuroinflammatory signal cascades (Tian *et al.*, 2009; Doll *et al.*, 2014). Additionally, the expression of cyclooxinase2 (COX-2), which is induced by IL-1β, has been found in early stages of Alzheimer's disease (AD) (Hoozemans and O'Banion 2005).

1.1.2.4 Peripheral immune cells recruited into the CNS

Chronic CNS inflammation and subsequent activation of microglia triggers cells of the adaptive immune system to invade the brain. Degenerative disorders usually are characterized by local inflammation from the above mentioned CNS resident cells and by the infiltration of peripheral leucocytes alike (McGeer *et al.*, 1989). Indeed, under healthy conditions T-cells are nearly non-present in the CNS while in patients suffering from Parkinson's Disease, multiple sclerosis or traumatic brain injuries were observed to enter affected areas (Mantovani *et al.*, 2009; Ankeny and Popovich 2009; Neumann *et al.*, 2002). Especially in Alzheimer's Disease, it has been shown that patients have an atypical inflammatory response, mainly from macrophages and microglia and additional recruitment of monocytes into the CNS (Perry *et al.*, 2007). A distinction between macrophage and microglia versus infiltrated CD8, CD4 monocytes and T-cells has yet to be established (Lucin and Wyss-Conray 2009).

1.1.3 Pro-inflammatory markers

In direct consequence of a CNS insult, a variety of cytokines is expressed to cope with the injury and to facilitate repair. The primary source are the activated microglial cells, producing IL-1, TNFα, NO, PGE2 and more. These are mainly involved in prolonged inflammation (Swardfager *et al.*, 2010; Murray *et al.*, 2015) and have been studied to great extend in Parkinson's Disease (Allan *et al.*, 2010), multiple sclerosis (Block and Hong 2005), Alzheimer's Disease (Misiak *et al.*, 2012; Lue *et al.*, 1996; Akiyama *et al.*, 2000), amyotrophic lateral sclerosis (Henkel *et al.*, 2004) but also in general ageing processes (Lucin and Wyss-Conray 2009; Villeda *et al.*, 2011). Griffin *et al.* could show (1995) that in AD patients IL1β show a 6 fold increase compared to healthy control patients, emphasizing it playing a role in chronic CNS diseases. Additionally, Swardfager *et al.* also showed (in 2010)

that AD is accompanied with an elevated inflammatory response by showing an increased concentration of IL-6, IL-12, IL-18, IL1β, and TNF in the periphery. Pro-inflammatory cytokines initiate downstream cascades which details still need to be defined.

1.2 Pyramidal cell - dendritic structure

The discrimination of individual neuronal morphology was first possible after the development of the Golgi staining in the late nineteenth century. This silver staining labels sparsely but intensely neuronal structures and allowed the neuroanatomist Ramón y Cajal (1888) meticulously draw and describe for the first time the elaborate dendritic aborization of diverse neuronal populations.

One major distinction proved to be that some neurons appear to have smooth dendrites, while some have plenty dendritic protrusions (dendritic spines). Nearly a century later it was shown that neuron with many spines are excitatory and glutamatergic and smooth neurons mostly inhibitory and GABAergic. Sophisticated electron microscopy experiments on Golgi-stained cells showed that each spine contains a synapse characterized by presynaptic vesicles and a broad postsynaptic density (Gabbott and Somogyi 1986; Kubota 2014; Morishima *et al.*, 2011; Thomson and Deuchars 1997).

With the advancements in electron microscopy experiments were conducted on Golgi-stained neurons, which showed that every synapse is characterized by round presynaptic vesicles and a postsynaptic density (Hersch and White 1981; LeVay 1973; Parnavelas *et al.*, 1977).

Pyramidal neurons are named after the shape of their cell soma. They are further characterized by distinct basal and apical dendritic trees, and one single axon usually emanates from the basal part of the soma making several excitatory glutamatergic synaptic contacts along its length. (fig. 1.1). While pyramidal neurons are by no means identical, they share distinct functional principles. Pyramidal cells are found in various CNS regions, and they have been studied to great length, especially in the hippocampal CA1 area and in the cortical layer V.

Synaptic input takes place at different domains in pyramidal neurons. The axon and the soma receive inhibitory input by GABAergic (γ-aminobutyric acid) neurons. Excitatory input arrives mainly through the dendrites from multiple sources. Generally it has been observed that proximal dendrites receive their input from

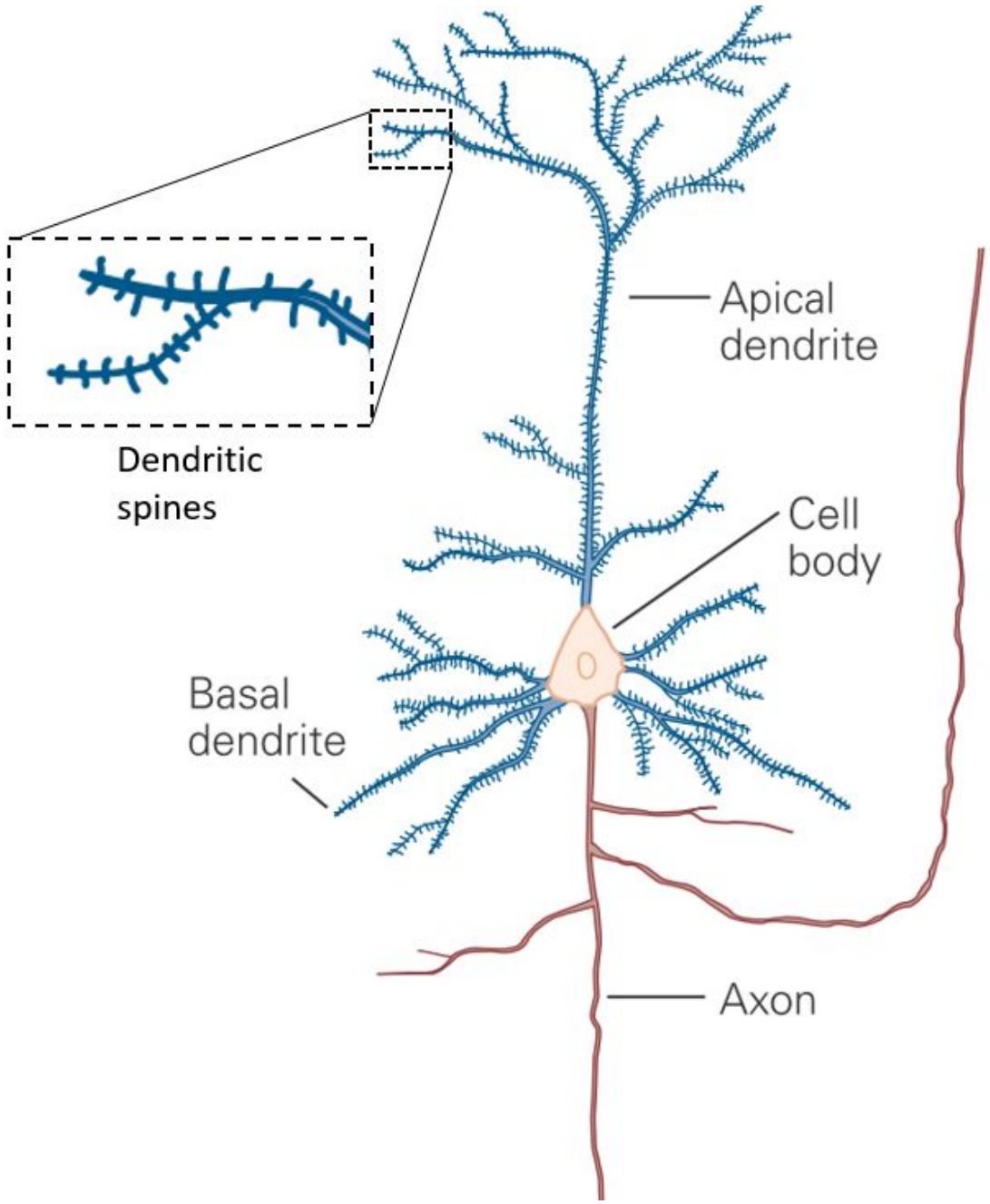

Figure 1.1: Pyramidal neuron of the hippocampus - Pyramidal cells depict a approximately triangular cell soma; the dendrites emerge from both the apex (the apical dendrite) and the base (the basal tuft). Pyramidal cells are present in the hippocampus and throughout the cerebral cortex. The dendrites are covered in dendritic spines (Adapted from Kandel *et al.*, 2012).

locally adjacent excitatory sources and the distal apical tuft from more distant locations (Cauller and Connors, 1994; Larkum *et al.*, 2004). The different morphological properties of apical and basal dendrites suggest a distinct integration of

their input (Spruston, 2008).

Hippocampal CA1 pyramidal neurons receive input from the entorhinal cortex to the distal tuft trough the perforant pathway. The proximal dendrites receive their excitatory input via the Schaffer collaterals from the hippocampal CA3 region (Ishizuka *et al.*, 1990; Li *et al.*, 1994).

1.2.1 Dendritic spines

In his descriptions and drawings of neuronal structures, Ramón y Cajal also showed dendritic spines for the first time. Since then technical advances have driven our knowledge beyond the limits of classic light microscopy. Several neuron types throughout the CNS form small membrane protrusions from the dendritic shaft which then differentiate into various types of dendritic spines. Depending on the CNS region and neuron type, different spine densities occur in all vertebrates. The variance in size and shape of spines strongly indicates a high degree of functional diversity (fig. 1.2).

Dendritic spines are commonly classified into three to four distinct types: mushroom, thin, stubby and filopodia-like. Mushroom spines have a large head with a substantial post-synaptic density. Thin spines have a thinner spine neck and a small bulbous head. Stubby spines lack a visible neck and filopodia like spines are long, hair-like and devoid of a head.

The changes in spine morphology are tightly linked to biochemical reactions taking place within the spine. The spine head is isolated from the metabolism of the dendrite by the spine neck. Compartmentalization also effects calcium dynamics, revealing a link between function and morphology (Yuste *et al.*, 2000).

1.3 Neurotrophins

Any secreted factor that has sustaining or nourishing effects on neurons can be understood as neurotrophic factors. While many different molecules do have those effects on neurons (e.g., neutrin, artemin and persephin) the family of neurotrophins has been subjected to intense study for more than half a century. The most archetypical neurotrophic factor, the neurotrophin "nerve growth factor" (NGF) was already discovered in 1952, and its essential role in survival and neurite outgrowth was shown by Levi-Montalcini and Angeletti in 1963, work for which she

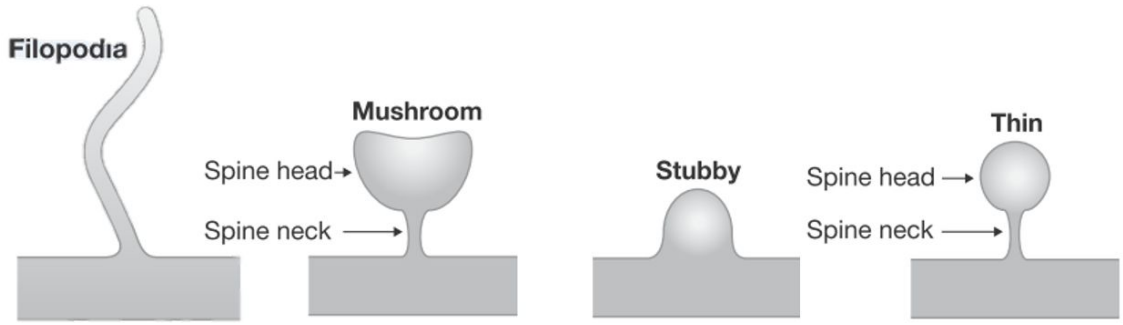

Figure 1.2: Structure and organization of spines Schematics of the most common spine morphologies based on an established classification system with four main categories. On a single dendrite a continuum of these shapes can be found and the morphology of a given spine can change rapidly (adapted from Rochefort and Konnerth, 2012).

was awarded the Nobel Prize in Physiology or Medicine in 1986 (together with Stanley Cohen). The other members of the neurotrophin family (BDNF, NT-3, and NT-4) were discovered in the 1980s and 1990s after PCR analysis. NGF and BDNF belong to a genetically conserved family (Barde *et al.*, 1982; Hohn *et al.*, 1990; Jones and Reichardt 1990; Maisonpierre *et al.*, 1990; Rosenthal *et al.*, 1990; Berkemeier *et al.*, 1991; Hallbook *et al.*, 1991; Ip *et al.*, 1992). All the neurotrophins are short peptides and have an approximate molecular weight of 13 kDa and exist as non-covalently linked homodimers. Neurotrophins mainly interact with two different cell surface receptor types (fig. 1.3); the members of Trk family of receptor tyrosine kinases and the p75 neurotrophin receptor ($p75^{NTR}$).

This research emphasis has since then shifted a little away from pursuing a role for neurotrophins in neuroprotection, nevertheless the last 15 years has generated formidable progress in elucidating the functional roles of the neurotrophins and their receptors in normal development and adult physiology, their mechanisms, and also their role in the pathophysiology in a state of disease.

The last decade has widely expanded the knowledge on neurotrophins and their receptors, following the discovery that the neurotrophin pro-peptides have distinct neuronal effects mediated by novel receptor constellations (homo- and heterodimers), including sortilin, Nogo-A, and the low-affinity neurotrophin receptor $p75^{NTR}$.

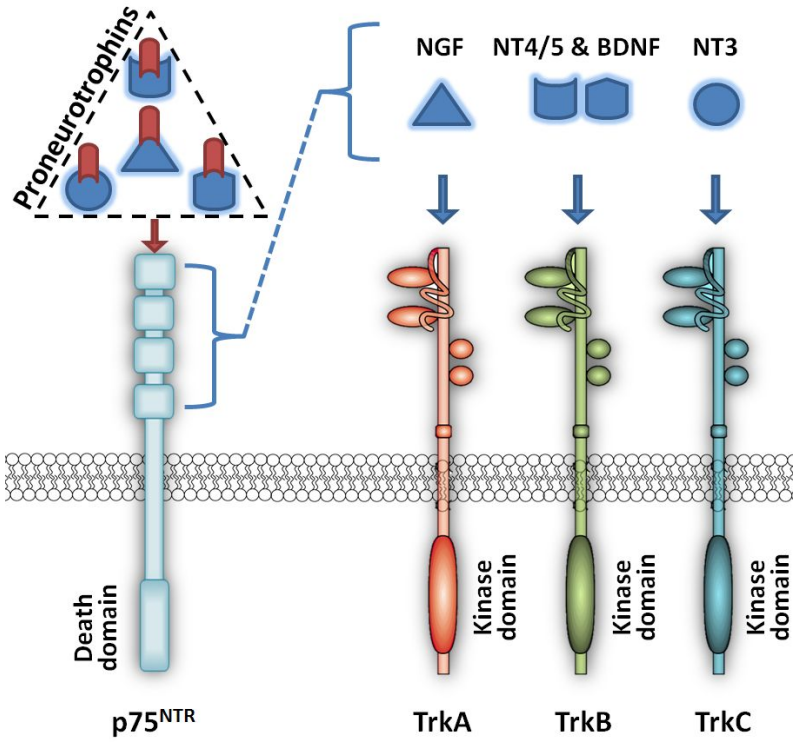

Figure 1.3: Neurotrophins bind to the Trk receptors and p75^{NTR} - Each neurotrophin binds to its cognate Trk receptor. The p75^{NTR} can bind all the neurotrophins with low affinity, and the proneurotrophins with high affinity.

1.3.1 Receptor Activation by Mature Versus Pro-neurotrophin

Neurotrophins are generated by translating from their mRNA as pro–neurotrophins which are post-translationally processed by proteolytically cleaving them. The pro forms of the neurotrophins were initially categorized as inactive precursor proteins in contrast to the processed peptides. Numerous studies afterward showed that the pro-neurotrophins are ligands for $p75^{NTR}$, recognizing them as physiologically active. Nowadays it is well understood that neurotrophin signaling depends on the balance between pro-neurotrophins vs. mature as well as the configuration of the target receptor complex. The affinity of pro versus mature neurotrophins depends mainly on the interactions of $p75^{NTR}$ and its present co-receptor (Chao *et al.*, 2003).

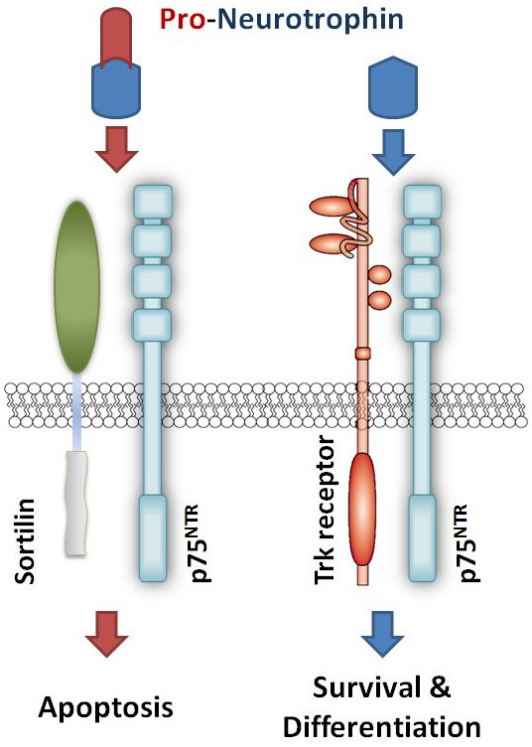

Figure 1.4: Pro-neurotrophins bind $p75^{NTR}$ with high affinity- Pro-neurotrophins possess a high binding affinity to a receptor complex composed of $p75^{NTR}$ and sortilin, inducing apoptosis. Cleaved, mature neurotrophins in contrast prefer binding a complex composed of a $p75^{NTR}$ with a Trk receptor to mediate survival and differentiation. Adapted from Siegel *et al.*, 2011

Cell growth, differentiation, and survival is enhanced by mature neurotrophin signaling via Trk receptors which is in turn increased by heterodimerization with $p75^{NTR}$ (Chao 1994; Esposito *et al.*, 2001; Hempstead 2006). In opposition, $p75^{NTR}$ pairing with sortilin increases the binding affinity to pro-neurotrophins, resulting in apoptosis inducing cell signaling (fig. 1.4). ProNGF and proBDNF have both been demonstrated to activate a $p75^{NTR}$ -dependent apoptotic cascade (Beattie *et al.*, 2002; Harrington *et al.*, 2004; Teng *et al.*, 2005; Lebrun-Julien *et al.*, 2010; Nykjaer and Willnow 2012).

As NGF has been the primary focus at the beginning of neurotrophin research, its pro-form has analogously been best studied, compared to the other pro-neurotrophins. Different groups demonstrated proNGF as being released by various cell types

Hasan *et al.*, 2003; Bruno and Cuello 2006; Domeniconi *et al.*, 2007; Yang *et al.*, 2009a, b). It was also shown that ProNGF gets cleaved intracellularly as well as extracellularly by different types of enzymes (Lee *et al.*, 2001). This indicates yet another potential for cell-cell interactions mediated by the neurotrophin system.

Loss-of-function experiments confirmed the role of the different pro-neurotrophins (proBDNF, proNGF) by blocking the binding by specific antibodies(Harrington *et al.*, 2004; Volosin *et al.*, 2008; Fan *et al.*, 2008). $P75^{NTR}$ knockout mice (Exon3 $^{-/-}$) suffer less from seizures (Volosin *et al.*, 2008), ligation by proNGF (Beattie *et al.*, 2002) or after axotomy (Ferri *et al.*, 1998; Syroid *et al.*, 2000). Comparable effects are observed in sortilin knockout mice (Jansen *et al.*, 2007).

The ambivalence between the consequences of mature neurotrophin and pro-neurotrophin signaling has raised the conjecture that a dysregulation could facilitate the progression of many neurodegenerative diseases. Further evidence arouse from, e. g., Fahnstock *et al.* (2001), who showed that proNGF is increased two-fold in the parietal cortex of individuals with Alzheimer's disease (AD).

1.3.2 The p75 neurotrophin receptor

The first receptor identified for NGF was the $p75^{NTR}$ (Chao *et al.*, 1986; Radeke *et al.*, 1987), and was initially named after being a low-affinity receptor for NGF (low-affinity NGFR). The high-affinity NGFR, TrkA, was identified half a decade later (Hempstead *et al.*, 1991; Kaplan *et al.*, 1991; Klein *et al.*, 1991). The receptors were renamed as more members of the Trk receptor family were identified.

The functionality of $p75^{NTR}$ remained elusive and was questioned for many years, because of the absence of kinase activity. In order to understand the bandwidth of effects downstream of $p75^{NTR}$, it has to be understood that there are various interactions with co-receptors. The $p75^{NTR}$ is a single membrane spanning protein from the tumor necrosis factor (TNF) receptor family, containing four cysteine rich areas within the extracellular region that are consequential for neurotrophin binding affinity and receptor-receptor interactions. The $p75^{NTR}$ forms both homodimers and heterodimers. The specific receptor interactions provide a wide range of signaling pathways, allowing a few receptors to fulfill many different responses. The $p75^{NTR}$ partners with three different types of co-receptors: the Trk receptors (A, B and C), sortilin or Nogo receptors (fig. 1.5).

1.3.2.0.1 p75^{NTR} interactions with the Trk receptors An important difference between other death receptors and the p75^{NTR} is the inability to auto-activate the apoptotic pathway, additionally to its above-mentioned lack of a kinase domain. Therefore p75^{NTR} exerts its functions by interacting with other receptors. Heterodimers consisting of Trk receptors and p75^{NTR} promote growth and pro-survival signaling while increasing the affinity of major neurotrophins to the respective Trk receptor 100-fold compared to the Trk homodimer (Hempstead 1991; Bibel 1999). This is especially important during development when the increased efficacy of TrkA–p75^{NTR} signaling initiates NGF dependent neuronal survival and growth. Downstream pathways of Trk activation typically includes the PI3K-Akt, extracellular regulated kinases (Erk) and phospholipase C–γ (PLC γ). Bui *et al.* could demonstrate in 2002 that in the absence of p75^{NTR} (ExonIII Knockout; Lee *et al.*, 1992), the ability to activate Akt signaling on PC12 cells via TrkA is decreased. The fact p75^{NTR} interacts with TrkA, B and C stresses the ability for p75^{NTR} to control a wide range of aspects of neurotrophin signaling.

1.3.2.0.2 p75^{NTR} interactions with truncated Trk receptors TrkA, B and C have variants that are derived from alternate splicing, which lack the kinase domain. The truncated TrkB is best characterized for being expressed in the mature CNS and has been suggested to modulate full-length TrkB signaling. Formation of dendritic spines (Michaelsen *et al.*, 2010) and filopodia (Hartmann *et al.*, 2004) is controlled by these splice variants working in concert with p75^{NTR}. Long-term potentiation (LTP) and long-term depression (LTD) are both impaired in truncated TrkB over-expressing transgenic mice. This suggests that truncated TrkB together with p75^{NTR} promotes the opposite effect as the full-length TrkB, limiting its actions.

Transactivation of Trk Receptors Another level to regulate neurotrophin receptor signaling remains still mainly elusive: the potential for Trk receptors to signal through transactivation. Studies showed (Lee *et al.*, 2001, 2002; Poo, 2001) that other receptors catalyze the phosphorylation of Trk receptors. Puehringer *et al.* (2013) could show that in the absence of BNDF and NT-3 epidermal growth factor (EGF) binding to its receptor (EGFR) and promotes the activation of TrkB and TrkC to regulate the migration of newborn cortical neurons. In other cases, transactivation promotes cell survival by increasing Akt activity (Chao *et al.*, 2006).

Known events are connected to interactions with G-protein protein coupled receptors (Filardo, 2002), as observed with adenosine receptors.

1.3.2.0.3 p75^{NTR} interactions with sortilin Aside the Trk receptors sortilin has been the most intensely studied co-receptor of p75^{NTR}. Sortilin itself is a protein with many different functions and interaction partners (Nykjaer and Willnow 2012). Two discoveries put a greater focus on its interaction with p75^{NTR} though: a) p75^{NTR}- sortilin heterodimers downstream activate apoptotic pathways, a process generally used during development of the CNS (Hempstead 2006; Kraemer *et al.*, 2014a, b) especially pro-neurotrophins bind the p75^{NTR}-sortilin heterodimer with high affinity, initiating the cell death signal (Lee *et al.*, 2001), by the JNK-3–c-Jun pathway. Different neuronal sub-populations are partly driven to initiate apoptosis during development by means of p75^{NTR}, e. g. in sympathic neurons, retinal neurons and oligodendrocytes (Frade and Barde, 1998; Huang and Reichardt, 2001; Beattie *et al.*, 2002; Teng, 2005; Jansen *et al.*, 2007; Kenchappa *et al.*, 2010; Nykjaer and Willnow, 2012; Roberti *et al.*, 2014). Cell death is by no means the only known function of sortilin, although intensely studied, it has also been described principally as an intracellular sorting protein. Vaegter *et al.* demonstrated in 2011 that sortilin controls pro-BDNF secretion by assisting in intracellular, anterograde trafficking. This underlines its importance for neuronal function and survival.

1.3.2.0.4 p75^{NTR} interactions with Nogo Another mechanism to control neuronal growth is provided by interactions of Nogo-receptor 1 (NgR1) with p75^{NTR}. Axonal growth is suppressed by signaling via NgR1 interacting with the p75^{NTR} in a receptor complex which is bound by MOG, MAG or Nogo. This ligand-receptor conglomerate mediates the dissociation of Rho-GDI from RhoA (Yamashita *et al.*, 1999), triggering growth cone collapse by interaction with LINGO-1 (Mi *et al.*, 2004.). Coincidentally, Rac gets inhibited, which does limit the stimulus to initiate the growth cone formation (Deinhardt *et al.*, 2011). This is important in development and after injuries, when the CNS needs to recover and repair the former structures. Therefore these processes have been studied and focused on to target neuronal growth restoration therapeutically (McDonald *et al.*. 2011).

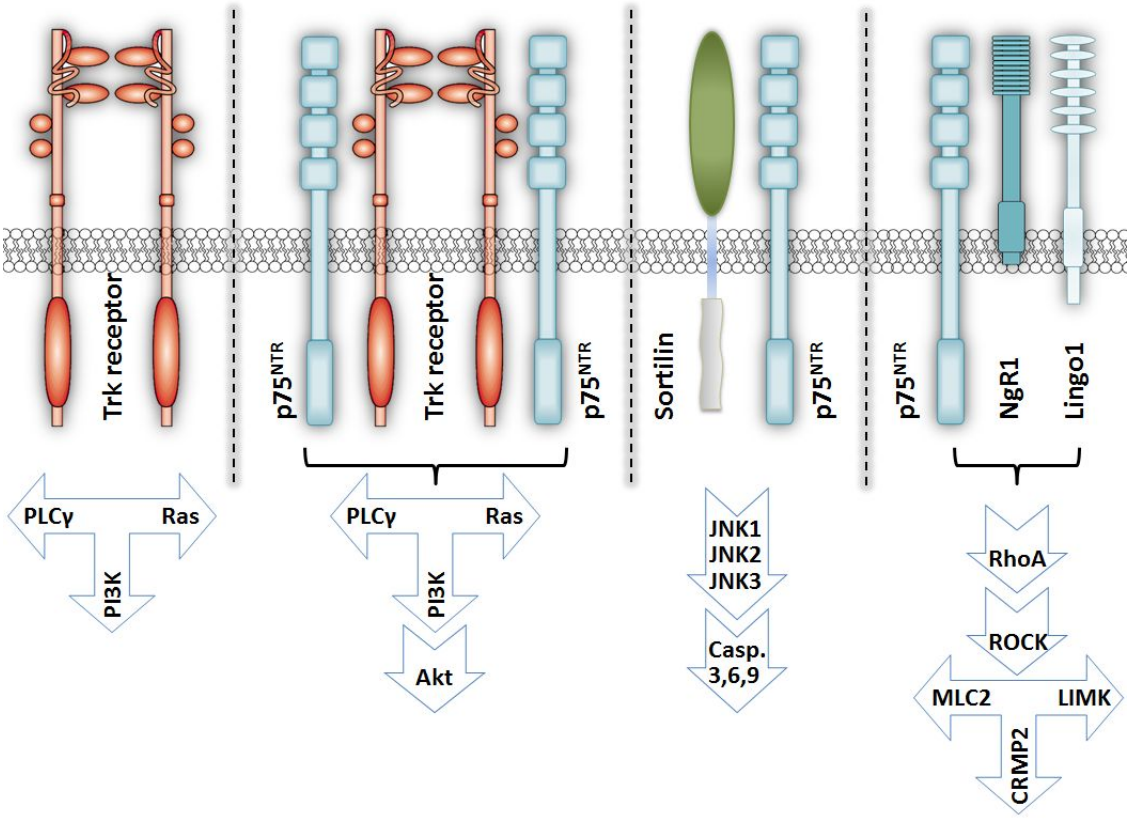

Figure 1.5: Neurotrophin receptor dimerization and signaling - The Trk (tyrosine receptor kinase) receptors can form homodimers and heterodimers with the $p75^{NTR}$. The $p75^{NTR}$ is a membrane-spanning neurotrophin receptor belonging to the tumor necrosis factor receptor superfamily (TNF) that binds all the four neurotrophins: BDNF, NGF, NT–3 or NT–4, the mature isoforms with low affinity and the pro-neurotrophins with high affinity. The intracellular domain (ICD) of the $p75^{NTR}$ contains a death domain that, because of the $p75^{NTR}$'s lack of kinase activty, is not able to activate itself and therefor requires interactions with other receptors or effector proteins. The $p75^{NTR}$ interacts with three different receptor classes: Nogo receptor, the Trk receptors and sortilin. Heterodimers with one of the Trk receptors leads to a higher affinity to mature neurotrophins and mediates surival and growth signaling PI3K-Akt, ERK or PLCγ pathways. In contrast dimerization of $p75^{NTR}$ with sortilin allow high affinity binding of the pro-forms of the neurotrophins. The Ras/MAPK pathway gets subsequently activated, finally leading to apoptosis by JNK3 and caspase pathways. Interactions of the $p75^{NTR}$ with the Nogo receptor and Lingo–1 participate in the control of neuronal growth. The RhoA activation and a concurrent suppression of Rac leads to collapse of neuronal growth cones, neurite retraction and also leads to reduction in spine density.

1.3.3 Neurotrophins participating in immunological functions

During the development of the CNS $p75^{NTR}$ plays an important part in neuron selection and while the nervous system matures, $p75^{NTR}$ gets substantially down regulated. However, it has been published that $p75^{NTR}$ expression can increase

profoundly in response to disease or injury, highlighting a considerable role of the neurotrophic system in regulating nervous system function in a healthy as well as in a pathological state (Ibanez and Simi, 2012; Kraemer *et al.*, 2014; Meeker and Williams, 2014).

Increased expression of $p75^{NTR}$ on macrophages and microglia during pathological states (Meeker and Williams, 2014) reveals a relatively unexplored area which may ultimately influence our understanding of neuroinflammation. Detailed research on $p75^{NTR}$ function in microglia and macrophages has yet to be published but indicated by the presence of Trk receptors, NOGO receptors and sortilin, similar signal transduction pathways as present in neurons could be involved. Several studies suggest that macrophage/monocyte chemotaxis in the CNS may be regulated by neurotrophins (Fry *et al.*, 2007; David *et al.*, 2008; Yan *et al.*, 2012).

Additionally activated macrophages/microglia potentially release neurotrophins (Heese *et al.*, 1998; Srinivasan *et al.*, 2004). This could either provide an autocrine signaling pathway or raise the possibility of a direct signaling link between CNS and immune system.

1.3.4 Microglia express and release neurotrophins

Microglia release several factors that are contributing to neuronal health and survival including neurotrophins (NGF and BDNF) and glial-derivedneurotrophic factor (GDNF) (Mallat *et al.*, 1989; Elkabes *et al.*, 1996; Wang *et al.*, 2013). Both microglia and macrophages produce NGF early in development *in vivo* (Frade and Barde, 1998), while increased secretion of BDNF upon neuronal damage has also been reported *in vitro* (Lai and Todd, 2008). This suggests that in response to CNS insult microglia may upregulate neurotrophin release in support to neuronal health. The regulation of BDNF synthesis and release in microglial cells appear to be associated with the purinergic receptor P2X4R (Ulmann *et al.*, 2008; Beggs *et al.*, 2012).

In a study by Parkhurst *et al.* (2013) the BDNF locus was deleted exclusively in microglial cells, by crossing BDNF floxed mice with CX_3CR_1-CreER and treated with tamoxifen to induce BDNF depletion during the desired time frame. These mice were additionally crossed with Thy1-eYFP mice in order to visualize neuronal structures and analyze dendritic spines with *in vivo* imaging. The experiments revealed that after removal of microglial BDNF a significant decrease in the formation rate of dendritic spines was induced. Unexpectedly these findings revealed a role

for microglial cells in spinogenesis and synapse formation in the healthy CNS.

The microglial release of BDNF also mediates synaptic plasticity in a mouse model of neuropathic pain (Coull *et al.*, 2005). The function of microglial BDNF is established in mediating pain in the spinal dorsal horn (Trang *et al.*, 2011), but the immunological effects of BDNF or microglial TrkB receptor activation are less clear. Asami *et al.* showed in 2006 that BDNF treated macrophages increased phagocytosis and upregulates IL-1β secretion. Given the similarities of macrophages and microglia, similar effects could be present in these.

1.4 *Toxoplasma gondii* - a protozoan in the central nervous system

Toxoplasmosis is an infection by *Toxoplasma gondii* (*T. gondii*), an obligate intracellular, microscopic protozoan, so named after the organism it was first identified in 1907 in North African rodents called gondis (*Ctenodactylus gundi*). *T. gondii* belongs to the phylum Apicomplexa, subclass coccidia. It can take several different forms: the oocyst; the tachyzoite; and the bradyzoite containing cyst. The *T. gondii* genome usually is haploid, except during sexual division in cats, and contains about $8x10^7$ base pairs. In its attempt to conceal it's presence from the host's immune response it invades the CNS and its cells. Following sections will introduce the current understanding of the mechanisms important for this thesis.

1.4.1 Epidemiology of a world wide pathogen - *T. gondii* is omnipresent

T. gondii can infect all warm blooded animals, namely mammals, including humans, and birds. As *T. gondii* is present in migratory birds, the parasite exits on every continent but Antarctica. Humans most often acquire the infection by ingesting oocysts or tissue cysts. Cat feces are the usual source of oocysts, while tissue cysts are commonly found in undercooked meat. Cat feces contaminated soil and water can act as vehicles, transferring the oocysts to vegetables and fruits meant for human consumption.

The parasites sexual life cycle occurs in the intestine of felidae (the family of the cats), the definitive hosts, which subsequently shed infectious oocysts with their feces. Mammals and birds feeding off the ground become infected. Tissue

cysts remain in brain and muscle until the intermediate host gets eaten by a cat, thereby completing the life cycle. Ground-feeding livestock can become infected and consequently become sources of infection for humans. *T. gondii* can be transferred to a new host by infected donor organs. Fetuses can be infected via the mother's bloodstream in utero if the mother develops a primary infection during pregnancies.

In immunocompetent hosts the risk of developing an encephalitis during primary Toxoplasmosis is negligible: 10-50% of North American citizens and up to 80% people in Central America have measurable antibody titers against *T. gondii* and no history of a disease. In the moist tropical places of South America, almost 100% of the population over age 45 years could be positive for antibodies. Approximately 10% of immunocompetent individuals have clinical signs and symptoms, which are usually mild, upon acute *T. gondii* infection.

The risk of *in utero* infection is highest if *T. gondii* infection is acquired shortly before delivery. In HIV infected patients (with acquired immune deficiency syndrome (AIDS)) with *T. gondii* antibody, the risk of recurring active toxoplasmosis is given at the time $CD4^+$ cell counts fall below 200 per mm^3.

1.4.2 Pathophysiology in humans

As previously mentioned *T. gondii* are common infections in humans, and typically without severe symptoms because adaptive immunity is acquired swiftly to the widely spreading and multiplying tachyzoites.

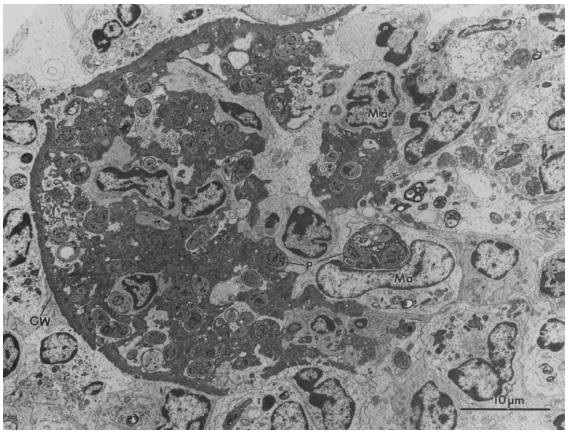

Figure 1.6: *Toxoplasma gondii* cyst - Electron micrograph of a disrupting bradyzoite cyst in the CNS of a mouse chronically infected with *T. gondii*. Remnants of the cyst's wall (CW) and spreading parasites (P) can be distinguished. Note the influx of numerous macrophages (Ma). Scale bar is 10 µm (Micrograph from Ferguson JP *et al.*, 1989).

There are certain exceptions to the above-mentioned asymptomatic progressions: in immature fetuses, immunocompromised patients or when the infection takes place at immune privileged body parts, e. g., brain or eye. Delayed adaptive immune response leads to a higher strain of the host's organism. As adaptive immunity develops, encysted bradyzoites colonize the tissue (brain, muscle, testicles). In immunocompromised patients cysts that rupture leave necrotic tissue and the freed bradyzoites

reverse their transformation back into tachyzoites that multiply and injure tissue.

1.4.3 *T. gondii* entering the brain through the blood brain barrier

1.4.3.1 The blood brain barrier

Besides the blood-brain barrier (BBB) the CNS contains two more main barrier sites, the arachnoid epithelium and the epithelium of the choroid plexus. The BBB is built by highly specialized microvascular endothelial cells, forming a functional and structural barrier with low permeability, limited pinocytosis activity, lacking endothelial pores (fenestrations), and high transendothelial resistance (Abbott *et al.*, 2006).

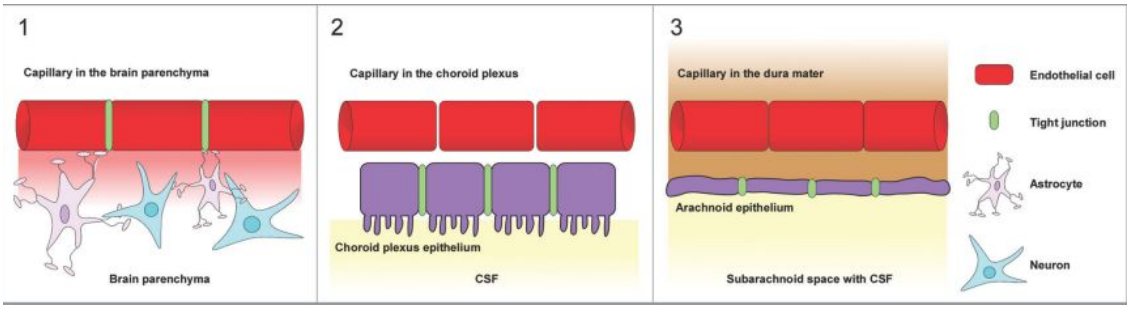

Figure 1.7: Barrier sites in the CNS - (1) The blood-brain barrier is formed by endothelial cells in the brains capillary system. **(2)** At the choroid plexus epithelial cells the barrier between the blood and the cerebrospinal fluid exists. **(3)** The arachnoid epithelium protects the cerebrospinal fluid. The intercellular between endothelial and epithelial cells spaces are sealed by tight junctions (Adapted from Feustel *et al.*, 2012).

Surrounding cells like microglia and astrocytes interact with the cells the BBB is composed off and support the maintenance of the barrier and its functions by releasing soluble agents such as transforming growth factor-β (TGFβ), basic fibroblast growth factor (bFGF) and glial-derived neurotrophic factor (GDNF). Intracellular cAMP elevating signaling molecules (like adrenomedullin) and hydrocortisones decrease the permeability between cells and strengthen barrier. To the contrary reactive oxygen species (ROS), inflammatory cytokines (IL-1, IL-6, TNF) , nitric oxide (NO) and other mediators impair the impermeability of the BBB. Adherence junctions and tight junctions restrict hydrophilic molecules to fluctuate between cells and limit the migration of the various cell types through the endothelial barrier (Deli *et al.*, 2005; Haseloff *et al.*, 2005; Dohgu *et al.*, 2005).

Regardless of this cellular mechanics, there exist several pathways for molecular trafficking across the BBB. E. g., the lipid membranes of the endothelium permit the diffusion of lipophilic agents (Abbott *et al.*, 2006). Also, there are specific receptors (e. g., transferrin and insulin receptors), which transport their ligands through the endothelium by means of receptor-depended endocytosis and exocytosis. As the brain needs to be provided with nutrients and other substances transport proteins for glucose, amino acids, purine bases and nucleosides are included in the BBB while the transport protein P-glycoprotein is an efflux pump that actively transports lipophilic drugs out of endothelial cells (Löscher and Potschka 2005).

During inflammation blood stream circulating leukocytes crawl across the endothelial barrier into the CNS (Ley *et al.*, 2007). This migration follows a specific sequence adhesion and extravasation steps, allowing to cross the extracellular matrix, basal lamina and the endothelial barrier (Rahman and Fazal, 2008). Leucocytes express P-selectin glycoprotein ligand 1 (PSGL-1), which is a ligand for E- and P-selectin, which are in turn expressed by endothelial cells (Kansas, 1996). Leukocyte extravasation involves a paracellular or a transcellular route with different cell signaling pathways included (Zarbock *et al.*, 2009).

1.4.3.2 Dissemination and Neuroinvasion of *T. gondii*

The tachyzoite form of *T. gondii* are effected by several aspects of the host's adaptive immune response. Whilst IgG against *T. gondii* in sera mediate parasite lysis *T. gondii* specific IgM inhibit tachyzoites from invading host cells. To protect itself against the immune system an intracellular habitat for *T. gondii* poses a mandatory solution for survival and subsequent dissemination.

T. gondii lacks flagella or cilia for locomotion (Soldati and Meissner, 2004; Wetzel *et al.*, 2002). Invading host cells is anyhow achieved without the host cells cooperation (Morisaki *et al.*, 1995; Carruthers *et al.*, 1999). After gaining proximity by gliding motility, the invasion itself is mediated by the secretion of a subset of parasite proteins into the host cells. These micronemal proteins (MICs) are apically exocytosed into the host cell. MIC2 is also displayed apically, binding the cell adhesion molecule ICAM-1, to anchor the parasite to the host cell (Dowse and Soldati, 2004). *T. gondii* infection induces the expression of different adhesion molecules and cytokines in host cells: brain endothelial cells upregulate 2 h post infection ICAM-1 expression while the chemokine MCP-1 is expressed 12 h post infection (Lachenmaier *et al.*, 2011). Upregulation of adhesion molecules and proinflamma-

tory chemokine secretion seem to be important parts of host cells response to *T. gondii* infection.

1.4.3.3 *T. gondii* as a model for neuroinflammation

Toxoplasmic encephalitis is one of the most prominent opportunistic infections in immunocompromised patients. When not kept low by the immune system it can cause severe brain injury, coma and even death (Osunkalu *et al.*, 2011). Especially in patients with AIDS, the pathogen is responsible for lesions and necrosis in different parts of the CNS (e.g., substantia nigra, ventral striatum, ventral pallidum). Already slightly immunocompromised patients may develop neurological symptoms; additionally to anxiety, depression and schizophrenic episodes (El Lakkis *et al.*, 2015).

Nevertheless, even in immunocompetent patients bradyzoites within the neurons produce a protein, which is functionally homologues to tyrosine hydroxylase and thereby being able to manipulate dopamine synthesis and also the release (Prandovszky *et al.*, 2011). This raises the possibility that by changing dopamine levels *T. gondii* actively interferes with the behavior (Money and Stanwood, 2013).

Moreover, the parasite also stimulates the secretion of cytokines (IFN-γ and IL-12) and initiates NFκB signal pathways via MAPK (Kim *et al.*, 2004). This establishes a stable host-parasite interaction (Vallochi, 2008). IFN-γ is seen to be the most important cytokine, released by T-cells which invade the CNS upon infection (Schlüter *et al.*, 1995). Beyond T-cells, B-cells (Schlüter *et al.*, 1998), NK cells (Schlüter *et al.*, 1995), macrophages (Suzuki *et al.*, 2005), and dendritic cells (Fischer *et al.*, 2000) also cross into the CNS upon infection.

T. gondii infection induces a variety of other cytokines (e.g., IL-1 and TNF-α; IL-10 and TGF-β) by neurons, astrocytes, and microglia (Fischer *et al.*, 1997; Schlüter *et al.*, 1997, 2001). *T. gondii* actively blocks TNF-α expression in monocytes by blocking the host's chromatin structures and inhibiting promoter - transcription factor interaction (Leng *et al.*, 2009). Inducing anti-inflammatory cytokines, such as TGF-β, IL-10 and IL-27 are thought to prevent tissue destruction by balancing Th1/Th2 response (Damsker *et al.*, 2010).

Several CNS cells, including neurons, astrocytes, and microglia, are invaded by *T. gondii* (Jones *et al.*, 1986; Chao *et al.*, 1993; Fischer *et al.*, 1997; Halonen *et al.*, 1998). The recognition of the parasite in these cells has been connected to the toll-like receptor 11 (TLR11), generating various downstream immune responses

(Atmaca *et al.*, 2014).

The general importance of inflammatory mediators in neurodegenerative disease and brain disorders has been a documented intensely for schizophrenia, brain injury, depression and bipolar disorders (Parlog *et al.*, 2015; Stich *et al.*, 2015).

Considering the broad adaptability of *T. gondii* to its many possible hosts, as well as its potential to immunomodulate, this pathogen is a great model to study CNS - immune system interactions.

1.5 Aim of the study

As previously outlined, there is plenty of evidence that neurotrophic factors play a major role in the regulation of immunological response to pathological events within the central nervous system (c.f. section 1.3.3). Intriguingly it is also known that the $p75^{NTR}$ is not only important in a broad variety of signalling pathways within neurons, by its potential to bind all neurotrophins and form heterodimers with the other receptors (c.f. section 1.3.2), it is also expressed on several immunological active cells and its expression is increased during different pathological states. The role of $p75^{NTR}$ in this context is yet unclear.

To elucidate the role of the $p75^{NTR}$ in chronic CNS inflammation, the protozoan parasite *Toxoplasma gondii* was used for its natural occurrence in human and the scientific model organism of choice, the mouse, alike (c.f. section 1.4). The characterization of hippocampal and cortical neurons depending on the presence of the $p75^{NTR}$ in context of a persistent *T. gondii* infection is a novel step to gain a deeper understanding of neurotrophic contribution to neuroinflammation. Also, the possible change of the quantity of neurotrophin receptors upon *T. gondii* infection is of interest. Additional to neuronal reaction microglial reaction to the parasite, representing the CNS immune system, is to be characterized morphologically to gain broader insights into the interleaving connections between CNS and immune system by $p75^{NTR}$.

Another question is whether the C57BL/6 (B6) mouse strain infected with *T. gondii* is an appropriate model for chronic toxoplasmosis - by comparing results to another mouse strain (BALB/c).

2 Material and Methods

2.1 Mouse strains and *T. gondii* infection

The $p75^{NTR}$ exonIV knockout mouse generated by von Schack et al.(2001) were crossed into C57BL/6-*Thy1*-eGFP line M mice (Feng et al., 2000) and used for the analysis of neuronal architecture. For biochemistry experiments, p75NTR exonIV knockout mice not expressing eGFP were used. Additionally BALB/c animals were used. In this thesis, only female mice have been analyzed.

Except for the BALB/c mice, all mice have been bred and housed at the animal facility of the TU Braunschweig until the age of 8 to 12 weeks. Then they have been transported to the animal facility of the Otto von Guericke Universität in Magdeburg and been infected with *T. gondii* (cf subsection 2.1.1).

All animals were housed at a standard day-night cycle of 12:12 h, at $\approx 22\,^{\circ}C$ with 4-5 animals each cage. Food and water were provided for *ad libitum*.

2.1.1 Infecting mice with *Toxoplasma gondii* cysts

Infections with the protozoan *Toxoplasma gondii* were carried out and planned by Dr. Ildiko Dunay and colleagues at the Institute of Medical Microbiology, Otto von Guericke University Magdeburg. Female mice (8-12 w old, cf section 2.1) were infected with 2 cysts of the *T. gondii* strain ME49 type II. For this means a previously infected (4-5 months prior) NMRI mouse was sacrificed, and the isolated brain was homogenized in 1 ml PBS.

Cyst concentration was determined by counting the number of cysts within 10 µl homogenate under a light microscope. After repeating this step at least three times, the total concentration was calculated. Two cysts were then administered to each mouse intraperitoneally (i.p.) in a total volume of 200 µl (diluted in PBS). Control mice received 200 µl PBS instead.

Infected mice and healthy controls were kept in the same room at a standard

day-night cycle of 12:12 h, at ≈ 22 °C with 4-5 animals each cage. Food and water were provided for *ad libitum*.

2.1.2 Genotyping of transgenic mice

To verify the lack of the forth exon of the $p75^{NTR}$ gene and the inclusion of the eGFP construct (cf section 2.1) genomic DNA was extracted from tail tips. This small amount of tissue was digested on a shaker (650 rpm) in 500 µl lysis buffer (containing proteinase K) at 55 °C overnight. The DNA was cleared from cellular debris by centrifugation with 14000 x g for 10 min. Afterwards, the DNA was precipitated with 500 µl isopropanol, and the resulting pellet washed with 70% ethanol.

The DNA was stored in 10 mM Tris/ HCl (pH 8) at -20 °C. 3 µl of genomic DNA were used for one polymerase chain reaction (PCR) to detect the presence or absence of the above-mentioned genes (cf table 2.2). Results were visualized via agarose gel electrophoresis. Table 2.1 contains detailed information about the used primers.

Table 2.1: These primers were used for genotyping. All primers were pre-diluted 1:5 before using in a PCR.

Gene	sequence tag	sequence
$p75^{NTR}$	1	AAGGGGCCACCAAAGAACGG
	2	GTTGGAGGATGAATTTAGGG
	3	GATGGATCACAAGGTCTACGC
eGFP	sense	AAGTTCATCTGCACCACCG
	anti-sense	TGCTCAGGTAGTGGTTGTCG
Thy1	Thy1 F1 (forward)	TCTGAGTGGCAAAGGACCTTAGG
	Ey PP RI (reverse)	GCTGAACTTGTGGCCGTTTACG
TrkB-Tk+/T1	TrkB (upper)	CTCCCACTTCCTTGGCTT
	TrkB (lower)	GCCCCACGTAAGCTTCGA

2.2 Perfusion and brain dissection

In order to preserve neurons in their *ex vivo* state mice were deeply anesthetized by placing the mice in a glass beaker with an isoflurane soaked paper tissue. In order to confirm the genotype the tip of the tail was cut and frozen (-20 °C). Then

Table 2.2: Following components were included in every PCR mix.

Component	volume
DNA-Sample	0.5 µl
Taq-Buffer	5 µl
dNTP's (10 mM each)	0.5 µl
Primers (cf table 2.1)	0.5 µl each
Taq polymerase	0.25 µl
$MgCl_2$	3 µl
$Aqua_{purificata}$	14.25 µl

the abdominal cavity was opened and the transcardial perfusion with ice cold 4% PFA in 0.1 M PB was performed by inserting a needle into the left ventricle and opening the right atrium to allow the liquid to flow through the entire circulation. The cranium was opened and the brain removed, the cerebellum cut away and the hemispheres divided.

Hemispheres meant for immunohistochemistry (cf section 2.4) were post-fixed in ice cold 4% PFA in 0.1 M PB for 30 min, briefly washed in PBS and subsequently put into 30% sucrose in 0.1 M PB and stored for 3 d at 4 °C to dehydrate them. Afterwards, these hemispheres were embedded in Tissue-Tek® O.C.T. ™ (A.Hartenstein Laborversand) and stored at -80 °C until being further processed.

Hemispheres meant for spines analysis, and neuronal morphological analysis (cf section 2.5) were postfixed in ice cold 4% PFA in 0.1 M PB for half an hour and subsequently stored in PBS. These hemispheres were then cut with a vibratome (Leica, VT1000S) into 150 µm and 300 µm sections and mounted on glass slides with Fluoro-Gel mounting medium (EMS; 17985-10) and imaged within one week.

For biochemical experiments (cf section 2.6) the mice were sacrificed by cervical dislocation, the brain removed and quickly dissected into hippocampus (HC) and cortex (C). The different parts were put in weighted reaction vessels and flash frozen in liquid LN_2. Afterwards, the samples were stored in the freezer (-20 °C) until being further processed.

2.3 DiOlistic labeling

Hippocampal and cortical neurons of BALB/c mice were labeled utilizing DiOlistics on PFA fixed brain sections. For this purpose, DiI bullets were prepared with

tungsten particles (50 mg; Ø 0.7 µm, 1.7 µm) spread on a glass slide. These particles were then mixed with 100 µl dye solution (3 mg DiI dissolved in 100 µl methylene-chloride; Invitrogen, Sigma-Aldrich). Methylene-chloride evaporates rapidly at RT. The DiI coated tungsten was then scratched off the glass slide with a razor blade and suspended in 3 ml $Aqua_{purificata}$, vortexed and sonicated. Dilutions of 1:20, 1:30, 1:40 and 1:50 were used to coat TEFZEL tubes (Bio-Rad). These bullets can be stored in the dark at RT for months. Hemispheres were then cut with a vibratome (Leica, VT1000S) into 400 µm coronal sections and post-fixed with 4% PFA and 4% sucrose in 0.1 M PB for 1 h. After washing briefly with PBS, 3-4 sections were placed within a tissue-culture insert (Merck Millipore).

The DiI-tungsten coated bullets were loaded into a gene-gun (Bio-Rad) and shot at the sections from a distance of roughly 1.5 cm with a pressure of ≈ 8200 hPa (120 psi). In order to prevent clusters of DiI coated particles to reach the sections and protect the section from direct exposure to the pressur,e a membrane filter (Ø 3 µm; Merck Millipore) was held between the gene-gun and the sections. The sections were kept in PBS overnight at RT. During this time the lipophilic DiI diffused on the membranes of cells. The day after the sections were quickly checked visually to confirm the success the of the shootings the prior day with a fluorescence microscope (Axioplan 2 microscope; Zeiss). Consecutively sections were stained with DAPI solution 1:1000 (1 mg/ml in PBS) for 10 min and mounted on glass slides with Fluoro-Gel mounting medium (EMS; 17985-10) and imaged within one week, because of the rapidly increasing background.

2.4 Immunohistochemistry

The hemispheres (cf section 2.2) were mounted on a freezing microtome (≈ -30 °C) within a frozen block of Tissue-Tek® O.C.T. ™ (A.Hartenstein Laborversand). The 30 µm sections were collected in PBS and afterwards were incubated in a blocking and permeabilizing solution (cf table 2.3) for 1 h at RT on a shaker to permeabilize the membrane and saturate unspecific binding sites. Section were then incubated with the primary antibody (cf table 2.4) diluted in PBS with 0.2% Triton X-100 and 10% goat serum at 4 °C covered in plastic wrap on a shaker overnight. Additionally a 30 min of incubation at RT took place on a shaker. That sections were then washed 3 x with PBS for 10 min at RT on a shaker. Secondary antibodies were diluted in PBS and incubated at RT for 2 h and in the dark on a

Table 2.3: The **blocking solution** for immunohistochemistry is prepared in **sterile PBS**. It can be stored in -20 °C for several weeks.

Substance	concentration
Goat serum	10%
BSA	1%
Triton X-100®	0.2%

shaker.

Table 2.4: The following table contains all **antibodies used for immunohistochemistry** staining in 30 µm sections.

Antigen	Clonality	Organism	Work dilution	Source
CD11b	monoclonal	mouse	1:250	abcam® ab64347
F4/80	monoclonal	rat	1:1000	abd Serotec®
Iba-1	polyclonal	rabbit	1:1000	Synaptic Systems
Mouse/rabbit Cy2/Cy3/Cy5	monoclonal	goat	1:500	Jackson Immuno Res.

A DAPI-solution (1 mg/ml in PBS) 1:1000 was applied for 5 min and then the sections were washed 4 x with PBS for 10 min at RT on a shaker. Then the sections were mounted on glass slides with anti-fading aqueous Fluoro-Gel mounting medium (EMS; 17985-10).

2.5 Imaging

2.5.1 Image acquisition and analysis for neuronal architecture

$B6^{Thy1\text{-}eGFP}$ and $B6^{Thy1\text{-}eGFP}$-$p75^{NTR/ExonIV\text{-}/\text{-}}$ mice were analyzed 4 weeks and 8 weeks post *T. gondii* infection (cf section 2.1).

EGFP expressing neurons were imaged using an Apotome® (Zeiss) equipped Axioplan 2 microscope (Zeiss). To reconstruct dendritic architecture a 20 fold 0.8 NA Plan-APO objective (Zeiss, 0.32 µm per pixel) was used to acquire hippocampal CA1 neurons. Controlled by the Axiovision® software (Zeiss) a z-stack step distance of 1 µm was achieved.

To simplify the analysis isolated, not overlapping eGFP expressing hippocampal CA1 neurons were chosen. Morphological analysis and reconstruction ("tracing")

were accomplished by using Neurolucida® version 6 and Neurolucida Explorer® software version 4.50.3 (Microbrightfield Bioscience).

Sholl analysis was used to quantify dendritic arborization. The software draws concentric circles around the soma at increasing distance and counts the number of intersections with dendrites for each circle. Raw values were exported to GraphPad Prism 6. For total complexity, the raw values obtained from the Sholl analysis were added to each other for each neuron. In comparisons between two data sets unpaired two-tailed Student's t-test was utilized. Comparing three or more data sets was done by ordinary one-way ANOVA with Tukey's *post hoc* test. P values of less than 0.05 were considered significant and plotted as follows: * = $p < 0.05$; ** = $p < 0.01$; *** = $p < 0.001$; **** = $p < 0.0001$. The n plotted refers to the number of cells analyzed, at least three animals per category were analyzed.

2.5.2 Image acquisition and analysis for dendritic spines

Dendrites of eGFP expressing hippocampal and cortical neurons were imaged using a laser scanning confocal microscope (Olympus, BX61WI FluoView 1000). A 40 fold oil objective (NA 1.3) and a z-step size of 0.35 µm were used. Depending on how straight a dendrite was an image of a variable vertical size (128-512) pixels times a horizontal size of 1014 pixels was used in a 6 fold zoom resulting in final pixel sizes ranging from 72 nm to 65 nm respectively.

As the background in slices labeled by Diolistic tents to fastly increase. These samples were imaged as fast as possible with as lowest a laser intensity as possible while trying to avoid dendrites which extend deep into the z-axis.

Raw confocal images (oif.-files) were deconvolved using AutoQuantX2 (Media cybernetics, Inc.; TIFF-files) and analyzed with ImageJ (US National Institutes of Health). The length of dendrites was determined with the segmented line tool, and the number of spines was calculated with the multipoint selection tool. Raw values were exported to GraphPad Prism 6 for statistical analysis. The n plotted refers to the number of animals analyzed. Per animal and region, 5 dendrites were analyzed and averaged. In comparisons between two data sets unpaired two-tailed Student's t-test was utilized. Comparing three or more data sets was done by ordinary one-way ANOVA with Tukey's *post hoc* test. P values of less than 0.05 were considered significant and plotted as follows: * = $p < 0.05$; ** = $p < 0.01$; *** = $p < 0.001$; **** = $p < 0.0001$.

2.5.3 Image acquisition immunohistochemistry

Additionally to the neuronal response to the *T. gondii* infection the phenotype of microglia upon *T. gondii* infection was characterized. For this purpose microglia cells/macrophages were labeled with an anti-Iba1 antibody (cf section 2.4). Images of the *stratum radiatum* and *dentate gyrus* within the CA1 area of the hippocampus and the cortex were taken with a 20 fold 0.8 NA Plan-APO objective (Zeiss, 0.32 µm per pixel) with a z-sectioning of 1 µm at an Apotome® (Zeiss) equipped Axioplan 2 microscope (Zeiss). Iba1+ cells were then counted in overlap with the DAPI signal. Per area and animal three regions of interest (ROIs) were analyzed. The n plotted in the results is the number of ROIs.The multipoint tool of ImageJ (V1.49 US National Institutes of Health) was used. Data were analyzed with GraphPad Prism 6.01 as mean ± SEM. In comparisons between two data sets unpaired two-tailed Student's t-test was utilized. Comparing three or more data sets was done by ordinary one-way ANOVA with Tukey's *post hoc* test. P values of less than 0.05 were considered significant and plotted as follows: * = $p < 0.05$; ** = $p < 0.01$; *** = $p < 0.001$; **** = $p < 0.0001$.

2.6 Biochemical methods

2.6.1 Brain lysates

Tissue was weighed frozen and thawed on ice. The weight in mg was used to determine the amount of brain lysate buffer (cf Table 2.5), equaling the amount of mg in µl. The tissue was homogenized with a pestle and dissociated with the tip of an ultrasonic processor (Hielscher UP50H; cycle 1; 80% amplitude). The ultrasonic tip was briefly applied for 5 s and then cooled down on ice again. This step was repeated four times. When tissue was still attached to the pestle $\frac{1}{4}$ of the initial buffer volume was used to rinse it. The resulting lysate was centrifuged for 1.5 h at 4 °C with 15500 x g (Servall® Hereaus Biofuge primoR; rotor: 7599B). The supernatant was divided into 15 µl aliquots and stored at -20 °C until further processed.

Table 2.5: The **brain lysis buffer** can be stored at 4°C for several months. The pH is to be adjusted to 7.3 at this temperature. This buffer contains distinct levels of Triton X-100® and therefore cannot be used directly in a Bradford protein assay. Samples must be diluted at least 1:5 with PBS before determining protein concentration. Protease inhibitors should always be applied to the mixture immediately before homogenization.

Substance	concentration
HEPES	50 mM
NaCl	150 mM
EGTA	2 mM
Triton X-100®	0.5%
AEBSF	0.4 mM
Pepstatin A	2 µM
Trasylol (Aprotinin)	1%

2.6.2 Bradford assay

Protein concentrations within the different brain lysates were determined using protein the Bradford protein assay. A calibration curve was derived from several dilutions of a 1 mg/ml BSA in PBS solution.

Protein dilutions ranging from 1:100 to 1:800 were prepared and duplicates were measured and their mean used in calculations. 20 µl of each dilution was mixed with 100 µl Bradford solution in a 96-well plate and incubated for 5 min at RT. The following readout via ELISA at 595 nm, the protein concentration was calculated referring to the BSA calibration curve (linear regression analysis).

Table 2.6: The Bradford protein assay reagent was prepared with $\text{Aqua}_{\text{purificata}}$. The blow mentioned **amounts suffice for 1 l**. When stored under dark conditions the Bradford reagent can be used for several years. Freshly prepared **Bradford reagent** needs to be filtered.

Substance	concentration
Coomassie Brilliant Blue G-250	100 mg
Ethanol	50 ml
Phosphoric acid	85 % (v/v) 100 ml

2.6.3 SDS-PAGE

The gels were prepared by mixing and chemically linking acrylamide and bisacrylamide (crosslinker; ratio 37.5:1). The polymerization was started by ammonium

persulfate (APS; source of free radicals) and catalyzed by TEMED (N,N,N,N'-tetramethylenediamine). The detailed gel composition is listed in Table 2.8. Protein samples were boiled (100°C; 5 min) before electrophoresis with SDS. Additionally β-mercaptoethanol was added to reduce disulfide bonds (cysteine residues) resulting in a complete denaturation of the proteins. In order to get sharper, well defined bands a discontinuous system usually was applied (cf table 2.7). The stacking gel atop the separation gel had a pH of 6.8. The power supply was set for 240 V and 10 mA until the sample was in a thin line, indicated by the bromphenol blue band, which is part of the loading buffer. Afterwards, the electric current was raised to 20 mA and kept constant until the end of the electrophoresis.

Table 2.7: Discontinuous SDS-PAGE need two different gels and these need to have different buffers to work..

Buffer	SDS	Tris	pH
Separation gel buffer	0.4%	1.5 mol/l	8.8
Stacking gel buffer	0.4%	0.6 mol/l	6.8

Table 2.8: The aqueous 30% acrylamide bisacrylamide ready-to-use stock solution Rotiphorese® Gel 30 (Carl Roth; 37.5:1) was used in several concentrations. The here specified quantities suffice for 11 gels. Gradient gels comprised of half the below mentioned amount for each concentration.

Substance	4% gel	10% gel	20% gel	stacking gel
$Aqua_{demin}$	74 ml	50 ml	10 ml	46,5 ml
Separation gel buffer	30 ml	30 ml	30 ml	
Stacking gel buffer				25 ml
Rotiphorese® Gel 30	16 ml	40 ml	80 ml	13 ml
TEMED (SERVA)	50 µl	50 µl	50 µl	50 µl
APS (10% (w/v))	800 µl	800 µl	800 µl	1000 µl

2.6.4 Western Blot (Towbin *et al.*, 1979; Burnette, 1981) and ECL reaction

Before proteins can be labeled and identified with antibodies, they need to be vertically transferred and immobilized on a polyvinylidene fluoride membrane (Rothi® Flouro PVDF; Roth) while preserving the separation pattern the tank-blot variance ($\hat{=}$ wet blot) of Western blotting was applied (Biometra 013-300). Therefore the

sandwich cassette was placed between the two electrodes in a pre-cooled buffer (cf Table 2.10) filled tank (cf Figure 2.1). This tank was then placed in a crushed-ice filled box and kept in the cool room (4°C) overnight. The power supply was set to 35 V and 200 mA per gel. To verify the majority of the protein within the gel transferred to the membrane the gel was stained with coomassie to visualize remnant protein (cf table 2.9).

Table 2.9: The following components suffice for 2 l of the Coomassie staining solution.

Substance	concentration
$C_2H_4O_2$	200 ml
C_3H_8O	500 ml
$Aqua_{purificata}$	1300 ml
Coomassie	0.5 g

The PVDF membrane was incubated in 5% skim milk powder diluted in TBS-T for one hour at RT on a shaker to block free binding sites and afterward washed 3 times with 1 x TBS-T for 10 min each.

Table 2.10: The **blotting buffer** was prepared a day ahead of the experiment and stored at 4°C.

Substance	concentration
Methanol	20%
SDS	0.05%
EGTA	2 mM
Glycine	1.5 mol/l
Tris	0.25 mol/l
10x blot buffer stock	10%

Table 2.11: The **TBS-T** was prepared as 10 fold stock solution in $Aqua_{purificata}$. The pH was adjusted to 7.6 with HCl.

Substance	concentration
NaCl	150 mM
Tris	50 mM
Tween-20	0.05%

The Membrane was then cut to remove the overhang above the original gel size and to divide the protein of interest from the internal standard horizontally. Sub-

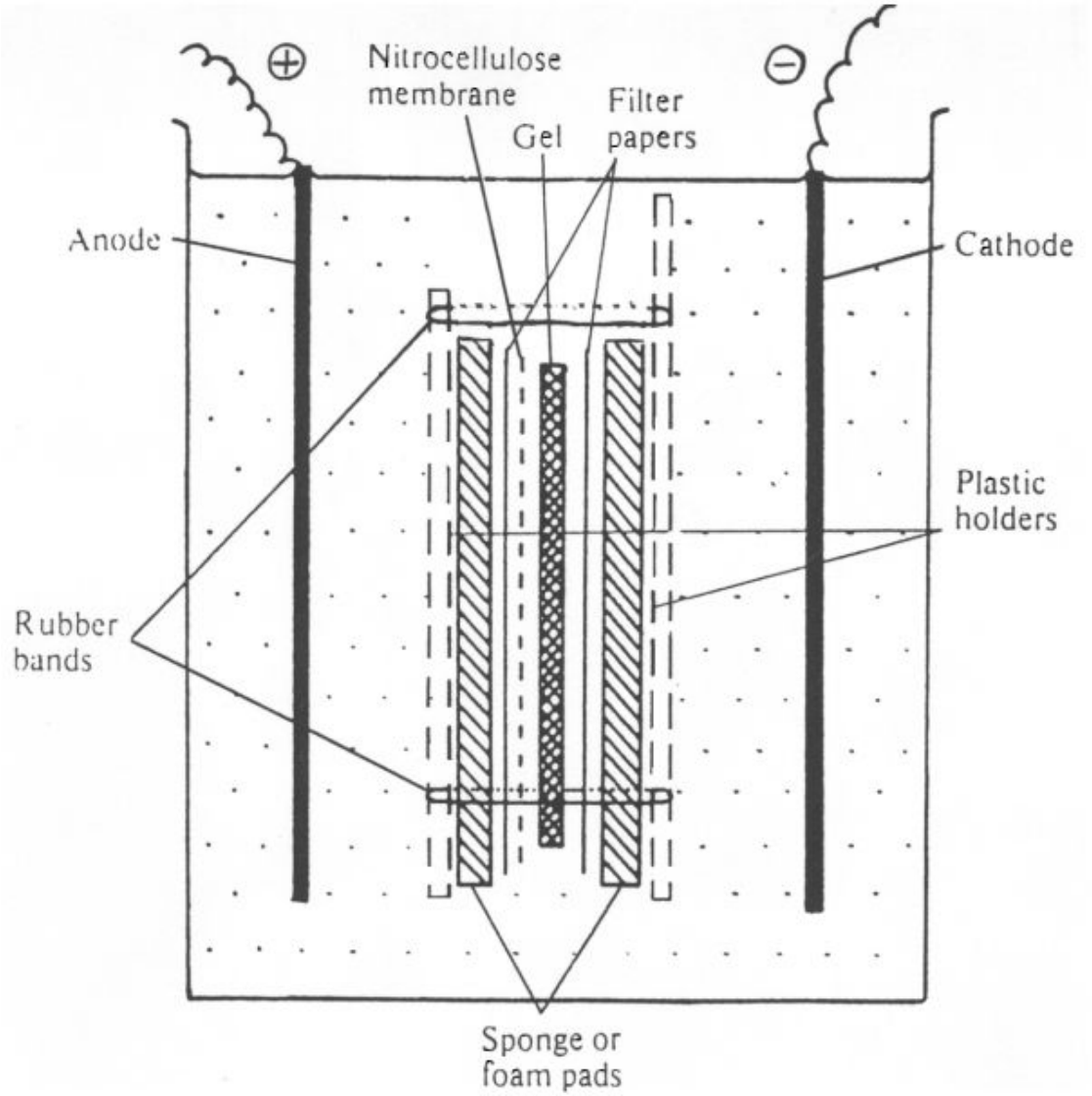

Figure 2.1: Schematic diagram of the Tankblot including the blot-sandwich. Instead of nitrocellulose a PVDF membrane was used in this thesis. Image taken from the Biometra manual.

sequently the membrane pieces were incubated with diluted primary antibodies (cf Table 2.12) over night at 4°C in a 10 ml falcon tube on a rotating wheel, and subsequently washed 3 times 10 min with 1 x TBS-T for removing unbound antibodies. Incubation with the secondary antibody (goat anti mouse/rabbit IgG HRP conjugated, cf Table 2.12) took place at RT for at least 1 h. The following washing steps differ from the previous by washing two times with TBS-T for 10 min at RT and once with TBS-X for 1 min at RT. The membrane was then put into $\text{Aqua}_{\text{demin}}$ for

5 min to wash off the remains of the Triton X-100®.

Table 2.12: The following antibodies were used in Western blots. Each was diluted in 1x TBS-T and incubated on a rotating wheel.

Antigen	clonality	supplier and reference number	concentration
$p75^{NTR}$	rabbit monoclonal	abcam ab52987	1:50000
$p75^{NTR}$	rabbit polyclonal	abcam ab38335	1:1000
TrkB	rabbit polyclonal	Milipore 07-225	1:2000
α-Tubulin	mouse monoclonal	Sigma-Aldrich® T9026	1:10000
GAPDH	rabbit polyclonal	Acris AP21839PU-N	1:3000

Following Luminata™ Crescendo HRP substrate solution was applied directly onto the membrane for 2 min. In a darkroom, the emitted light was detected with X-Ray films (LucentBlue™; Pierce). After developing and fixing the films in the dark, they were dried at RT and then scanned (600 dpi). The densiometric analysis was performed with the freely available GelAnalyzer2010a software (www.gelanalyzer.com). Per animal 3 repetitions were analyzed and every repetition consisted of triplets. In comparisons between two data sets unpaired two-tailed Student's t-test was utilized. Comparing three or more data sets was done by ordinary one-way ANOVA with Tukey's *post hoc* test. P values of less than 0.05 were considered significant and plotted as follows: * = $p < 0.05$; ** = $p < 0.01$; *** = $p < 0.001$; **** = $p < 0.0001$.

As loading controls, α-Tubulin and GAPDH (Glyceraldehyde 3-phosphate dehydrogenase) were used. These proteins are constitutively expressed at high levels in almost all tissues and cell lines making them ideal for use as loading control markers in immunoblots.

3 Results

In this work the effect of chronic *Toxoplasma gondii* infection, as a model for direct immune insult and prolonged neuroinflammation, on B6 wild type and $p75^{NTR}$ knock out mice, was analyzed. Additionally, mouse strain specific differences in the effect of the parasite infection were analyzed by comparing the results from the B6 mouse strain to the BALB/c mouse strain. The following sections will include results about neuronal architecture, dendritic spine densities, microglial response and neurotrophin receptor expression upon *Toxoplasma gondii* infection in the aforementioned mouse strains for 4 and 8 weeks after infection with *T. gondii*.

3.1 Morphological analysis of hippocampal and cortical pyramidal neurons

Neuroinflammation caused by intraperitoneal infection with *T. gondii* tissue cysts and subsequent invasion of the CNS has been shown to cause morphological changes in hippocampal and cortical pyramidal cells (Parlog *et al.*, 2014) in rodents.

However, the molecular mechanisms mediating these alterations and especially the role of $p75^{NTR}$ and neurotrophins on the progression of the disease are still unknown. In this study, the architecture of hippocampal CA1 neurons and cortical layer V/VI pyramidal neurons were analyzed four and eight weeks after *Toxoplasma gondii* infection. The dendritic complexity of the excitatory pyramidal CA1 neurons was analyzed by the Sholl analysis for the apical and the basal dendrites (Sholl, 1953). Additionally, the spine density of these excitatory cortical and hippocampal neurons was determined.

3.1.1 Changes in dendritic complexity in *T. gondii* infected mice

Parlog *et al.*, have shown that upon *T. gondii* infection the dendritic architecture of pyramidal neurons is altered. Significant reduction in complexity in the basal tuft of cortex layer III neurons with a significantly decreased total dendritic length were shown in the 2014 publication.

Table 3.1: Descriptive statistics for total complexity of CA1 dendrites in fig. 3.1

Genotype	CNS area	*T. gondii*	Mean±SEM
B6 WT	CA1 apical	-	152.9±10.49 dendritic intersections
B6 WT	CA1 apical	4 w	133.3±4.708 dendritic intersections
B6 WT	CA1 apical	8 w	108.9±7.834 dendritic intersections
B6 WT	CA1 basal	-	125.2±6.895 dendritic intersections
B6 WT	CA1 basal	4 w	129.7±7.197 dendritic intersections
B6 WT	CA1 basal	8 w	86.41±5.45 dendritic intersections

Figure 3.1 shows how chronic *T. gondii* infection effects dendritic architecture of hippocampal pyramidal CA1 neurons in B6 wt mice. Figure 3.1 A, A' and A" show reproductions ("tracings") of B6 wt CA1 neurons of control, 4 w *T. gondii* infected and 8 w *T. gondii* infected mice. After 8 w infected with *T. gondii* the amount of dendrites is visibly reduced.

Figure 3.1 B and B' show the results of the Sholl analysis (c.f. section 2.5.1) for apical and basal CA1 neurons of control B6 wt *versus* 4 w *T. gondii* infected B6 wt mice. Both, the control and the 4 w *T. gondii* infected, show a similar distribution of dendritic complexity relative to the distance from the cell body.

Figure 3.1 C and C' show the results of the Sholl analysis for apical and basal CA1 neurons of control B6 wt *versus* 8 w *T. gondii* infected B6 wt mice. The curves do not overlap; the curves of the 8 w *T. gondii* infected B6 wt mice show a different distribution of dendritic complexity relative to the distance from the cell body compared to the wt control for both, apical and basal, dendrites of the hippocampal CA1 neurons.

Figure 3.1 D and D' show the total complexity for control, 4 w *T. gondii* infected and 8 w *T. gondii* infected B6 wt mice in CA1 neurons. For the apical dendrites (fig. 3.1 D) no significant difference between the B6 wt control and the 4 w *T. gondii* infected B6 wt mice could be shown, also no statistical significant difference between 4 w *T. gondii* infected B6 wt mice and 8 w *T. gondii* infected B6 wt mice

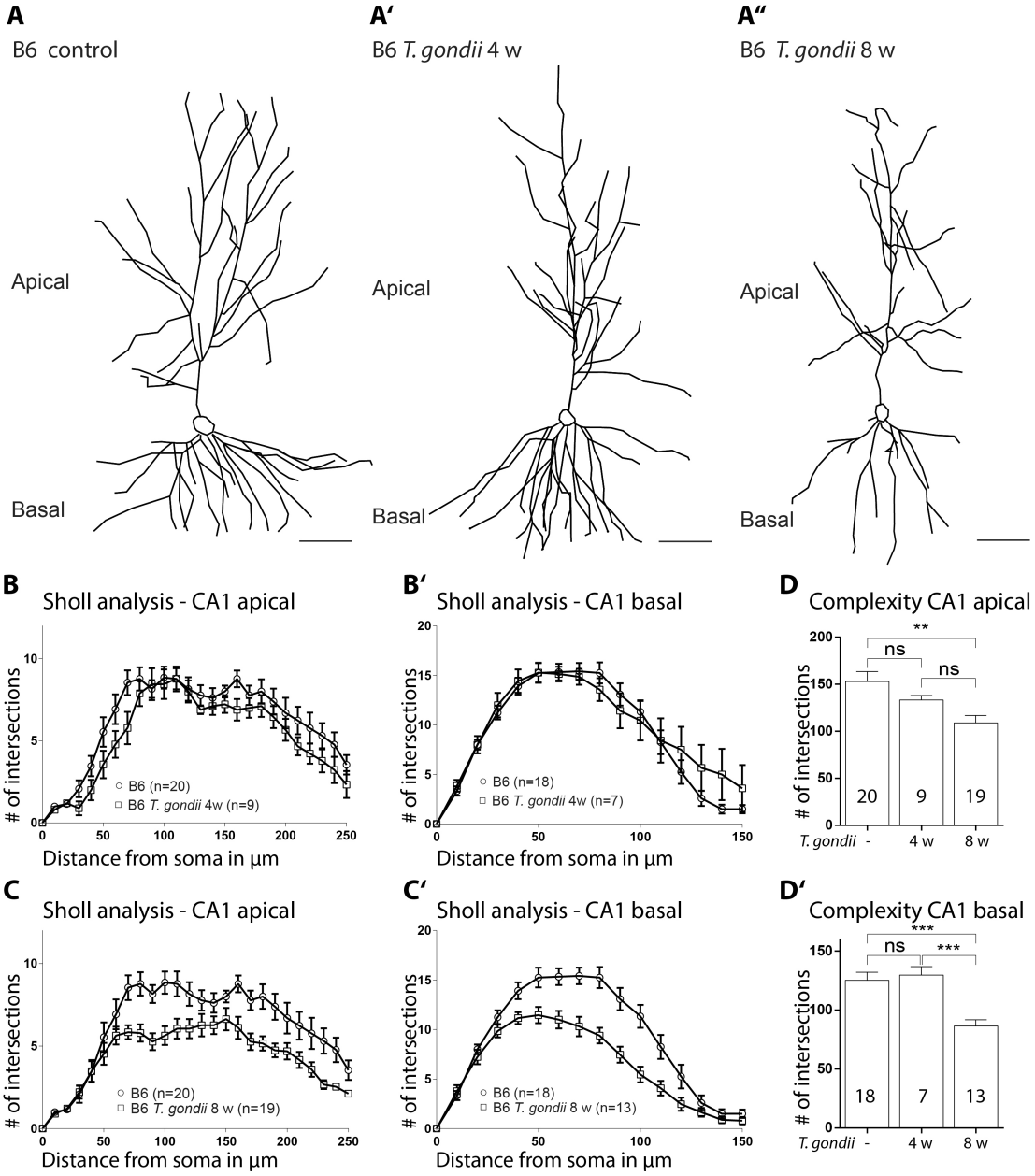

Figure 3.1: Influence of a chronic *Toxoplasma gondii* infection with different incubation times on dendritic complexity of hippocampal CA1 pyramidal neurons - (A, A', A") Exemplified morphology of hippocampal CA1 pyramidal neurons of B6 control, 4 w infected and 8 w infected, scale bar is 100 µm **(B, B')** Dendritic complexity of hippocampal CA1 pyramidal neurons (apical and basal tree), B6 control vs B6 4 w infected with *T. gondii* **(C, C')** Dendritic complexity of hippocampal CA1 pyramidal neurons (apical and basal tree), B6 control vs B6 8 w infected with *T. gondii* **(D, D')** Total complexity of hippocampal CA1 pyramidal neurons apical and basal dendrites. B6 control vs B6 4 w vs B6 8 w infected with *T. gondii*. Data presented as mean ± SEM. p***<0.001; p**<0.01; p*<0.05. The n represents the number of cells analyzed, at least 3 animals per condition were used.

can can be observed. The total complexity of B6 wt control *versus* 8 w *T. gondii* infected B6 wt mice shows a significant decrease in the total number of intersections in the 8 w *T. gondii* infected B6 wt mice.

For the basal dendrites (fig. 3.1 D') no significant difference between the B6 wt control and the 4 w *T. gondii* infected B6 wt mice could be shown. Both, B6 wt control and 4 w *T. gondii* infected B6 wt mice show significantly higher total numbers of intersections than the 8 w *T. gondii* infected B6 wt mice. Descriptive statistics for fig. 3.1 are listed in table 3.1.

Table 3.2: Descriptive statistics for total complexity of CA1 dendrites in fig. 3.2

Genotype	CNS area	*T. gondii*	Mean±SEM
B6-p75$^{NTR-/-}$	CA1 apical	-	158.6±15.98 dendritic intersections
B6-p75$^{NTR-/-}$	CA1 apical	4 w	155±7.785 dendritic intersections
B6-p75$^{NTR-/-}$	CA1 apical	8 w	144.8±5.808 dendritic intersections
B6-p75$^{NTR-/-}$	CA1 basal	-	133.2±7.468 dendritic intersections
B6-p75$^{NTR-/-}$	CA1 basal	4 w	126.6±8.643 dendritic intersections
B6-p75$^{NTR-/-}$	CA1 basal	8 w	115.8±7.306 dendritic intersections

Figure 3.2 shows how chronic *T. gondii* infection effects dendritic architecture of hippocampal pyramidal CA1 neurons in B6-p75$^{NTR-/-}$ mice. Figure 3.1 A, A' and A" show reproductions ("tracings") of B6-p75$^{NTR-/-}$ CA1 neurons of control, 4 w *T. gondii* infected and 8 w *T. gondii* infected mice.

Figure 3.2 B and B' show the results of the Sholl analysis (c.f. section 2.5.1) for apical and basal CA1 neurons of control B6-p75$^{NTR-/-}$ *versus* 4 w *T. gondii* infected B6-p75$^{NTR-/-}$ mice. Both conditions show a similar distribution of dendritic complexity relative to the distance from the cell body.

Figure 3.2 C and C' show the results of the Sholl analysis for apical and basal CA1 neurons of control B6-p75$^{NTR-/-}$ *versus* 8 w *T. gondii* infected B6-p75$^{NTR-/-}$ mice. Both conditions show a similar distribution of dendritic complexity relative to the distance from the cell body.

Figure 3.2 D and D' show the total complexity for control, 4 w *T. gondii* infected and 8 w *T. gondii* infected B6-p75$^{NTR-/-}$ mice in CA1 neurons. For the apical and basal dendrites (fig. 3.2 D, D') no significant difference between the B6-p75$^{NTR-/-}$ control and both *T. gondii* infected B6-p75$^{NTR-/-}$ mice can be observed regarding the total number of intersections. Descriptive statistics for fig. 3.2 are listed in table 3.2.

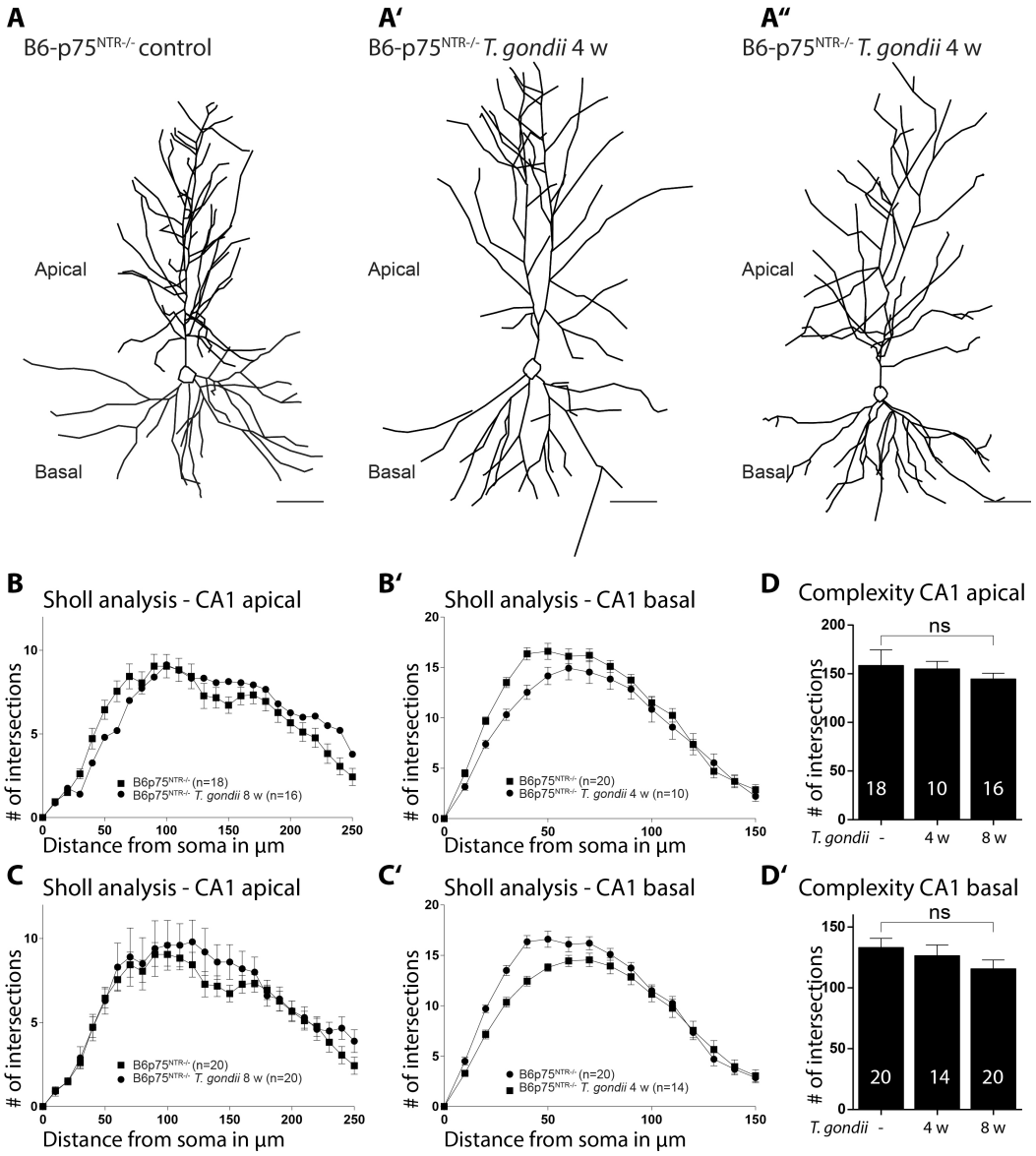

Figure 3.2: Influence of a chronic *Toxoplasma gondii* infection with different incubation times on dendritic complexity of hippocampal CA1 pyramidal neurons in p75$^{NTR-/-}$ mice - (A, A', A") Exemplified morphology of hippocampal CA1 pyramidal neurons of p75$^{NTR-/-}$, 4 w infected and 8 w infected, scale bar is 100 µm **(B, B')** Dendritic complexity of hippocampal CA1 pyramidal neurons (apical and basal tree), p75$^{NTR-/-}$ control vs p75$^{NTR-/-}$ 4 w infected with *T. gondii* **(C, C')** Dendritic complexity of hippocampal CA1 pyramidal neurons (apical and basal tree), p75$^{NTR-/-}$ control vs p75$^{NTR-/-}$ 8 w infected with *T. gondii* **(D, D')** Total complexity of hippocampal CA1 pyramidal neurons apical and basal dendrites. p75$^{NTR-/-}$ control vs p75$^{NTR-/-}$ 4 w vs p75$^{NTR-/-}$ 8 w infected with *T. gondii*. Data presented as mean ± SEM. p*<0.05. The n represents the number of cells analyzed, at least 3 animals per condition were used.

3.1.2 p75$^{NTR-/-}$ mice show no difference in dendritic architecture compared to wild type controls

Genetically deleting the exon IV in the p75^{NTR} gene has been shown to increase the dendritic complexity of the proximal apical dendrites in hippocampal CA1 neurons compared to wild type controls in *in vitro* experiments (Zagrebelsky *et al.*, 2005).

Figure 3.3 shows how genetically deleting the exon IV in the p75^{NTR} gene in B6 wt mice effects dendritic architecture of hippocampal pyramidal CA1 neurons. Figure 3.3 A is a fluorescence micrograph of an under the *Thy1* promoter eGFP expressing hippocampal CA1 neuron of a B6 wt mouse. Figure 3.3 B and B' show reproductions ("tracings") CA1 neurons of B6 wt and B6-p75$^{NTR-/-}$ mice.

Figure 3.3 C and C' show the results of the Sholl analysis (c.f. section 2.5.1) for apical and basal CA1 neurons of B6 wt *versus* B6-p75$^{NTR-/-}$ mice. Both genotypes show a similar distribution of dendritic complexity relative to the distance from the cell body.

Figure 3.3 D shows the total complexity for apical and basal CA1 neurons of B6 wt *versus* B6-p75$^{NTR-/-}$ mice. The total number of intersections in basal and apical dendrites of the wt and the p75^{NTR} KO do not differ significantly. Descriptive statistics for fig. 3.3 are listed in table 3.3.

Table 3.3: Descriptive statistics for total complexity of CA1 dendrites in fig. 3.3

Genotype	CNS area	*T. gondii*	Mean±SEM
B6 WT	CA1 apical	-	152.9±10.49 dendritic intersections
B6-p75$^{NTR-/-}$	CA1 apical	-	158.6±15.98 dendritic intersections
B6 WT	CA1 basal	-	125.2±6.895 dendritic intersections
B6-p75$^{NTR-/-}$	CA1 basal	-	133.2±7.468 dendritic intersections

3.1.3 Dendritic spine density is altered in *T. gondii* infected mice

Parlog *et al* ., have shown that upon *T. gondii* infection the dendritic architecture of pyramidal neurons is altered (2014). Dendritic spine densities in cortex LII/III have shown to be significantly reduced in *T. gondii* infected B6 wt mice. Following results will provide insight into the effect of chronic *T. gondii* infection on hippocampal CA1 neurons and cortical pyramidal LV/VI neurons in B6 controls and B6-p75^{NTR}

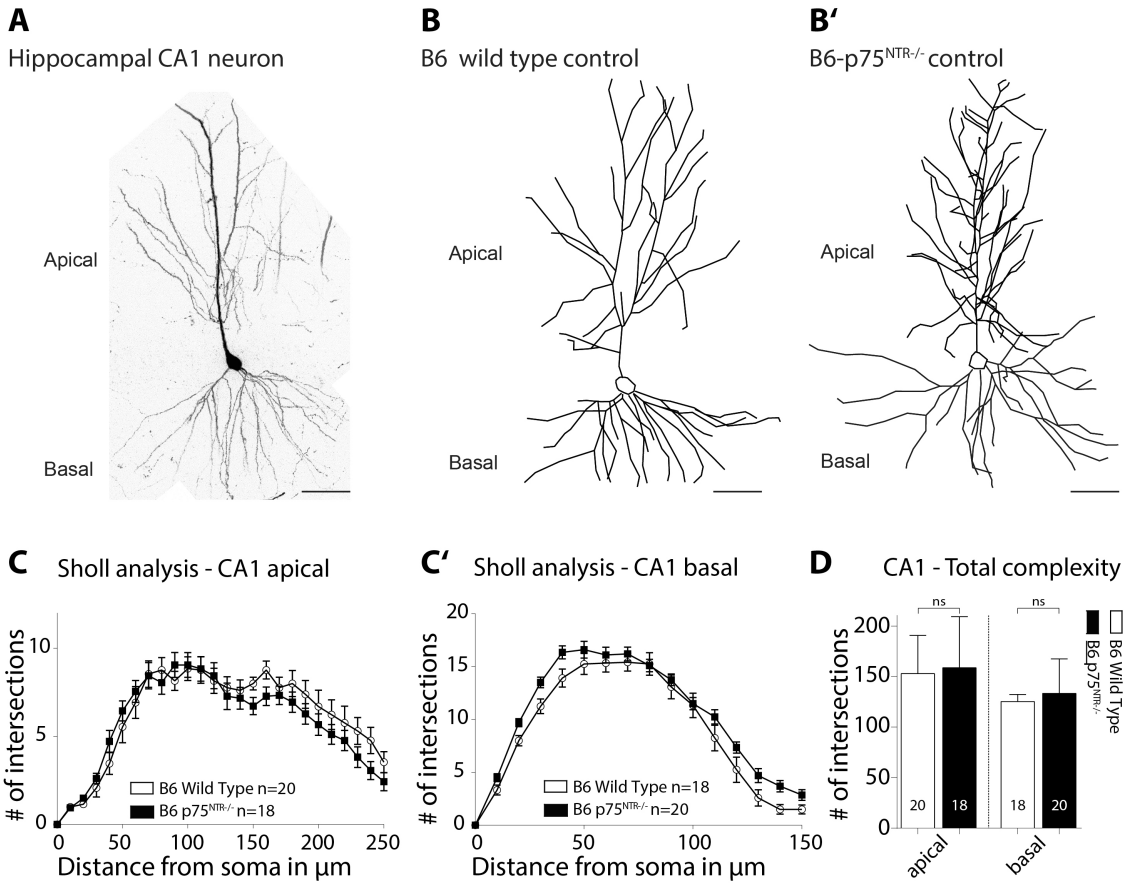

Figure 3.3: Influence of genetically deleting exon VI from the p75^{NTR} gene in B6 mice on dendritic complexity of hippocampal CA1 pyramidal neurons - (A) Example of a hippocampal CA1 neuron (Thy1-eGFP), scale bar is 100 µm **(B, B')** Exemplified morphology of hippocampal CA1 pyramidal neurons of B6 control and B6-p75$^{NTR-/-}$ control conditions, scale bar is 100 µm **(C, C')** Dendritic complexity of hippocampal CA1 pyramidal neurons (apical and basal tree) **(D)** Total complexity of hippocampal CA1 pyramidal neurons apical and basal dendrites. Data presented as mean ± SEM. * = $p < 0.05$, student's *t*-test. The n represents the number of cells analyzed, at least 3 animals per condition were used.

ko mice.

Figure 3.4 shows how chronic *T. gondii* infection effects apical dendritic spine densities of hippocampal pyramidal CA1 neurons in B6 wt and B6-p75^{NTR} ko mice. Figure 3.4 A shows representative confocal microscopic images of apical CA1 neuron dendrites in control, 4 w *T. gondii* infected and 8 w *T. gondii* infected B6 wt mice. Neurons are visualized by eGFP, which is expressed under the *Thy1* promoter (c.f. section 2.5.2). Figure 3.4 B shows representative confocal microscopic images of apical CA1 neuron dendrites in control, 4 w *T. gondii* infected and 8 w *T. gondii* infected B6-p75^{NTR} ko mice. Neurons are visualized by eGFP, which is expressed

under the *Thy1* promoter (c.f. section 2.5.2). Figure 3.4 C shows that 4 w *T. gondii* infected B6 wt mice have significantly less dendritic spines in CA1 apical neuron than the control B6 wt mice. Also, 8 w *T. gondii* infected B6 wt mice have significantly less dendritic spines in CA1 apical neuron than the control B6 wt mice. No significant difference in dendritic spine density between 4 w *T. gondii* infected *versus* 8 w *T. gondii* infected B6 wt mice can be observed. Figure 3.4 D shows that 4 w *T. gondii* infected B6-p75^{NTR} ko mice do not show significant differences in dendritic spine density in CA1 apical neurons than in the control B6-p75^{NTR} ko mice, but 8 w *T. gondii* infected B6-p75^{NTR} ko mice have significantly less dendritic spines in CA1 apical neuron than the control B6-p75^{NTR} ko mice. Also, significant differences in dendritic spine density between 4 w *T. gondii* infected *versus* 8 w *T. gondii* infected B6-p75^{NTR} ko mice can be observed. Descriptive statistics for fig. 3.4 are listed in table 3.4.

Table 3.4: Descriptive statistics for dendritic spine densities of apical CA1 dendrites in B6 wt and B6-p75^{NTR} ko mice (fig. 3.4)

Genotype	CNS area	*T. gondii*	Mean±SEM
B6 WT	CA1 apical	-	2.221±0.2027 spines per µm
B6 WT	CA1 apical	4 w	1.9±0.1287 spines per µm
B6 WT	CA1 apical	8 w	1.724±0.1304 spines per µm
B6-p75$^{NTR-/-}$	CA1 apical	-	2.324±0.2226 spines per µm
B6-p75$^{NTR-/-}$	CA1 apical	4 w	2.15±0.11066 spines per µm
B6-p75$^{NTR-/-}$	CA1 apical	8 w	1.664±0.2624 spines per µm

Figure 3.5 shows how chronic *T. gondii* infection effects basal dendritic spine densities of hippocampal pyramidal CA1 neurons in B6 wt and B6-p75^{NTR} ko mice. Figure 3.5 A shows representative confocal microscopic images of basal CA1 neuron dendrites in control, 4 w *T. gondii* infected and 8 w *T. gondii* infected B6 wt mice. Neurons are visualized by eGFP, which is expressed under the *Thy1* promoter (c.f. section 2.5.2). Figure 3.5 B shows representative confocal microscopic images of basal CA1 neuron dendrites in control, 4 w *T. gondii* infected and 8 w *T. gondii* infected B6-p75^{NTR} ko mice. Neurons are visualized by eGFP, which is expressed under the *Thy1* promoter (c.f. section 2.5.2). Figure 3.5 C shows that 4 w *T. gondii* infected B6 wt mice have significantly less dendritic spines in CA1 basal neuron than the control B6 wt mice. Also, 8 w *T. gondii* infected B6 wt mice have significantly less dendritic spines in CA1 apical neuron than the control B6 wt mice. No significant difference in dendritic spine density between 4 w *T. gondii* infected

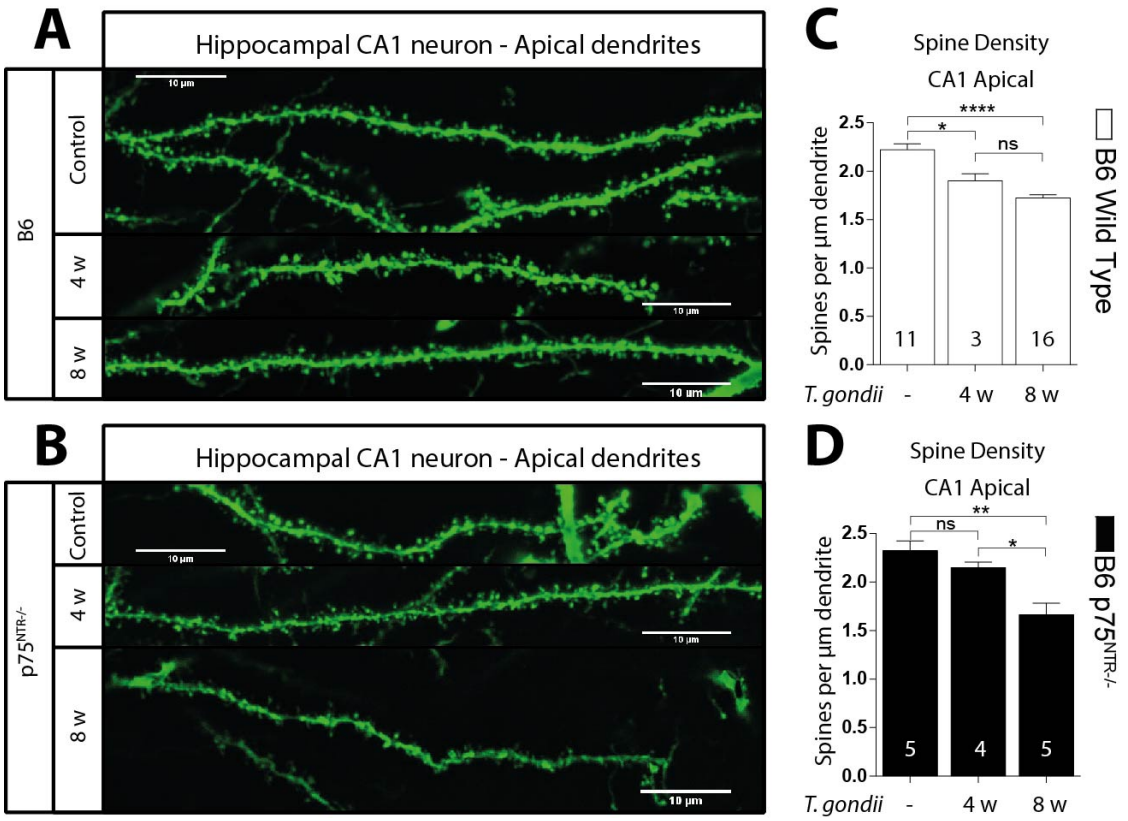

Figure 3.4: Dendritic spine density in apical dendrites of hippocampal CA1 neurons in B6 wt and p75$^{NTR-/-}$ mice 4 w and 8 w chronically infected with *Toxoplasma gondii* (A, B) Representative confocal microscopic images of apical dendrites of pyramidal CA1 neurons in B6 wt and B5-p75$^{NTR-/-}$ mice; control, 4 w and 8 w infected with *T. gondii*. Scale bar is 10 µm **C, D** Evaluation of dendritic spine density of apical dendrites of pyramidal CA1 neurons in B6 wt and B6-p75$^{NTR-/-}$ mice; control, 4 w and 8 w infected with *T. gondii*. Data presented as mean ± SEM, p****<0.0001; p***<0.001; p**<0.01; p*<0.05

versus 8 w *T. gondii* infected B6 wt mice can be observed. Figure 3.5 D shows that 4 w *T. gondii* infected B6-p75^{NTR} ko mice do not show significant differences in dendritic spine density in CA1 apical neurons than in the control B6-p75^{NTR} ko mice, but 8 w *T. gondii* infected B6-p75^{NTR} ko mice have significantly less dendritic spines in CA1 apical neuron than the control B6-p75^{NTR} ko mice. Also, significant differences in dendritic spine density between 4 w *T. gondii* infected *versus* 8 w *T. gondii* infected B6-p75^{NTR} ko mice can be observed. Descriptive statistics for fig. 3.5 are listed in table 3.5.

Figure 3.6 shows how chronic *T. gondii* infection effects apical dendritic spine densities of pyramidal cortex LV/VI neurons in B6 wt and B6-p75^{NTR} ko mice. Figure 3.6 A shows representative confocal microscopic images of cortex LV/VI

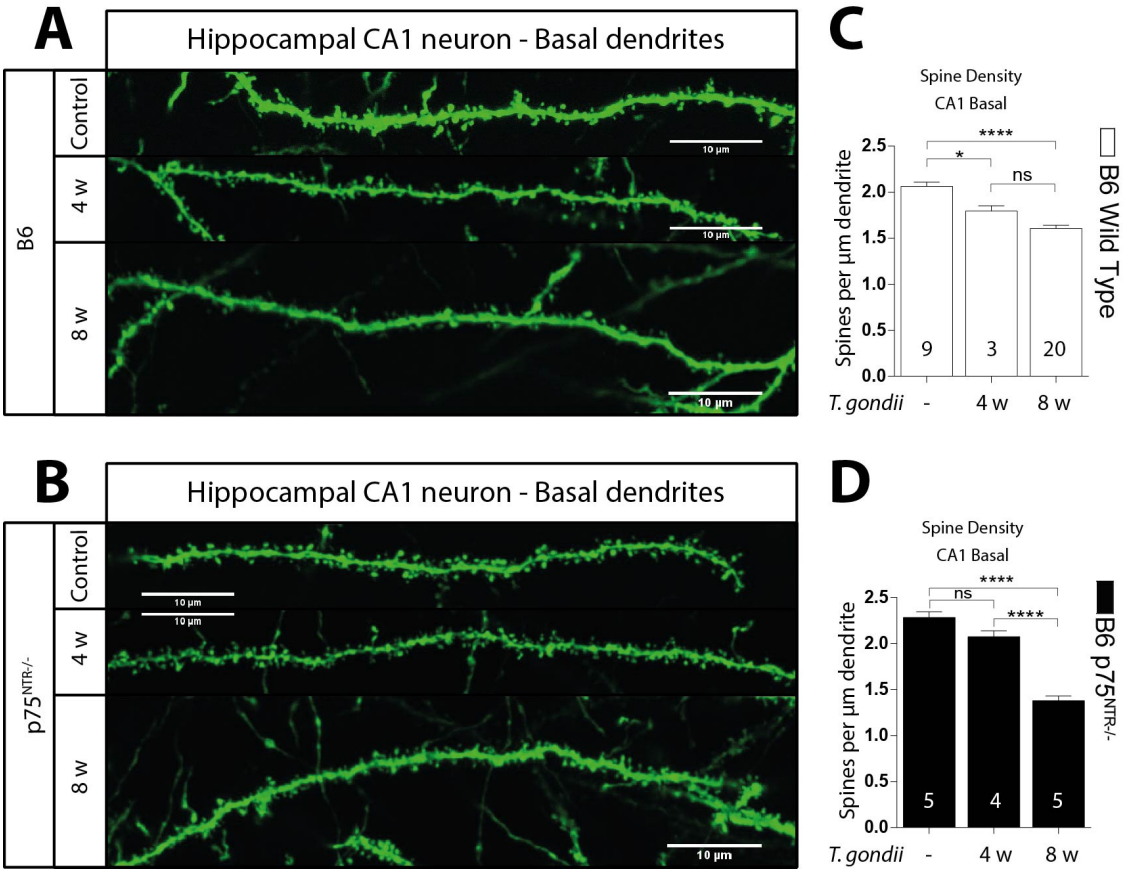

Figure 3.5: Dendritic spine density in basal dendrites of hippocampal CA1 neurons in B6 wt and p75$^{NTR-/-}$ mice 4 w and 8 w chronically infected with *Toxoplasma gondii* (A, B) Representative confocal microscopic images of basal dendrites of pyramidal CA1 neurons in B6 wt and B5-p75$^{NTR-/-}$ mice; control, 4 w and 8 w infected with *T. gondii*. Scale bar is 10 µm **C, D** Evaluation of dendritic spine density of basal dendrites of pyramidal CA1 neurons in B6 wt and B6-p75$^{NTR-/-}$ mice; control, 4 w and 8 w infected with *T. gondii*. Data presented as mean ± SEM, p****<0.0001; p***<0.001; p**<0.01; p*<0.05

neuron dendrites in control, 4 w *T. gondii* infected and 8 w *T. gondii* infected B6 wt mice. Neurons are visualized by eGFP, which is expressed under the *Thy1* promoter (c.f. section 2.5.2). Figure 3.6 B shows representative confocal microscopic images of cortex LV/VI neuron dendrites in control, 4 w *T. gondii* infected and 8 w *T. gondii* infected B6-p75^{NTR} ko mice. Neurons are visualized by eGFP, which is expressed under the *Thy1* promoter (c.f. section 2.5.2). Figure 3.6 C shows that 4 w *T. gondii* infected B6 wt mice have significantly less dendritic spines in cortex LV/VI neurons than the control B6 wt mice. Also, 8 w *T. gondii* infected B6 wt mice have significantly less dendritic spines in CA1 apical neuron than the control B6 wt mice. Additionally significant difference in dendritic spine density between

Table 3.5: Descriptive statistics for dendritic spine densities of basal CA1 dendrites in B6 wt and B6-p75^{NTR} ko mice (fig. 3.5)

Genotype	CNS area	*T. gondii*	Mean±SEM
B6 WT	CA1 basal	-	2.063±0.139 spines per µm
B6 WT	CA1 basal	4 w	1.931±0.159 spines per µm
B6 WT	CA1 basal	8 w	1.608±0.1571 spines per µm
B6-p75$^{NTR-/-}$	CA1 basal	-	2.283±0.1398 spines per µm
B6-p75$^{NTR-/-}$	CA1 basal	4 w	2.075±0.1289 spines per µm
B6-p75$^{NTR-/-}$	CA1 basal	8 w	1.379±0.1158 spines per µm

4 w *T. gondii* infected *versus* 8 w *T. gondii* infected B6 wt mice can be observed. Figure 3.6 D shows that 4 w *T. gondii* infected B6-p75^{NTR} ko mice have significantly less dendritic spines in cortex LV/VI neurons than the control B6-p75^{NTR} ko mice. Also, 8 w *T. gondii* infected B6-p75^{NTR} ko mice have significantly less dendritic spines in cortical apical neurons than the control B6-p75^{NTR} ko mice. Additionally significant difference in dendritic spine density between 4 w *T. gondii* infected *versus* 8 w *T. gondii* infected B6-p75^{NTR} ko mice can be observed. Descriptive statistics for fig. 3.6 are listed in table 3.6.

Table 3.6: Descriptive statistics for dendritic spine densities of apical cortex LV/VI dendrites in B6 wt and B6-p75^{NTR} ko mice (fig. 3.6)

Genotype	CNS area	*T. gondii*	Mean±SEM
B6 WT	Ctx LV/VI apical	-	1.358±0.05634 spines per µm
B6 WT	Ctx LV/VI apical	4 w	0.8851±0.02291 spines per µm
B6 WT	Ctx LV/VI apical	8 w	0.6305±0.03308 spines per µm
B6-p75$^{NTR-/-}$	Ctx LV/VI apical	-	1.6±0.07363 spines per µm
B6-p75$^{NTR-/-}$	Ctx LV/VI apical	4 w	1.198±0.08685 spines per µm
B6-p75$^{NTR-/-}$	Ctx LV/VI apical	8 w	0.5258 ±0.05506 spines per µm

Figure 3.7 shows how chronic *T. gondii* infection effects basal dendritic spine densities of pyramidal cortex LV/VI neurons in B6 wt and B6-p75^{NTR} ko mice. Figure 3.7 A shows representative confocal microscopic images of cortex LV/VI neuron dendrites in control, 4 w *T. gondii* and 8 w *T. gondii* B6 wt mice. Neurons are visualized by eGFP, which is expressed under the *Thy1* promoter (c.f. section 2.5.2). Figure 3.7 B shows representative confocal microscopic images of cortex LV/VI neuron dendrites in control, 4 w *T. gondii* and 8 w *T. gondii* B6-p75^{NTR} ko mice. Neurons are visualized by eGFP, which is expressed under the

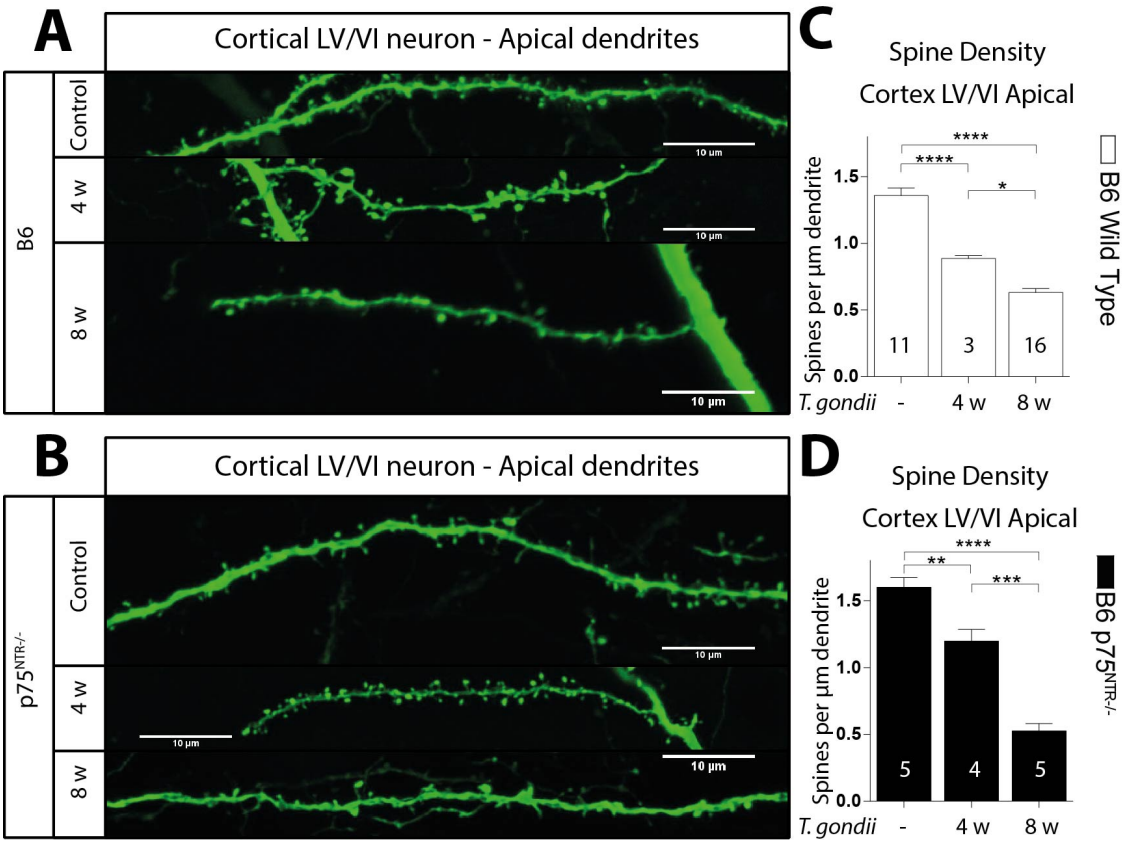

Figure 3.6: Dendritic spine density in apical dendrites of pyramidal LV/VI neurons of the cortex in B6 wt and p75$^{NTR-/-}$ mice 4 w and 8 w chronically infected with *Toxoplasma gondii* (A, B) Representative confocal microscopic images of apical dendrites of cortex LV/VI neurons in B6 wt and B5-p75$^{NTR-/-}$ mice; control, 4 w and 8 w infected with *T. gondii*. Scale bar is 10 µm **C, D** Evaluation of dendritic spine density of apical dendrites of pyramidal LV/VI neurons of the cortex in B6 wt and B6-p75$^{NTR-/-}$ mice; control, 4 w and 8 w infected with *T. gondii*. Data presented as mean ± SEM, p****<0.0001; p***<0.001; p**<0.01; p*<0.05

Thy1 promoter (c.f. section 2.5.2). Figure 3.7 C shows that 4 w *T. gondii* infected B6 wt mice have significantly less dendritic spines in cortex LV/VI neurons than the control B6 wt mice. Also, 8 w *T. gondii* infected B6 wt mice have significantly less dendritic spines in CA1 apical neuron than the control B6 wt mice. No significant difference in dendritic spine density between 4 w *T. gondii* infected *versus* 8 w *T. gondii* infected B6 wt mice can be observed. Figure 3.7 D shows that 4 w *T. gondii* infected B6-p75^{NTR} ko mice do not have significantly altered dendritic spine numbers in cortical LV/VI neurons than the control B6-p75^{NTR} ko mice. The 8 w *T. gondii* infected B6-p75^{NTR} ko mice have significantly less dendritic spines in cortical LV/VI neurons than the control B6-p75^{NTR} ko mice. Additionally significant difference in dendritic spine density between 4 w *T. gondii* infected *versus*

8 w *T. gondii* infected B6-p75^{NTR} ko mice can be observed. Descriptive statistics for fig. 3.7 are listed in table 3.7.

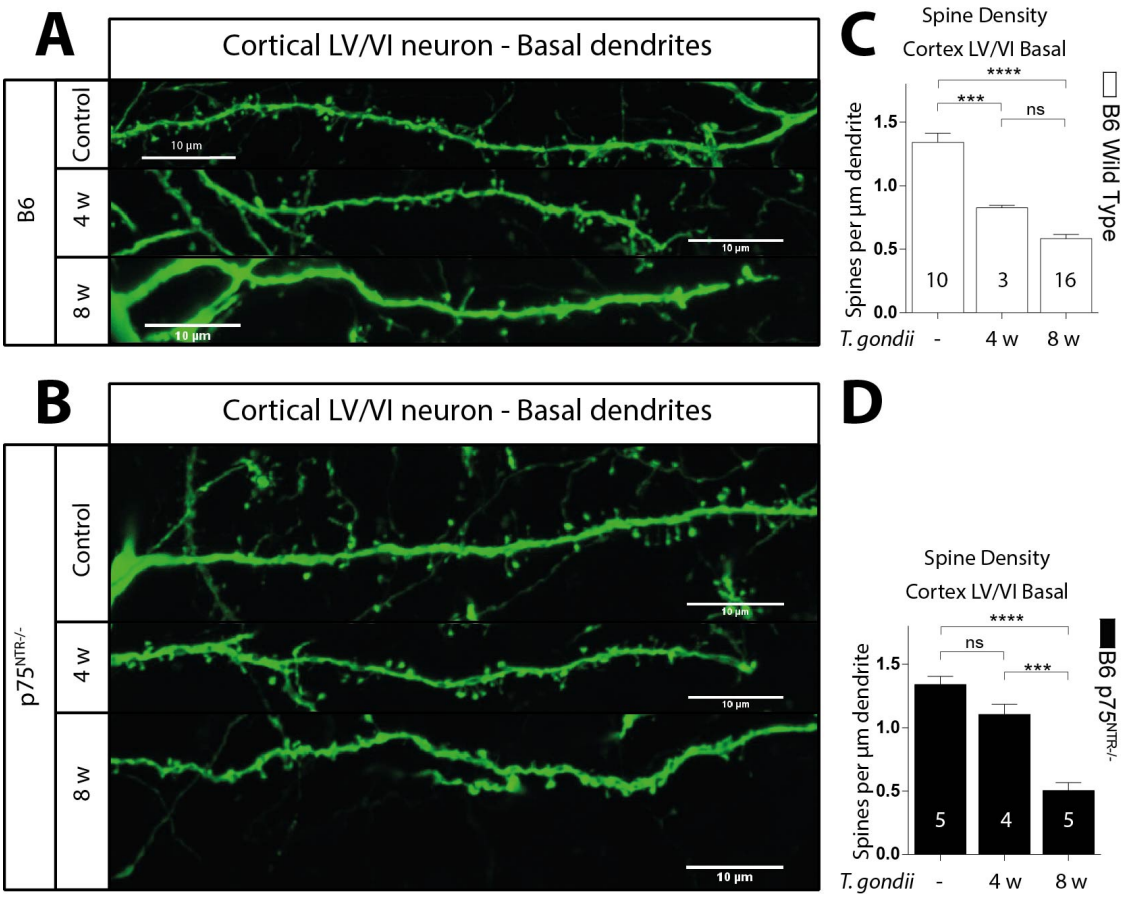

Figure 3.7: Dendritic spine density in basal dendrites of pyramidal LV/VI neurons of the cortex in B6 wt and p75$^{NTR-/-}$ mice 4 w and 8 w chronically infected with *Toxoplasma gondii* (A, B) Representative confocal microscopic images of basal dendrites of cortex LV/VI neurons in B6 wt and B5-p75$^{NTR-/-}$ mice; control, 4 w and 8 w infected with *T. gondii*. Scale bar is 10 µm **C, D** Evaluation of dendritic spine density of basal dendrites of pyramidal LV/VI neurons of the cortex in B6 wt and B6-p75$^{NTR-/-}$ mice; control, 4 w and 8 w infected with *T. gondii*. Data presented as mean ± SEM, p****<0.0001; p***<0.001; p**<0.01; p*<0.05

3.1.4 p75$^{NTR-/-}$ mice show increased spine density

Genetically deleting the Exon IV in the p75^{NTR} gene has been shown to increase spine density compared to wild type controls in *in vitro* experiments (Zagrebelsky *et al.*, 2005).

Figure 3.8 shows how genetically deleting the exon IV in the p75^{NTR} gene in B6 wt mice effects the dendritic spine density of hippocampal pyramidal CA1 neurons.

Table 3.7: Descriptive statistics for dendritic spine densities of basal cortex LV/VI dendrites in B6 wt and B6-p75^{NTR} ko mice (fig. 3.7)

Genotype	CNS area	*T. gondii*	Mean±SEM
B6 WT	Ctx LV/VI basal	-	1.358±0.05634 spines per µm
B6 WT	Ctx LV/VI basal	4 w	0.8851±0.02291 spines per µm
B6 WT	Ctx LV/VI basal	8 w	0.6305±0.03308 spines per µm
B6-p75$^{NTR-/-}$	Ctx LV/VI basal	-	1.6±0.07363 spines per µm
B6-p75$^{NTR-/-}$	Ctx LV/VI basal	4 w	1.198±0.08685 spines per µm
B6-p75$^{NTR-/-}$	Ctx LV/VI basal	8 w	0.5258 ±0.05506 spines per µm

Figure 3.8 A shows representative confocal microscopic images of apical dendrites of hippocampal CA1 neurons pf B6 wt and B6-p75^{NTR} ko mice (c.f. section 2.5.2). Figure 3.8 A' shows that there is no significant difference in spine density between the B6 wt and the B6-p75^{NTR} ko mice in apical dendrites of hippocampal CA1 neurons. Figure 3.8 B shows representative confocal microscopic images of basal dendrites of hippocampal CA1 neurons pf B6 wt and B6-p75^{NTR} ko mice. Figure 3.8 B' shows that there are significantly less spines on basal CA1 dendrites of B6 wt than of B6-p75^{NTR} ko mice. Descriptive statistics of fig. 3.8 are listed in table 3.8.

Table 3.8: Descriptive statistics for dendritic spine densities of apical and basal CA1 dendrites in B6 wt and B6-p75^{NTR} ko mice (fig. 3.8)

Genotype	CNS area	*T. gondii*	Mean±SEM
B6 WT	CA1 apical	-	2.221±0.006112 spines per µm
B6-p75$^{NTR-/-}$	CA1 apical	-	2.324±0.09957 spines per µm
B6 WT	CA1 basal	-	2.063±0.04633 spines per µm
B6-p75$^{NTR-/-}$	CA1 basal	-	2.283±0.06251 spines per µm

Figure 3.9 shows how genetically deleting the exon IV in the p75^{NTR} gene in B6 wt mice effects the dendritic spine density of cortical LV/VI pyramidal neurons. Figure 3.9 A shows representative confocal microscopic images of apical dendrites of cortical LV/VI pyramidal neurons pf B6 wt and B6-p75^{NTR} ko mice (c.f. section 2.5.2). Figure 3.9 A' shows that there is significantly higher spine spine density in the B6-p75^{NTR} ko than in the B6 wt mice in apical dendrites of cortical LV/VI pyramidal neurons. Figure 3.9 B shows representative confocal microscopic images of basal dendrites of cortical LV/VI pyramidal neurons pf B6 wt and B6-p75^{NTR} ko mice. Figure 3.9 B' shows that there is no significant difference in spine density on basal cortex LV/VI dendrites between B6 wt and B6-p75^{NTR} ko mice. Descriptive

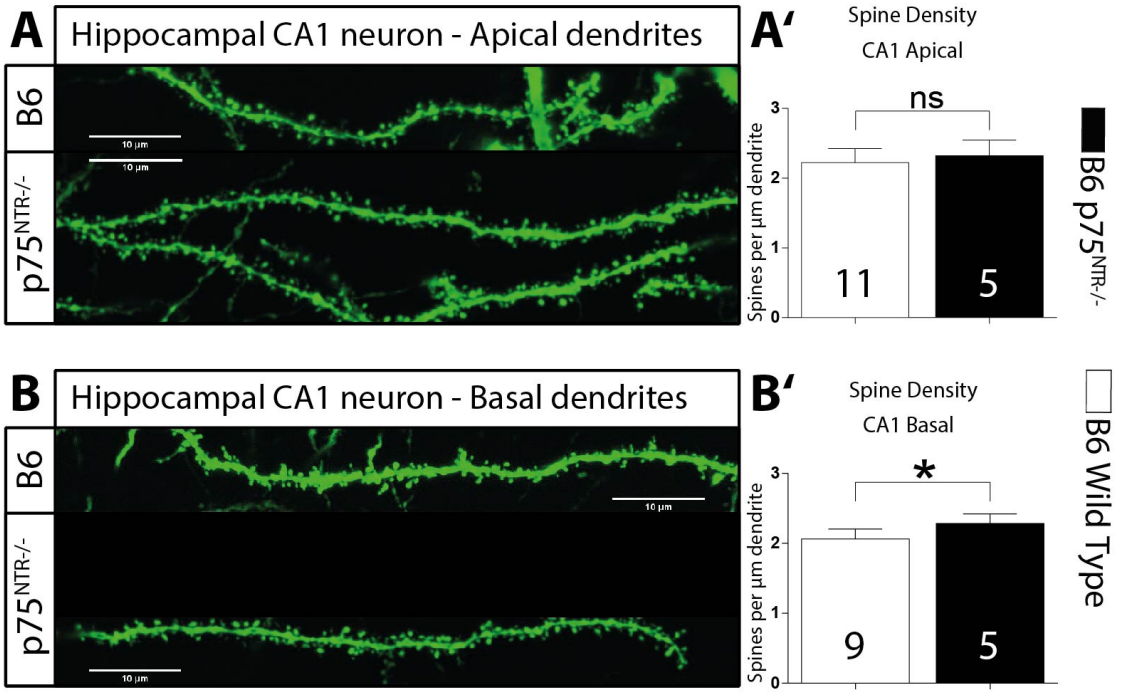

Figure 3.8: Spine density in apical and basal dendrites of hippocampal CA1 neurons in B6 wild type and p75$^{NTR-/-}$ mice – (A, A', B, B') Representative confocal microscopic images and evaluation of spine density from CA1 pyramidal neurons. Scale bar is 10 µm. Data presented as mean ± SEM, p*<0.05.

statistics of fig. 3.9 are listed in table 3.9.

Table 3.9: Descriptive statistics for dendritic spine densities of apical and basal cortex LV/VI dendrites in B6 wt and B6-p75^{NTR} ko mice (fig. 3.9)

Genotype	CNS area	*T. gondii*	Mean±SEM
B6 WT	Ctx LV/VI apical	-	1.358±0.05634 spines per µm
B6-p75$^{NTR-/-}$	Ctx LV/VI apical	-	1.6±0.07363 spines per µm
B6 WT	Ctx LV/VI basal	-	1.342±0.07196 spines per µm
B6-p75$^{NTR-/-}$	Ctx LV/VI basal	-	1.342±0.07196 spines per µm

3.1.5 The number of dendritic spines in BALB/c mice are mostly unchanged upon *T. gondii* infection

Strong challenge to the immune system is usually accompanied by quantifiable weight loss in mice. Silva *et al.* showed before that chronic toxoplasmosis takes a greater toll on B6 mice than on BALB/c mice by inflicting stronger neuroinflammation (2010). Figure 3.10 shows significant loss in weight for B6 mice (wt and

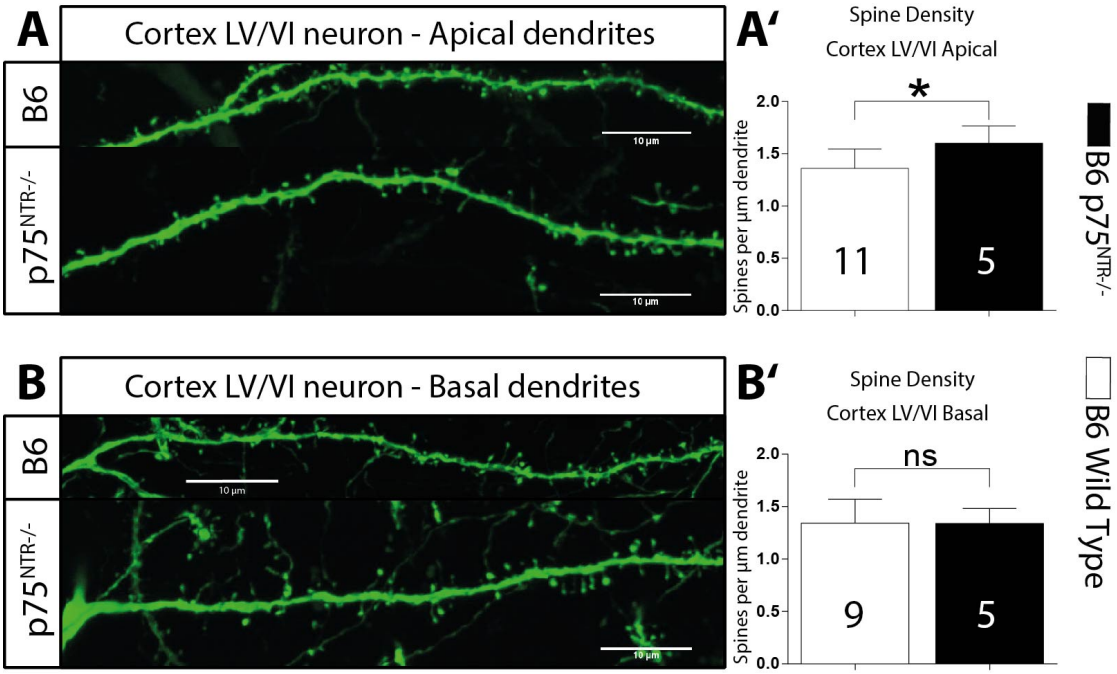

Figure 3.9: Spine density in apical and basal dendrites of cortical layer V/VI pyramidal neurons in B6 wild type and p75$^{NTR-/-}$ mice – (A, A', B, B') Representative confocal microscopic images and evaluation of spine density from cortex LV/VI neurons. Scale bar is 10 µm. Data presented as mean ± SEM, p*<0.05.

p75^{NTR} ko). BALB/c mice did not significantly lose weight. Descriptive statistics for fig. 3.10 are listed in table 3.10.

In this context it was of interest whether dendritic morphology in BALB/c mice is also less affected by *T. gondii* infection than B6 wt mice. BALB/c neurons have been vizualized with a diolistic approach.

Figure 3.11 shows the effect of chronic *T. gondii* infection on dendritic spine density of apical and basal dendrites in hippocampal CA1 neurons. Figure 3.11 A and B show representative confocal microscopic images of apical and basal CA1 neuron dendrites control and 8 w *T. gondii* infected BALB/c wt mice. Figure 3.11 A' shows that there is no significant difference in dendritic spine density of CA1 apical neurons in 8 w *T. gondii* infected BALB/c wt mice compared to the BALB/c wt controls. Figure 3.11 B' shows a significant decrease in dendritic spines of CA1 basal neurons in 8 w *T. gondii* BALB/c wt mice compared to the BALB/c wt controls. Descriptive statistics for fig. 3.11 are listed in table 3.11.

Figure 3.12 shows the effect of chronic *T. gondii* infection on dendritic spine density of apical and basal dendrites in cortical LV/VI neurons. Figure 3.12 A and B show representative confocal microscopic images of apical and basal cortex

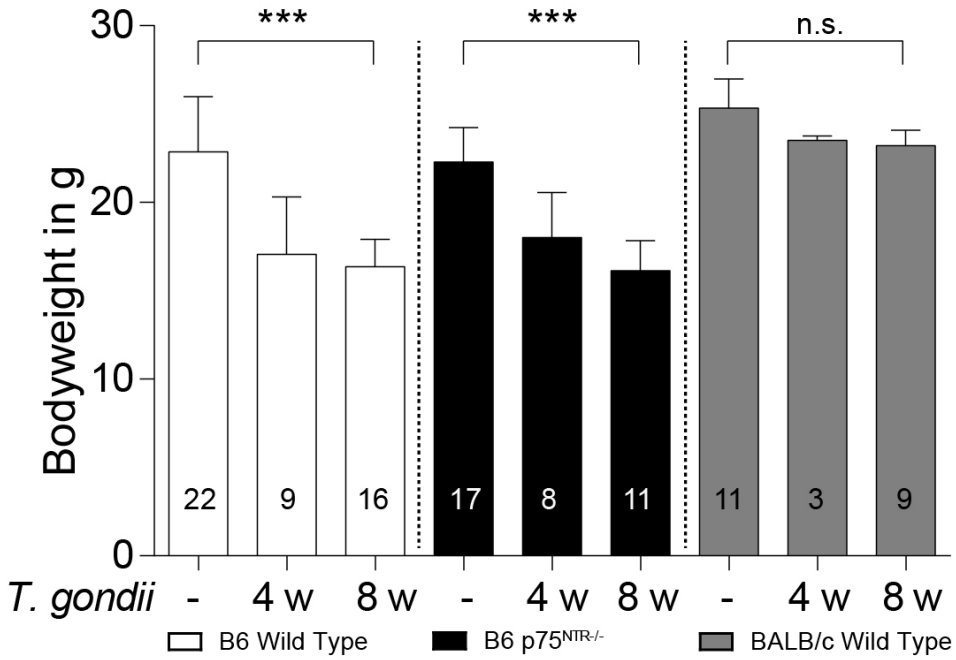

Figure 3.10: Bodyweight upon *T. gondii* infection in B6 and BALB/c mice four and eight weeks post infection - Bodyweight at $\sim$ 17 w of age of control mice, 4 w incubated and 8 w incubated B6 (wild type and p75$^{NTR-/-}$) and BALB/c mice. Data presented as mean $\pm$ SEM. *** = $p < 0.001$. One-way ANOVA, Fisher's LSD test

LV/VI neuron dendrites control and 8 w *T. gondii* infected BALB/c wt mice. Figure 3.12 A' and B' show that there is no significant difference in dendritic spine density of basal and apical dendrites in cortical LV/VI pyramidal neurons in 8 w *T. gondii* infected BALB/c wt mice compared to the BALB/c wt controls. Descriptive statistics for fig. 3.12 are listed in table 3.12.

3.2 Microglial activation upon *T. gondii* infection

Immunological response to *T. gondii* infection has been in the focus of research for many decades. While the characteristics of an infection on monocyte recruitment and monocyte marker distribution are described well, the underlying signaling mechanisms are not fully understood yet. Therefore, it was of a major interest do study microglial reaction to *T. gondii* infection in p75$^{NTR-/-}$ mice.

This work contributes to existing knowledge by adding novel morphological information. Additionally the microglia concentration within the brain was analyzed by determining the number of Iba1 positive (Iba1+) cells in the hippocampus as

Table 3.10: Descriptive statistics for bodyweight upon *T. gondii* infection B6 wt, B6-p75^{NTR} ko and BALB/c wt mice (fig. 3.10).

Genotype	*T. gondii*	Mean±SEM
B6 WT	-	22.87 g ± 3.12 g
B6 WT	4 w	17.07 g ±3.243 g
B6 WT	8 w	16.37 g ±1.540 g
B6-p75$^{NTR-/-}$	-	22.30 g ±1.933 g
B6-p75$^{NTR-/-}$	4 w	18.01 g ± 2.547 g
B6-p75$^{NTR-/-}$	8 w	16.13 g ±1.717 g
BALB/c	-	25.16 g ±1.516 g
BALB/c	4 w	23.50 g ± 0.2646 g
BALB/c	8 w	23.42 g ± 0.908 g

Table 3.11: Descriptive statistics for dendritic spine densities of apical cortex LV/VI dendrites in B6 wt and B6-p75^{NTR} ko mice (fig. 3.11)

Genotype	CNS area	*T. gondii*	Mean±SEM
BALB/c	CA1 apical	-	2.233±0.08198 spines per µm
BALB/c	CA1 apical	w	1.908±0.1226 spines per µm
BALB/c	CA1 basal	-	2.162±0.02343 spines per µm
BALB/c	CA1 basal	8 w	1.805±0.071 spines per µm

Table 3.12: Descriptive statistics for dendritic spine densities of apical cortex LV/VI dendrites in B6 wt and B6-p75^{NTR} ko mice (fig. 3.12)

Genotype	CNS area	*T. gondii*	Mean±SEM
BALB/c	Ctx apical	-	1.267±0.08399 spines per µm
BALB/c	Ctx apical	w	1.262±0.2140 spines per µm
BALB/c	Ctx basal	-	1.289±0.08656 spines per µm
BALB/c	Ctx basal	8 w	1.205±0.03976 spines per µm

well as in the cortex of in PFA fixed brains, which were deep frozen in 30 µm thick transversal sections and immunolabled with an Iba1 antibody. Iba1+ cells were counted in a defined region of interest (ROI) and compared to controls. Results are shown for B6 mice (WT and p75$^{NTR-/-}$) and BALB/c mice. They were infected for 4 and 8 weeks.

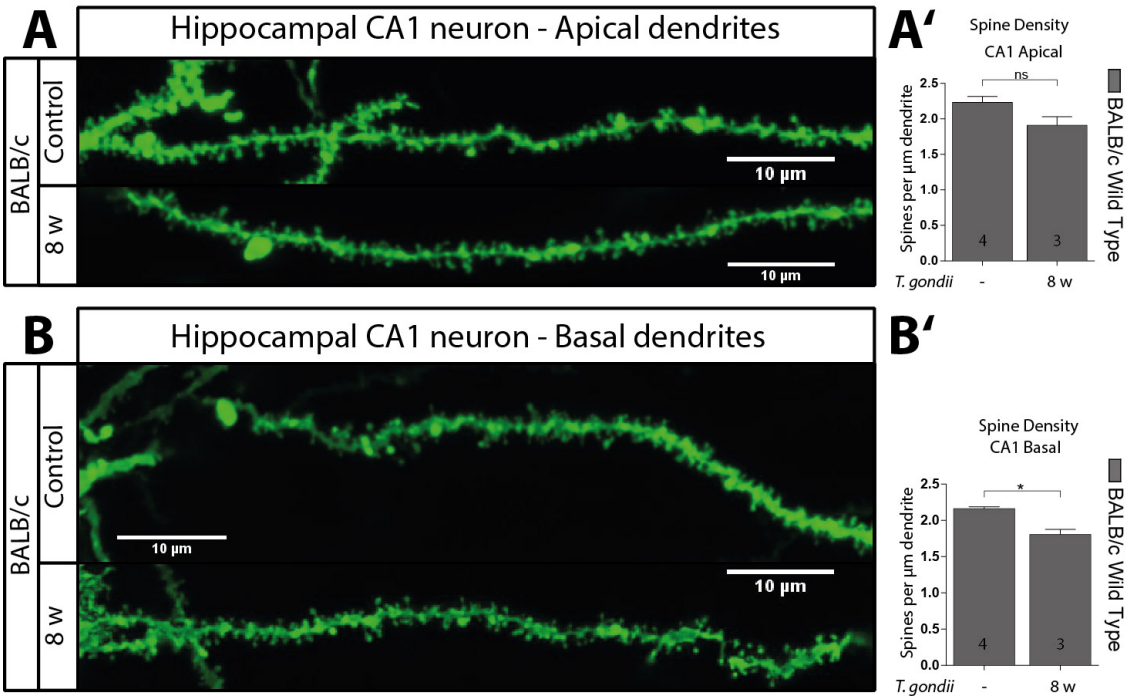

Figure 3.11: Dendritic spine density in apical and basal dendrites of hippocampal CA1 neurons in control BALB/c wt and 8 w chronically infected with *Toxoplasma gondii* (A, B) Representative confocal microscopic images of apical and basal dendrites of pyramidal CA1 neurons in control BALB/c wt and 8 w *T. gondii* infected BALB/c wt mice. Scale bar is 10 µm **A', B'** Evaluation of dendritic spine density of apical and basal dendrites of pyramidal CA1 neurons in control BALB/c wt mice and 8 w *T. gondii* infected BALB/c wt mice. Data presented as mean ± SEM, p****<0.0001; p***<0.001; p**<0.01; p*<0.05

3.2.1 Morphological changes in microglia upon *T. gondii* infection in B6 wt and B6-p75^{NTR} ko mice

Microglia cells continuously survey the CNS in a ramified morphology and, in response to injury, disease and most other CNS insults, undergo progressive morphological changes resulting in an amoeboid morphology.

Figure 3.13 shows representative confocal microscopic images of the hippocampal *stratum pyramidale* in a non-infected control B6 wt mouse. Pyramidal CA1 neurons are labeled green (*Thy1*-eGFP) while microglia and marcophages are labled red (Iba1+ cells). The upper left panel shows cell somata of the CA1 neurons are lined up in an ordered band and their primary apical neurons extend visibly from this cell band. The lower left panel shows several primary apical dendrites from CA1 neurons within the *stratum radiatum*. The upper middle panel shows the distribution of Iba1+ cells in the *stratum pyramidale* and the *stratum radiatum*.

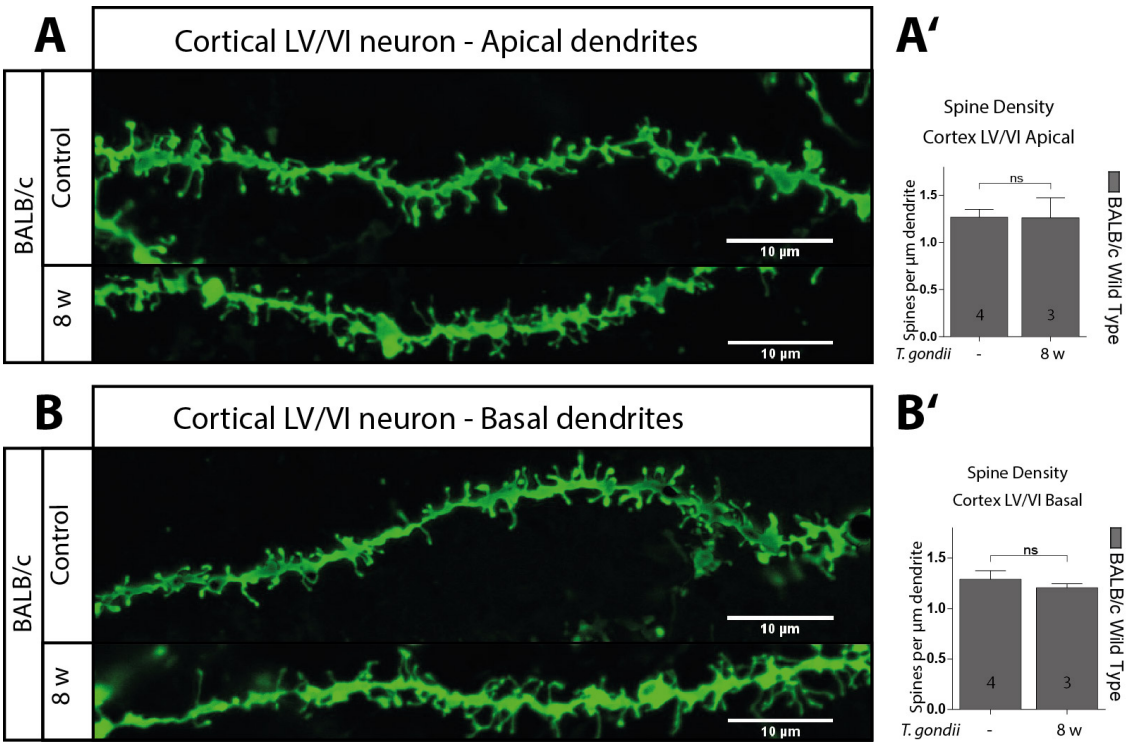

Figure 3.12: Dendritic spine density in apical and basal dendrites of cortex LV/VI neurons in control BALB/c wt and 8 w chronically infected with *Toxoplasma gondii* (A, B) Representative confocal microscopic images of apical and basal dendrites of pyramidal cortex LV/VI in control BALB/c wt and 8 w *T. gondii* infected BALB/c wt mice. Scale bar is 10 µm **A', B'** Evaluation of dendritic spine density of apical and basal dendrites of cortex LV/VI neurons in control BALB/c wt mice and 8 w *T. gondii* infected BALB/c wt mice. Data presented as mean ± SEM, p****<0.0001; p***<0.001; p**<0.01; p*<0.05

The lower middle panel shows a Iba1+ cell. A small cell body and numerous long processes stretch from the soma in every direction. The right panels show a merge of the former.

Figure 3.14 shows representative confocal microscopic images of the hippocampal *stratum pyramidale* in a 8 w *T. gondii* infected B6 wt mouse. Pyramidal CA1 neurons are labeled green (*Thy1*-eGFP) while microglia and marcophages are labled red (Iba1+ cells). The upper left panel shows cell somata of the CA1 neurons are lined up in an ordered band and their primary apical neurons extend visibly from this cell band. The lower left panel shows several primary apical dendrites from CA1 neurons within the *stratum radiatum*. The upper middle panel shows the distribution of Iba1+ cells in the *stratum pyramidale* and the *stratum radiatum*. The lower middle panel shows Iba1 staining in higher magnification. No single cells can be described in their morphology. The right panels show a merge of the former.

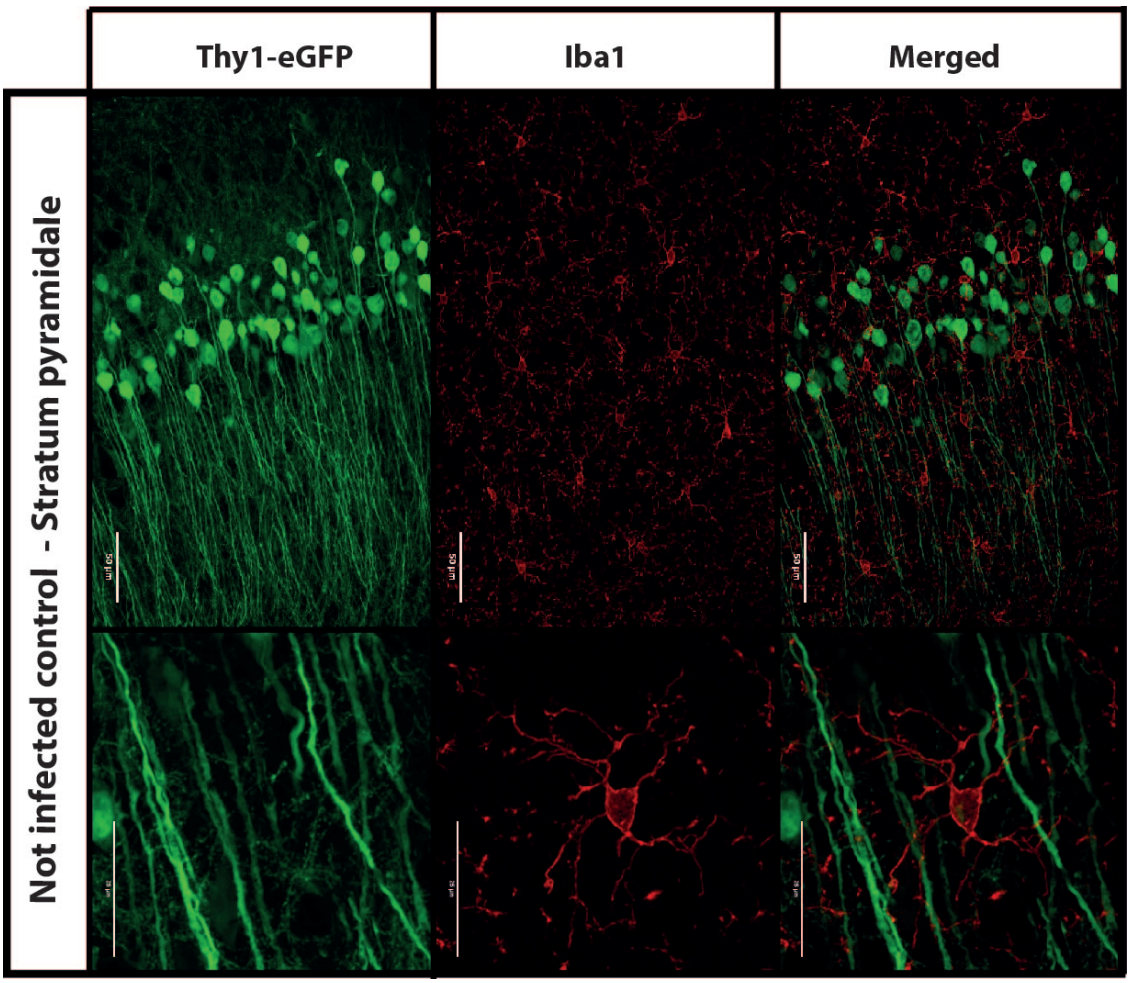

Figure 3.13: Maximum intensity projection of *Thy1*-eGFP labeled neurons and staining of microglia/macrophages in the stratum pyramidale of the CA1 area with primary antibodies against ionized calcium-binding adapter molecule 1 (Iba1) respectively in control animals not infected with *T. gondii*, scale bar in the large frame is 50 µm, smaller detail 25 µm.

This overlay shows a association of Iba1+ cells and CA1 neurons. This is observed in further detail in fig. 3.16.

Figure 3.16 shows representative confocal microscopic images of the hippocampal *stratum pyramidale* in control and 8 w *T. gondii* infected B6 wt mice. Pyramidal CA1 neurons are labeled green (*Thy1*-eGFP) while microglia and marcophages are labled red (Iba1+ cells). Figure 3.16 A shows a Iba1+ cell in red and CA1 neurons in green (*Thy1*-eGFP) of a control B6 wt mouse. Figure 3.16 B shows Iba1+ staining of a blood vessel in the hippocampus of a 8 w *T. gondii* infected B6 wt mouse. The blood vessel is completely covered. Figure 3.16 B' and B" show a close association of Iba1 staining with CA1 neurons in the hippocampus of *T. gondii*

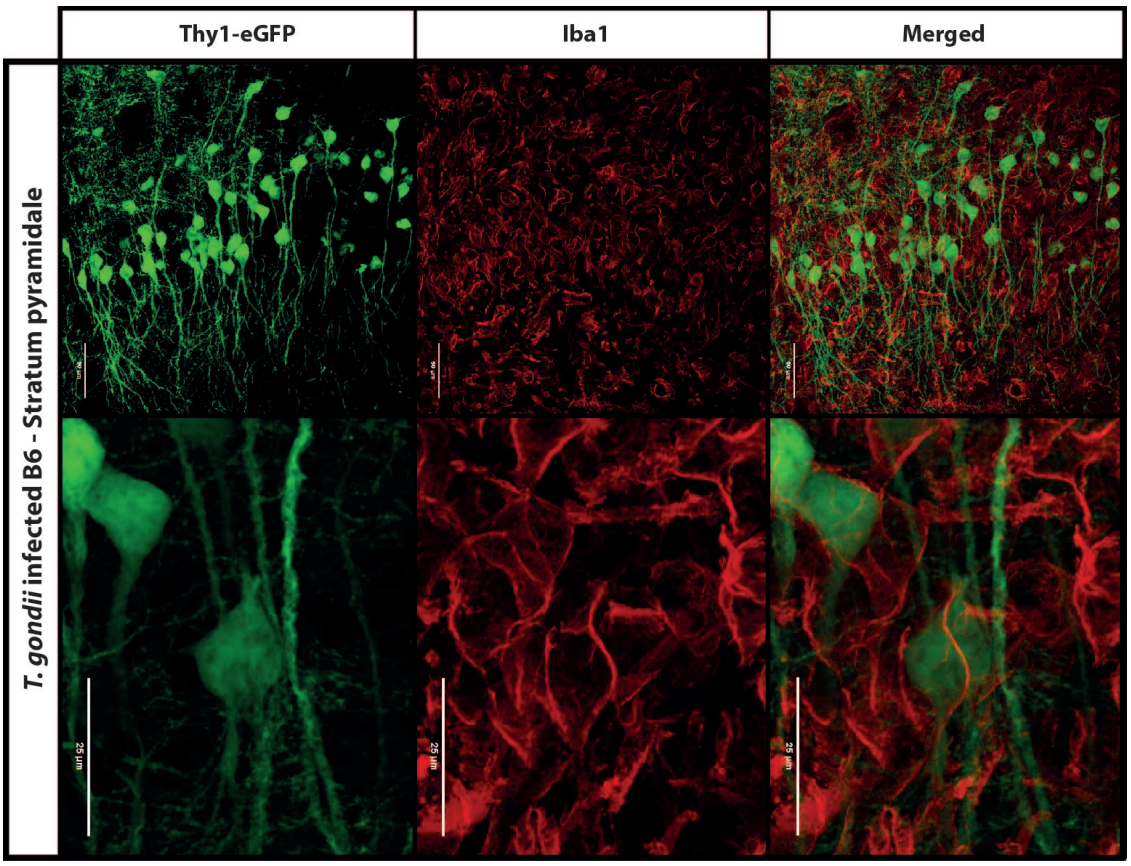

Figure 3.14: Maximum intensity projection of *Thy1*-eGFP labeled neurons and staining of microglia/macrophages in the stratum pyramidale of the CA1 area with primary antibodies against ionized calcium-binding adapter molecule 1 (Iba1) respectively in *T. gondii* infected B6 mice, scale bar in upper frame is 50 µm, in detail frame it is 25 µm.

infected B6 wt mice. Pyramidal cell somata are coated by Iba1 as well as primary apical dendrites.

Figure 3.15 shows that a similar picture as with the Iba1 staining can be observed with a F4/80 staining in *T. gondii* infected B6 wt mice.

3.2.1.1 Morphological changes in microglia upon *T. gondii* infection in BALB/c wt mice

Figure 3.17 shows representative confocal microscopic images of the hippocampal *stratum pyramidale* in a 8 w *T. gondii* infected BALB/c wt mouse. Microglia and marcophages are labled red (Iba1+ cells). The left panel shows an overview about microglial distribution in the hippocampal CA1 neurons. The right panel shows a microglia cell in detail. A big cell body is covered by numerous spiky processes.

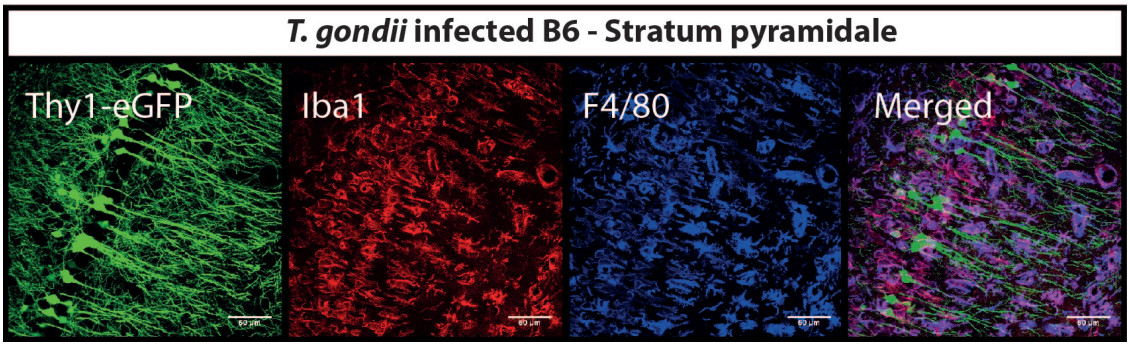

Figure 3.15: Maximum intensity projection of *Thy1*-eGFP labeled neurons and staining of microglia/macrophages in the stratum pyramidale of the CA1 area with primary antibodies against ionized calcium-binding adapter molecule 1 (Iba1) and EGF-like module-containing mucin-like hormone receptor-like 1 (F4/80) respectively in *T. gondii* infected B6 mice, scale bar is 50 µm.

3.2.2 The density of microglial cells increases upon *T. gondii* infection

T. gondii infection is widely known to induce microglia activation and monocyte recruitment (Dunay and Sibley, 2010). Most publications rely on fluorescence-activated cell sorting (FACS). To gain further morphological insight (cf. section 3.2.1) the brains of *T. gondii* infected mice were immunohistochemically stained with an Iba1 antibody. After receiving images via fluorescence microscopy I manually counted the Iba+ cells.

Figure 3.18 shows how chronic *T. gondii* infection effects microglia/macrophage numbers within the *stratum pyramidale* of the hippocampus in B6 wt and B6-p75^{NTR} ko mice. Figure 3.18 A indicates the distribution of Iba1+ cells within the hippocampal *stratum pyramidale* in B6 wt mice, control, 4 w and 8 w infected with *T. gondii*. Figure 3.18 A' shows that the total number of Iba1+ cells in the *stratum pyramidale* is significantly increased in *T. gondii* infected B6 wt mice compared to the controls. There is no statistical difference between 4 w and 8 w *T. gondii* infected mice. Figure 3.18 B indicates the distribution of Iba1+ cells within the hippocampal *stratum pyramidale* in B6-p75^{NTR} ko mice, control, 4 w and 8 w infected with *T. gondii*. Figure 3.18 B' shows that the total number of Iba1+ cells in the *stratum pyramidale* is significantly increased in *T. gondii* infected B6 wt mice compared to the controls. There is no statistical difference between 4 w and 8 w *T. gondii* infected mice. Descriptive statistics for fig. 3.18 are listed in table 3.13.

Figure 3.19 shows how chronic *T. gondii* infection effects microglia/macrophage

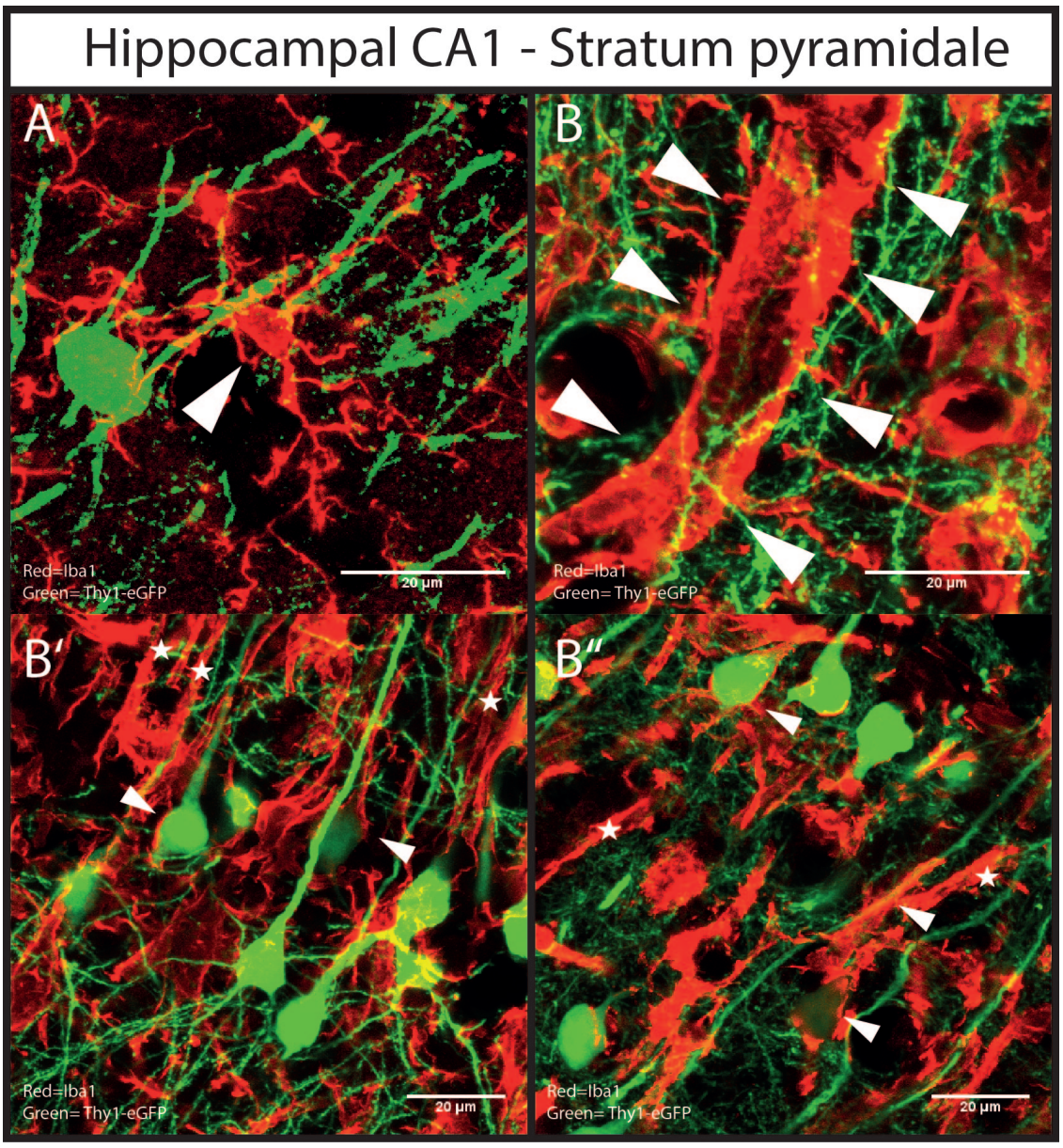

Figure 3.16: Maximum intensity projection of *Thy1*-eGFP labeled neurons and staining of microglia/macrophages in the stratum pyramidale of the CA1 area with primary antibodies against ionized calcium-binding adapter molecule 1 (Iba1) respectively in *T. gondii* infected B6 mice - (A) Healthy control B6 animal. Arrowhead indicates microglia cell, scale bar is 20 µm **(B)** *T. gondii* infected B6 mouse. Arrowheads point to microglia coating blood vessel, scale bar is 20 µm **(B', B'')** *T. gondii* infected B6 mouse. Arrowheads indicate microglia coating CA1 pyramidal neuron soma coating. Asterisks indicate CA1 pyramidal neuron apical dendrite coating, scale bar is 20 µm

numbers within the cortex in B6 wt and B6-p75^{NTR} ko mice. Figure 3.19 A indicates the distribution of Iba1+ cells within the cortex in B6 wt mice, control, 4 w and 8 w

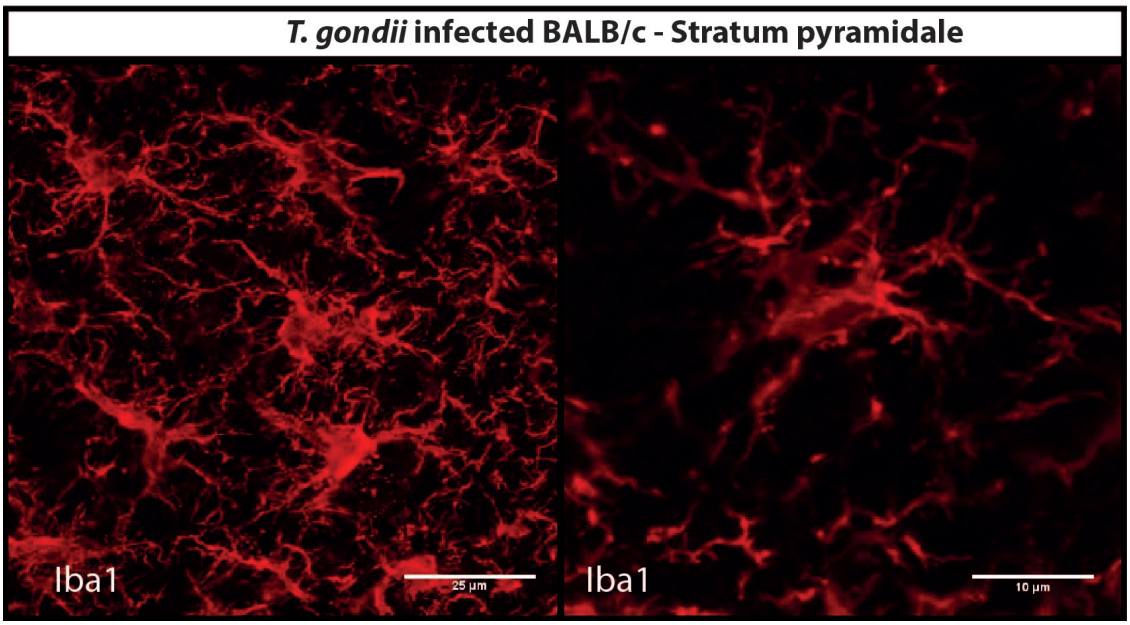

Figure 3.17: Maximum intensity projection of staining of microglia/macrophages in the stratum pyramidale of the CA1 area with primary antibodies against ionized calcium-binding adapter molecule 1 (Iba1) respectively in *T. gondii* infected BALB/c mice, scale bar in the left frame is 25 µm, detail frame 10 µm.

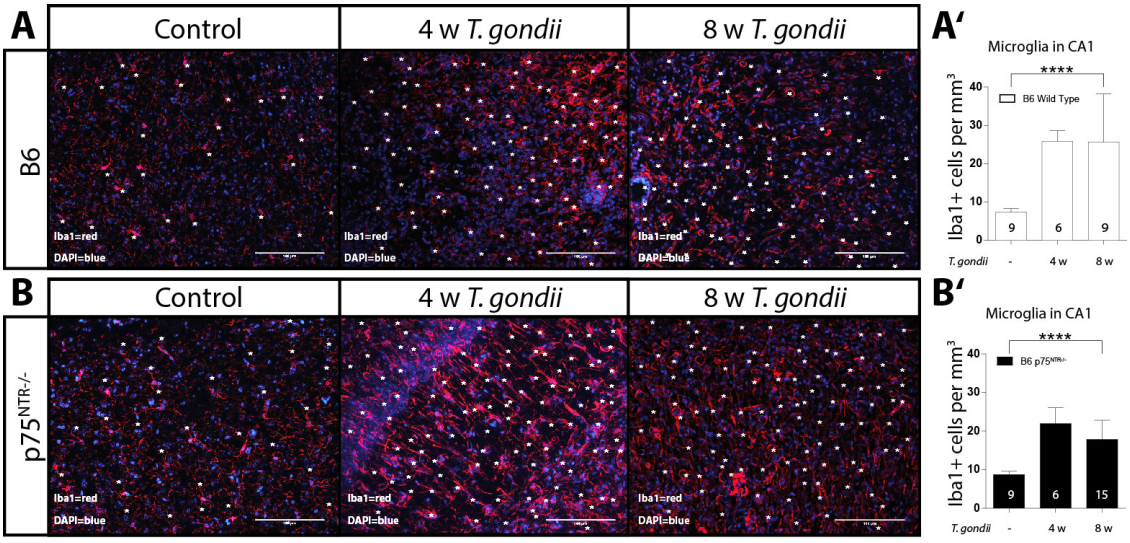

Figure 3.18: Quantification of microglia/macrophages in hippocampal *stratum pyramidale* B6 wt and B6-p75^{NTR} ko mice infected with *T. gondii* for 4 w and 8 w (A, B) Immunohistochemistry of *stratum pyramidale* CA1 area of B6 wt and B6-p75^{NTR} ko mice infected with *T. gondii* for 4 w and 8 w. Red is Iba1, blue is DAPI, scale bar is 100 µm. White asterisk indicate Iba1+ cells **(A', B')** Evaluation of the number of Iba1+ cells in the stratum pyramidale CA1 area of B6 and B6-p75^{NTR} ko mice infected with *T. gondii* for 4 w and 8 w. Data presented as mean ± SEM, p*<0.05; p****<0.0001.

Table 3.13: Descriptive statistics for hippocampal Iba1+ cell numbers in *T. gondii* infected B6 wt and B6-p75^{NTR} ko mice (fig. 3.18).

Genotype	CNS area	*T. gondii*	Mean±SEM
B6 WT	*stratum pyramidale*	-	7.36±0.2939 cells per mm^3
B6 WT	*stratum pyramidale*	4 w	25.73±1.234 cells per mm^3
B6 WT	*stratum pyramidale*	8 w	22.84±4.047 cells per mm^3
B6-p75$^{NTR-/-}$	*stratum pyramidale*	-	8.728±0.2841 cells per mm^3
B6-p75$^{NTR-/-}$	*stratum pyramidale*	4 w	21.94±1.68 cells per mm^3
B6-p75$^{NTR-/-}$	*stratum pyramidale*	8 w	17.85±1.274 cells per mm^3

infected with *T. gondii*. Figure 3.19 A' shows that the total number of Iba1+ cells in the cortex is significantly increased in *T. gondii* infected B6 wt mice compared to the controls. There is no statistical difference between 4 w and 8 w *T. gondii* infected mice. Figure 3.19 B indicates the distribution of Iba1+ cells within the cortex in B6-p75^{NTR} ko mice, control, 4 w and 8 w infected with *T. gondii*. Figure 3.19 B' shows that the total number of Iba1+ cells in the *stratum pyramidale* is significantly increased in *T. gondii* infected B6 wt mice compared to the controls. There is no statistical difference between 4 w and 8 w *T. gondii* infected mice. Descriptive statistics for fig. 3.19 are listed in table 3.14.

Table 3.14: Descriptive statistics for hippocampal Iba1+ cell numbers in *T. gondii* infected B6 wt and B6-p75^{NTR} ko mice (fig. 3.19).

Genotype	CNS area	*T. gondii*	Mean±SEM
B6 WT	Cortex	-	8.139±0.4066 cells per mm^3
B6 WT	Cortex	4 w	26.57±1.594 cells per mm^3
B6 WT	Cortex	8 w	22.84±4.047 cells per mm^3
B6-p75$^{NTR-/-}$	Cortex	-	10.57±0.3258 cells per mm^3
B6-p75$^{NTR-/-}$	Cortex	4 w	24.63±1.542 cells per mm^3
B6-p75$^{NTR-/-}$	Cortex	8 w	21.4±2.581 cells per mm^3

3.2.3 p75$^{NTR-/-}$ mice show increased numbers of Iba1+ cells compared to the B6 wt controls

The influence of the p75^{NTR} on microglia cells has been studied in last two decades (Nakajima *et al.*, 1998; Srinivasan *et al.*, 2004; Meeker *et al.*, 2016) and the overall participation of the p75^{NTR} in injury and disease rose to general interest (Meeker

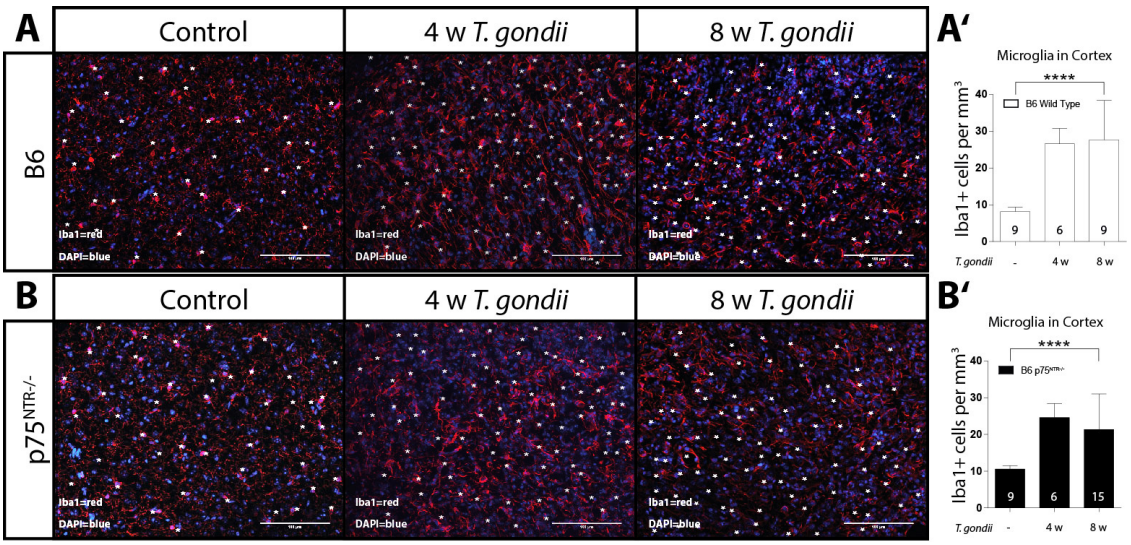

Figure 3.19: Quantification of microglia/macrophages in the cortex of B6 wt and B6-p75^{NTR} ko mice infected with *T. gondii* for 4 w and 8 w (A, B) Immunohistochemistry of cortex of B6 wt and B6-p75^{NTR} ko mice infected with *T. gondii* for 4 w and 8 w. Red is Iba1, blue is DAPI, scale bar is 100 µm. White asterisk indicate Iba1+ cells **(A', B')** Evaluation of the number of Iba1+ cells in the cortex of B6 and B6-p75^{NTR} ko mice infected with *T. gondii* for 4 w and 8 w. Data presented as mean ± SEM, p*<0.05; p****<0.0001.

and Williams, 2014).

Figure 3.20 shows deleting the exon IV from the p75^{NTR} gene effects microglia numbers within the *stratum pyramidale* of the hippocampus and the cortex in B6 wt and B6-p75^{NTR} ko mice. Figure 3.20 A indicates the distribution of Iba1+ cells within the hippocampal *stratum pyramidale* in B6 wt mice and B6-p75^{NTR} ko mice. Figure 3.20 B indicates the distribution of Iba1+ cells within the cortex in B6 wt and B6-p75^{NTR} ko mice. Figure 3.20 C shows that the total number of Iba1+ cells in the *stratum pyramidale* is significantly increased in B6-p75^{NTR} ko mice compared to B6 wt mice. Figure 3.20 D shows that the total number of Iba1+ cells in the cortex is significantly increased in B6-p75^{NTR} ko mice compared to B6 wt mice. Descriptive statistics for fig. 3.20 are listed in table 3.15.

3.2.4 The number of Iba1+ cells increases in BALB/c mice upon *T. gondii* infection

The findings of the impact of chronic *T. gondii* infection on microglial morphology raised the question on the number of Iba1+ cells upon infection in BALB/c wt mice and their relative numbers to the B6 wt strain.

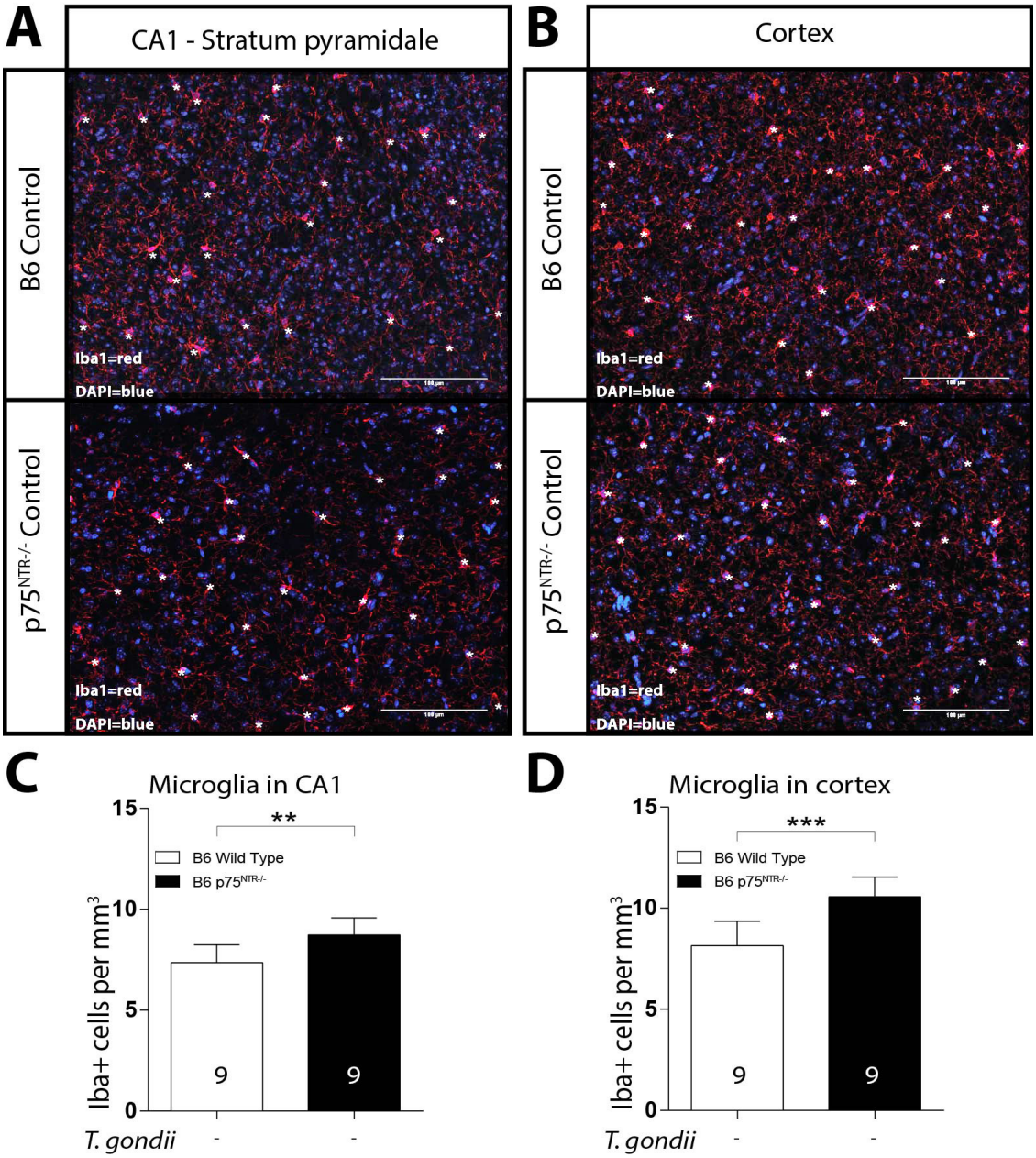

Figure 3.20: Quantification of microglia/macrophages in hippocampal *stratum pyramidale* and cortex sections of B6 wt controls and p75$^{NTR-/-}$ controls (A, B) Immunohistochemistry of *stratum pyramidale* CA1 area and cortex area of B6 wt controls and B6-p75^{NTR} ko controls mice. Red is Iba1, blue is DAPI, scale bar is 100 µm, asterisks indicate Iba1+ cells **(C, D)** The number of Iba1+ cells in the *stratum pyramidale* CA1 area and cortex area of B6 and B6-p75$^{NTR-/-}$ mice. Data presented as mean ± SEM, p*<0.05; p**<0.01; p***<0.001; p****<0.0001.

Figure 3.21 shows how chronic *T. gondii* infection effects microglia/macrophage numbers within the *stratum pyramidale* of the hippocampus and the cortex in

Table 3.15: Descriptive statistics for hippocampal and cortical Iba1+ cell numbers in B6 wt and B6-p75^{NTR} ko mice (fig. 3.18).

Genotype	CNS area	*T. gondii*	Mean±SEM
B6 WT	*stratum pyramidale*	-	7.36±0.2939 cells per mm^3
B6 WT	Cortex	-	8.139±0.4066 cells per mm^3
B6-p75$^{NTR-/-}$	*stratum pyramidale*	-	8.728±0.2841 cells per mm^3
B6-p75$^{NTR-/-}$	Cortex	-	10.57±0.3258 cells per mm^3

BALB/c wt mice. Figure 3.21 A indicates the distribution of Iba1+ cells within the hippocampal *stratum pyramidale* in BALB/c wt controls (upper panel) and 8 w *T. gondii* infected *T. gondii* BALB/c wt mice (lower panel).

Table 3.16: Descriptive statistics for hippocampal Iba1+ cell numbers in *T. gondii* infected B6 wt and B6-p75^{NTR} ko mice (fig. 3.22).

Genotype	CNS area	*T. gondii*	Mean±SEM
BALB/c WT	*stratum pyramidale*	-	6,476±0,5106 cells per mm^3
B6 WT	*stratum pyramidale*	-	7.36±0.2939 cells per mm^3
BALB/c WT	Cortex	-	6,900±0,3584 cells per mm^3
B6 WT	Cortex	-	8.139±0.4066 cells per mm^3

Figure 3.21 B indicates the distribution of Iba1+ cells within the cortex in BALB/c wt controls (upper panel) and 8 w *T. gondii* infected *T. gondii* BALB/c wt mice (lower panel). Figure 3.21 A' shows that the total number of Iba1+ cells in the *stratum pyramidale* is significantly increased in *T. gondii* infected BALB/c wt mice compared to the controls. Figure 3.21 B' shows that the total number of Iba1+ cells in the cortex is significantly increased in *T. gondii* infected BALB/c wt mice compared to the controls. Descriptive statistics for fig. 3.21 are listed in table 3.17.

Table 3.17: Descriptive statistics for hippocampal and cortical Iba1+ cell numbers in *T. gondii* infected BALB/c wt mice (fig. 3.21).

Genotype	CNS area	*T. gondii*	Mean±SEM
BALB/c WT	*stratum pyramidale*	-	6,476±0,5106 cells per mm^3
BALB/c WT	*stratum pyramidale*	8 w	16,84±0,9265 cells per mm^3
BALB/c WT	Cortex	-	6,900±0,3584 cells per mm^3
BALB/c WT	Cortex	8 w	17,94±0,9848 cells per mm^3

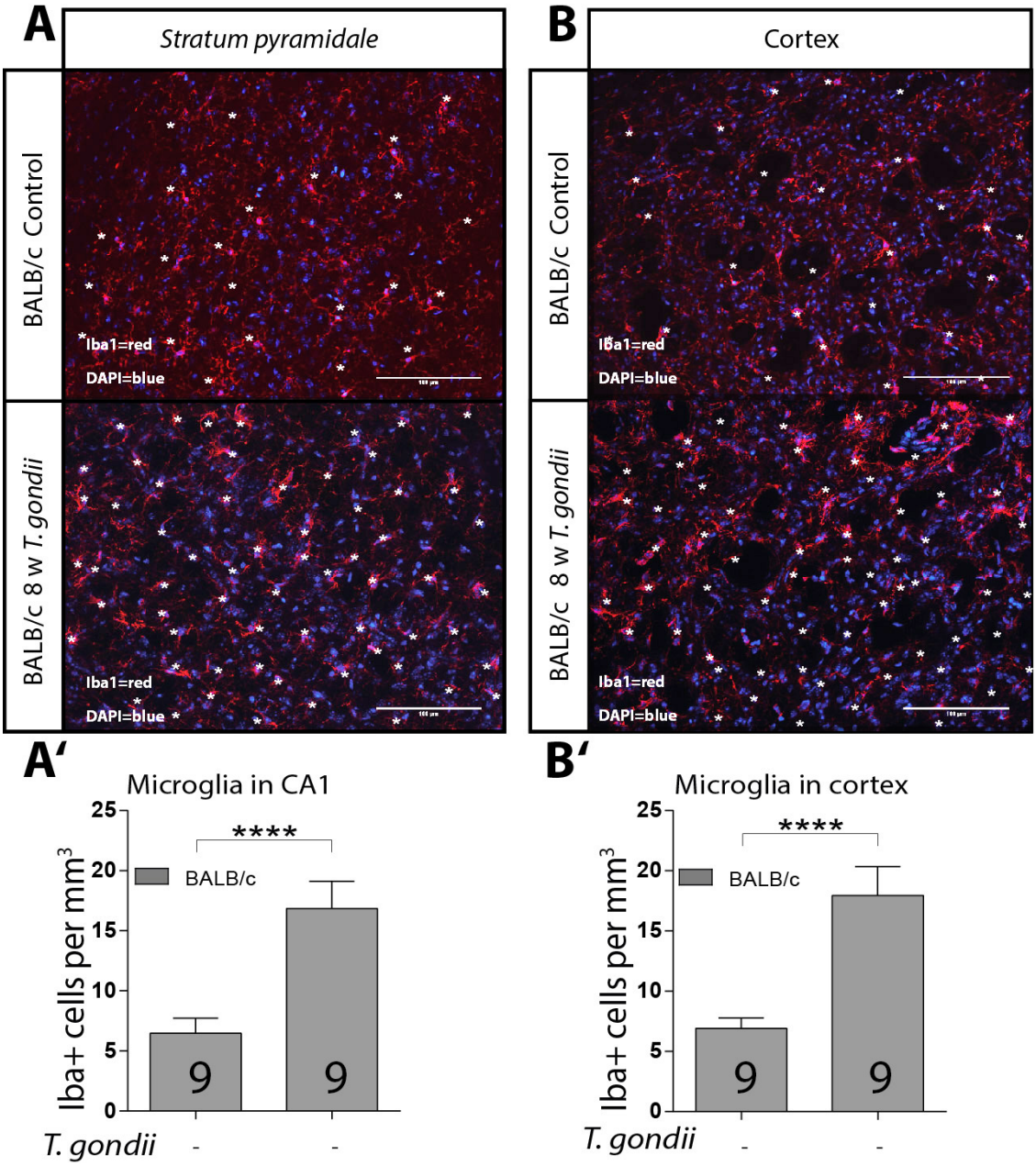

Figure 3.21: Quantification of microglia/macrophages in hippocampal *stratum pyramidale* and cortex sections of BALB/c wt controls 8 w *T. gondii* infected BALB/c wt mice (A, B) Immunohistochemistry of *stratum pyramidale* area and cortex area of BALB/c wt control mice and 8 w *T. gondii* infected BALB/c wt mice. Red is Iba1, blue is DAPI, scale bar is 100 µm, asterisks indicate Iba1+ cells **(C, D)** The number of Iba1+ cells in the *stratum pyramidale* and cortex area of BALB/c wt control mice and 8 w *T. gondii* infected BALB/c wt mice. Data presented as mean ± SEM, p*<0.05; p**<0.01; p***<0.001; p****<0.0001.

Figure 3.22 shows how microglia/macrophage numbers differ within the *stratum pyramidale* of the hippocampus and the cortex in BALB/c wt mice compared to

B6 wt mice. Figure 3.22 A indicates the distribution of Iba1+ cells within the hippocampal *stratum pyramidale* in BALB/c wt B6 wt mice. Figure 3.22 B indicates the distribution of Iba1+ cells within the cortex in BALB/c wt controls and B6 wt mice. Figure 3.22 A' shows that the total number of Iba1+ cells in the *stratum pyramidale* is not significantly different in BALB/c wt mice compared to B6 wt mice. Figure 3.22 B' shows that the total number of Iba1+ cells in the cortex is significantly increased BALB/c wt mice compared to B6 wt mice. Descriptive statistics for fig. 3.22 are listed in table 3.16.

3.2.5 Iba1 immuno reactivity increases upon *T. gondii* infection in B6 mice

Iba1 has also been used to analyze microglial activation. While microglia undergo cytoskeletal rearrangements that alter their morphology (Davalos *et al.*, 2005), morphological changes may not ultimately represent active inflammatory profiles accurately (section 3.2.1). Additionally to the number of Iba1+ cells I measured fluorescence intensity.

Table 3.18: Descriptive statistics for Iba1 immuno reactivity in B6 wt and B6-p75^{NTR} ko mice upon *T. gondii* infection (fig. 3.23).

Genotype	CNS area	*T. gondii*	Mean±SEM
B6 wt	Cortex	-	14473±1212 ID per 0.13 mm^3
B6 wt	Cortex	8 w	194656±19571 ID per 0.13 mm^3
B6-p75^{NTR} ko	Cortex	-	88407±3960 ID per 0.13 mm^3
B6-p75^{NTR} ko	Cortex	8 w	311053±13896 ID per 0.13 mm^3
B6-p75^{NTR} ko	CA1	-	62148±3102 ID per 0.13 mm^3
B6-p75^{NTR} ko	CA1	8 w	269276±23887 ID per 0.13 mm^3
B6-p75^{NTR} ko	DG	-	65989±33342 ID per 0.13 mm^3
B6-p75^{NTR} ko	DG	8 w	288935±9850 ID per 0.13 mm^3

Figure 3.23 shows the impact of chronic (8 w) *T. gondii* infection on Iba1 immuno reactivity in B6 wt and B6-p75^{NTR} ko mice. Figure 3.23 A and A' are representative confocal microscopic images of the cortex of B6 wt and B6-p75^{NTR} ko mice, which have been stained with an anti-Iba1 antibody. The increase in Iba1 immuno reactivity is clear. Figure 3.23 B, C and D show a significant increase in Iba1 immuno reactivity in B6-p75^{NTR} ko mice upon *T. gondii* infection in the CA1, DG and cortex region. Figure 3.23 D' shows there is significant increase in Iba1 immuno

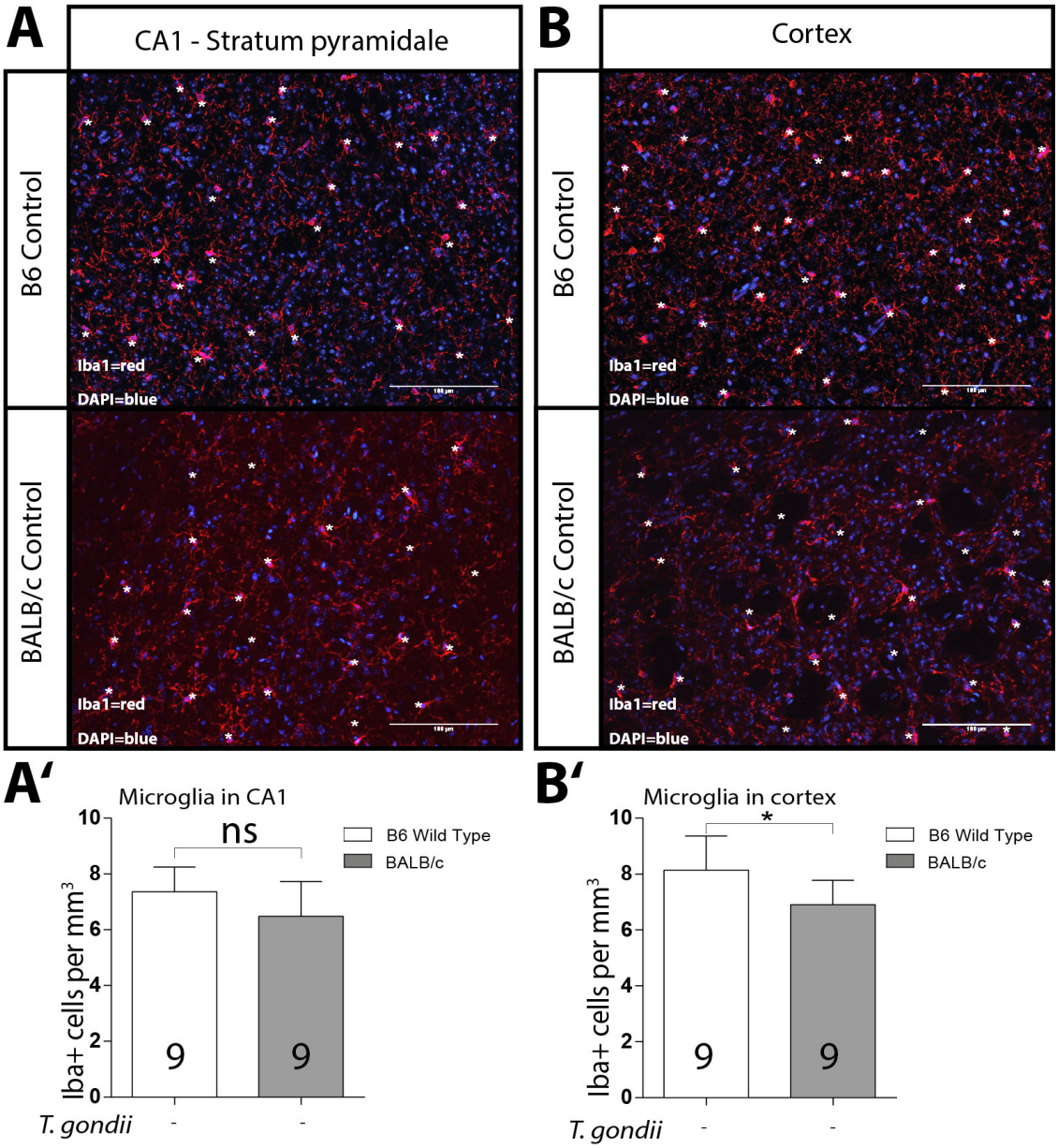

Figure 3.22: Quantification of microglia/macrophages in hippocampal *stratum pyramidale* and cortex sections of B6 wt controls and BALB/c wt controls (A, B) Immunohistochemistry of *stratum pyramidale* CA1 area and cortex area of B6 wt controls and BALB/c wt control mice. Red is Iba1, blue is DAPI, scale bar is 100 µm, asterisks indicate Iba1+ cells **(C, D)** The number of Iba1+ cells in the *stratum pyramidale* and cortex area of B6 and BALB/c wt mice. Data presented as mean ± SEM, p*<0.05; p**<0.01; p***<0.001; p****<0.0001.

reactivity in the cortex of 8 w *T. gondii* infected B6 wt mice. Descriptive statistics of fig. 3.23 are listed in table 3.18.

Figure 3.24 shows the impact of chronic (8 w) *T. gondii* infection on Iba1 immuno

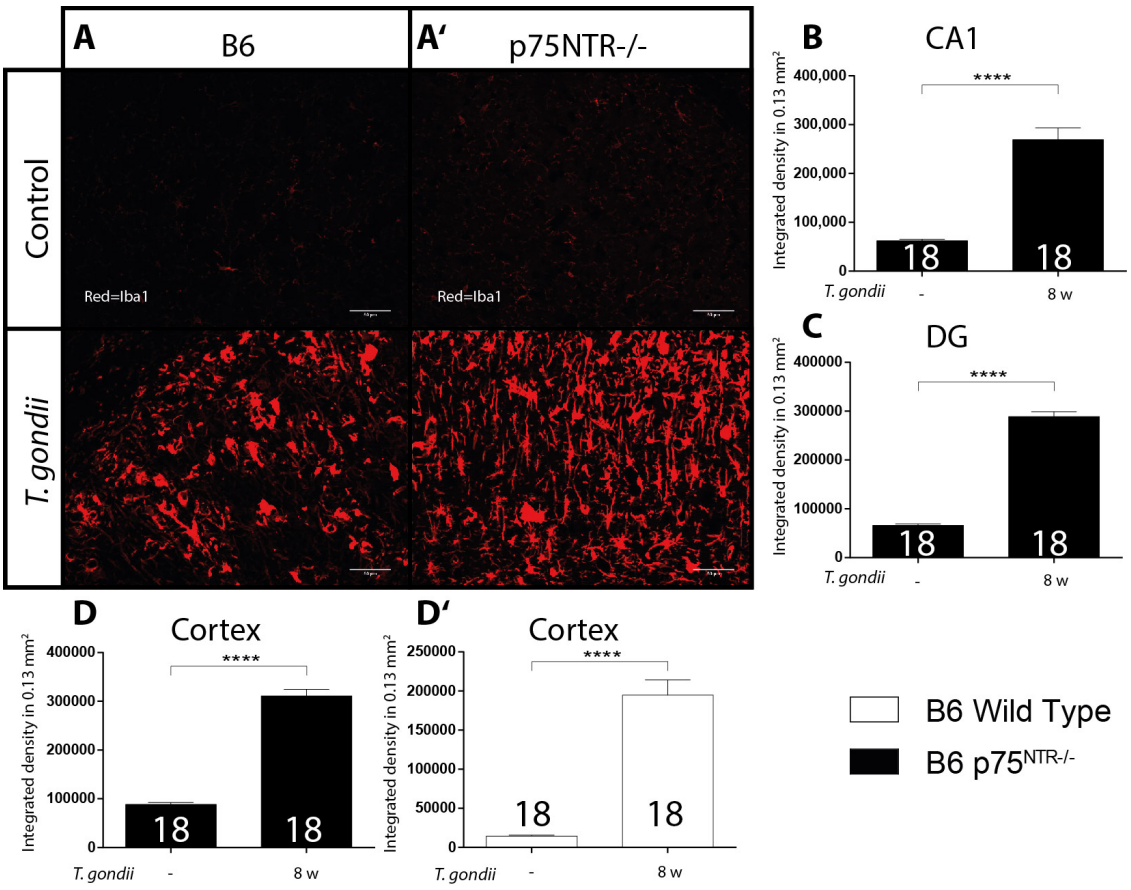

Figure 3.23: Influence of a chronic *Toxoplasma gondii* infection on Iba1 immunoreactivity in B6 wild type and B6-p75$^{NTR-/-}$ mice - (A, A') Exemplified intensity measurements (100 ms exposure) for B6 wild type and B6-p75^{NTR} ko mice. Control upper panels, *T. gondii* infected lower panels. Scale bar is 50 µm. Pictures were taken within the cortex. **(B, C, D,)** Integrated density of B6-p75$^{NTR-/-}$ mice in hippocampal *stratum pyramidale*, dentate gyrus and the entorhinal cortex, control and 8 w *T. gondii* infected. **(D')** Integrated density of *T. gondii* infected and control B6 wild type mice in entorhinal cortex. Data presented as mean ± SEM. p**** < 0.0001

reactivity in B6 wt and B6-p75^{NTR} ko mice. Figure 3.24 A and A' are representative confocal microscopic images of the cortex of 8 w *T. gondii* infected B6 wt and B6-p75^{NTR} ko mice, which have been stained with an anti-Iba1 antibody. The difference in Iba1 immuno reactivity is visibly higher in the B6-p75^{NTR} ko mice. Figure 3.24 B, C and D show a significant increase in Iba1 immuno reactivity in B6-p75^{NTR} ko mice upon *T. gondii* infection in the CA1, DG and cortex region compared to the B6 wt mice. Descriptive statistics of fig. 3.24 are listed in table 3.19.

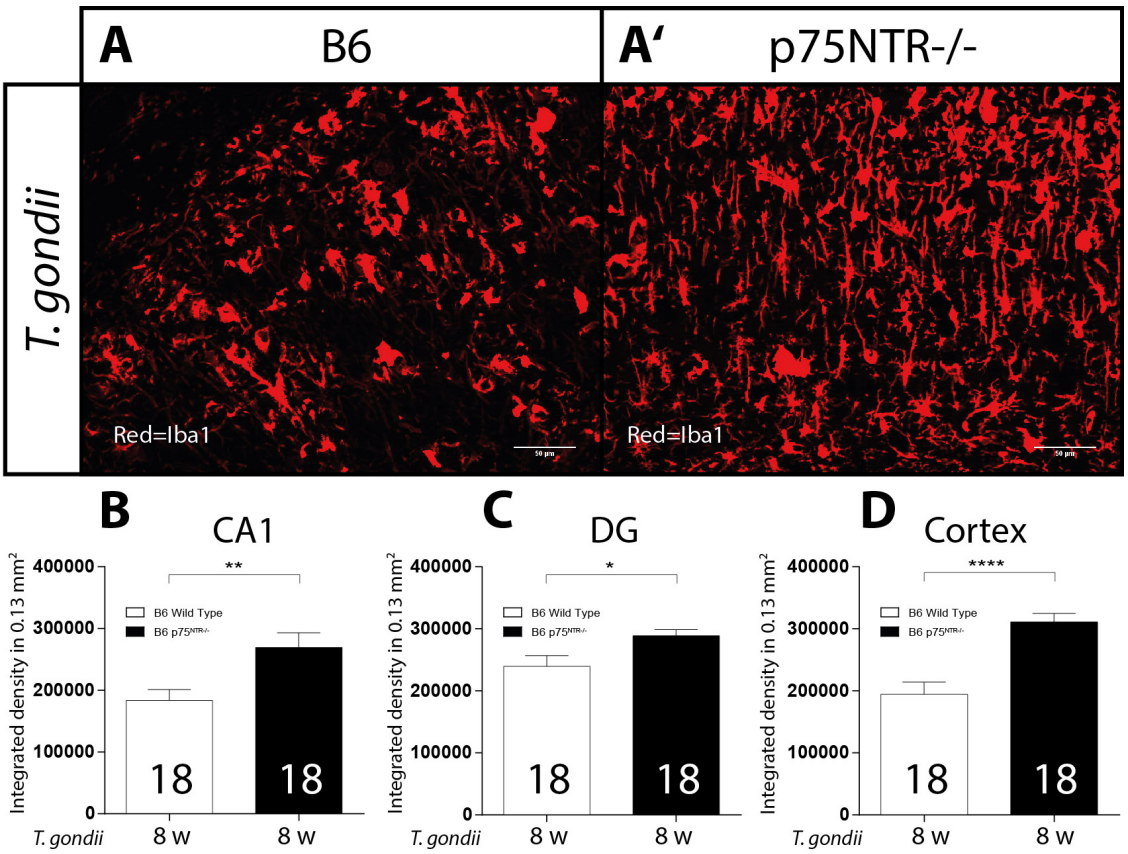

Figure 3.24: Influence of chronic *T. gondii* infection on Iba1 immunoreactivity in the cortex of B6 wild type and B6-p75^{NTR} ko mice - (A, A') Exemplified intensity measurements (100 ms exposure) for control B6 wild type and control B6-p75^{NTR} ko mice in the cortex. Scale bar is 50 µm. **(B)** Integrated density of control B6 wt mice and B6-p75$^{NTR-/-}$ mice in entorhinal cortex. Data presented as mean ± SEM. p**** < 0.0001

Table 3.19: Descriptive statistics for Iba1 immuno reactivity in B6 wt and B6-p75^{NTR} ko mice upon *T. gondii* infection (fig. 3.24).

Genotype	CNS area	*T. gondii*	Mean±SEM
B6 wt	Cortex	8 w	194656±19571 ID per 0.13 mm^3
B6 wt	CA1	8 w	183406±17616 ID per 0.13 mm^3
B6 wt	DG	8 w	239470±17309 ID per 0.13 mm^3
B6-p75^{NTR} ko	Cortex	8 w	311053±13896 ID per 0.13 mm^3
B6-p75^{NTR} ko	CA1	8 w	269276±23887 ID per 0.13 mm^3
B6-p75^{NTR} ko	DG	8 w	288935±9850 ID per 0.13 mm^3

3.2.6 Iba1 immuno reactivity is increased in the cortex of B6-p75^{NTR} ko control mice compared to B6 wt control mice

Figure 3.25 shows the impact of the deletion of the exon IV of the p75^{NTR} gene in B6 mice on Iba1 immuno reactivity compared to B6 wt control mice. Figure 3.25 A and A' are representative confocal microscopic images of the cortex of B6 wt and B6-p75^{NTR} ko mice, which have been stained with an anti-Iba1 antibody. Figure 3.25 B shows a significant increase in Iba1 immuno reactivity in B6-p75^{NTR} ko mice compared to the control B6 wt mice in the cortex region. Descriptive statistics of fig. 3.25 are listed in table 3.20

Table 3.20: Descriptive statistics for Iba1 immuno reactivity in B6 wt and B6-p75^{NTR} ko mice (fig. 3.25).

Genotype	CNS area	*T. gondii*	Mean±SEM
B6 wt	Cortex	-	14473±1212 ID per 0.13 mm^3
B6-p75^{NTR} ko	Cortex	-	88407±3960 ID per 0.13 mm^3

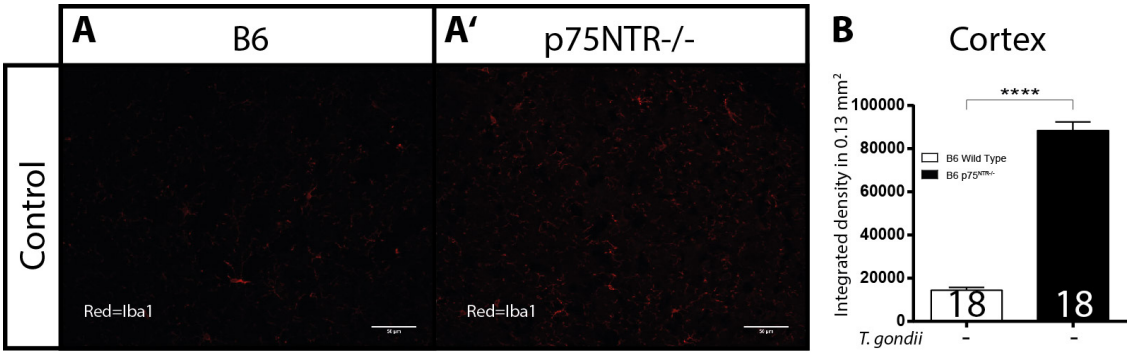

Figure 3.25: Influence of p75^{NTR} ko on Iba1 immunoreactivity in the cortex of B6 wild type mice - (A, A') Exemplified intensity measurements (100 ms exposure) for control B6 wild type and control B6-p75^{NTR} ko mice in the cortex. Scale bar is 50 µm. **(B)** Integrated density of control B6 wt mice and B6-p75$^{NTR-/-}$ mice in entorhinal cortex. Data presented as mean ± SEM. p**** < 0.0001

3.2.7 Iba1 immuno reactivity increases upon *T. gondii* infection in BALB/c mice

Figure 3.26 shows the impact of chronic (8 w) *T. gondii* infection on Iba1 immuno reactivity in BALB/c wt mice. Figure 3.26 A and A' are representative confocal

Table 3.21: Descriptive statistics for Iba1 immuno reactivity in BALB/c wt mice upon *T. gondii* infection (fig. 3.26).

Genotype	CNS area	*T. gondii*	Mean±SEM
BALB/c wt	Cortex	-	45144±1603 ID per 0.13 mm^3
BALB/c wt	Cortex	8 w	611254±62942 ID per 0.13 mm^3
BALB/c wt	CA1	-	36770±2290 ID per 0.13 mm^3
BALB/c wt	CA1	8 w	557094±88116 ID per 0.13 mm^3
BALB/c wt	DG	-	36338±2651 ID per 0.13 mm^3
BALB/c wt	DG	8 w	662142±73075 ID per 0.13 mm^3

Table 3.22: Descriptive statistics for Iba1 immuno reactivity in BALB/c wt mice upon *T. gondii* infection (fig. 3.27).

Genotype	CNS area	*T. gondii*	Mean±SEM
BALB/c wt	Cortex	-	45144±1603 ID per 0.13 mm^3
B6 wt	Cortex	-	14473±1212 ID per 0.13 mm^3

microscopic images of the cortex of BALB/c wt mice, which have been stained with an anti-Iba1 antibody. The increase in Iba1 immuno reactivity is clear in the 8 w *T. gondii* infected mice. Figure 3.26 B, C and D show a significant increase in Iba1 immuno reactivity in BALB/c mice upon *T. gondii* infection in the CA1, DG and cortex region. Figure 3.23 Descriptive statistics of fig. 3.26 are listed in table 3.21.

Figure 3.27 shows differences in Iba1 immuno reactivity between B6 wt and BALB/c wt mice in the cortex. Figure 3.27 A and A' are representative confocal microscopic images of the cortex of B6 wt and BALB/c ko mice, which have been stained with an anti-Iba1 antibody. Figure 3.27 B shows a significant increase in Iba1 immuno reactivity in BALB/c mice compared to the control B6 wt mice in the cortex region. Descriptive statistics of fig. 3.27 are listed in table 3.22

Figure 3.28 shows the impact of chronic (8 w) *T. gondii* infection on Iba1 immuno reactivity in B6 wt and BALB/c wt mice. Figure 3.28 A and A' are representative confocal microscopic images of the cortex of 8 w *T. gondii* infected B6 and BALB/c wt mice, which have been stained with an anti-Iba1 antibody. The difference in Iba1 immuno reactivity is visibly higher in the BALB/c wt mice. Figure 3.28 B, C and D show a significant increase in Iba1 immuno reactivity in BALB/c wt mice upon *T. gondii* infection in the CA1, DG and cortex region compared to the B6 wt mice. Descriptive statistics of fig. 3.28 are listed in table 3.23.

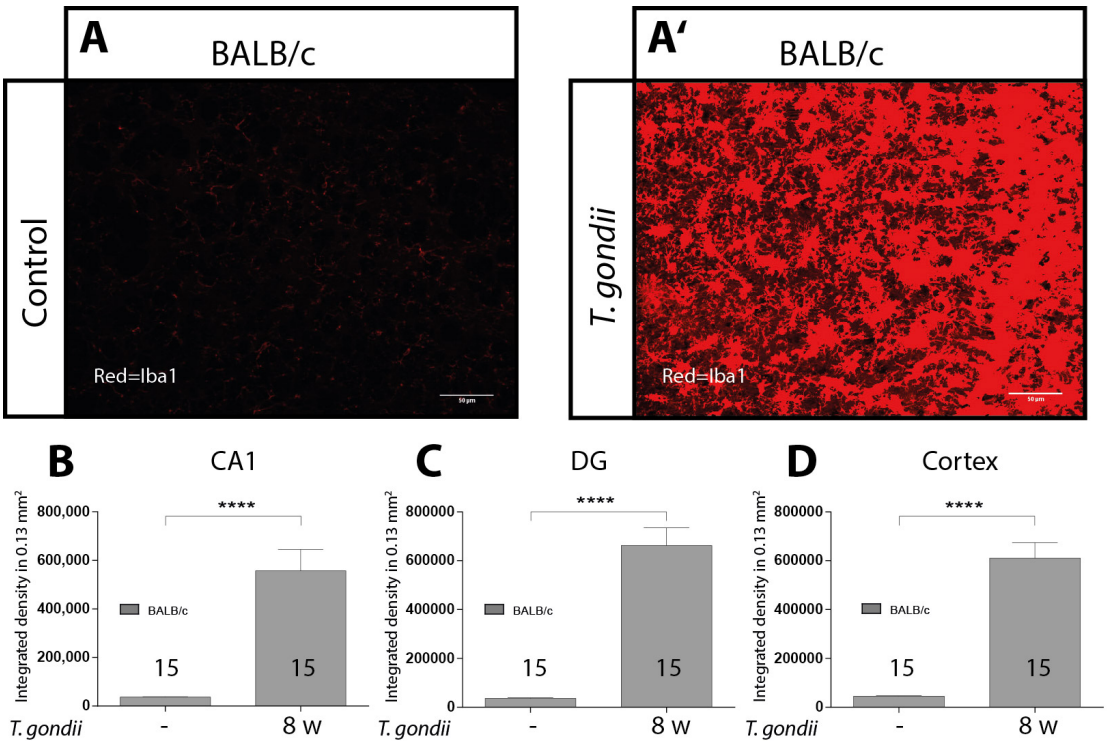

Figure 3.26: Influence of a chronic *Toxoplasma gondii* infection on Iba1 immunoreactivity in BALB/c wild type mice - (A, A') Exemplified intensity measurements (100 ms exposure) for BALB/c wt mice. Control left panels *T. gondii* infected right panel. Scale bar is 50 µm. Pictures were taken within the cortex. **(B, C, D,)** Integrated density of BALB/c wt mice in hippocampal *stratum pyramidale*, dentate gyrus and the entorhinal cortex, control and 8 w *T. gondii* infected. Data presented as mean ± SEM. p**** < 0.0001

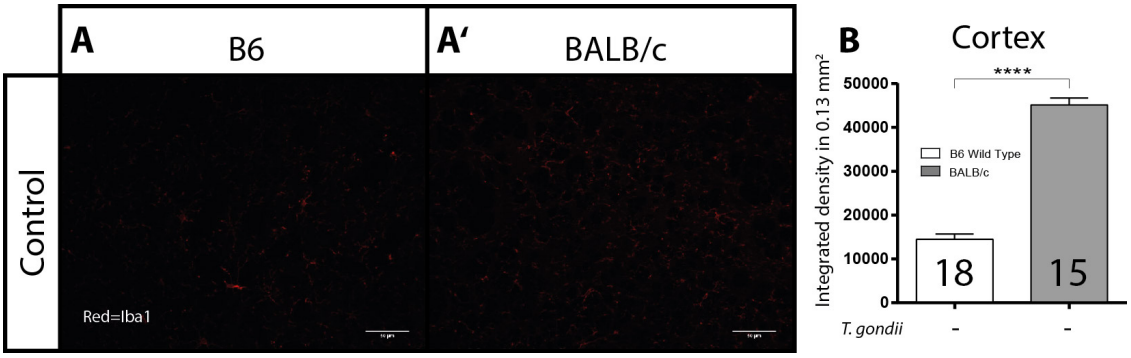

Figure 3.27: Comparison between the Iba1 immuno reactivity of B6 wt and BALB/c wt mice in the cortex - (A, A') Exemplified intensity measurements (100 ms exposure) for control B6 wild type and control BALB/c wt mice in the cortex. Scale bar is 50 µm. **(B)** Integrated density of control B6 wt mice and BALB/c wt mice in entorhinal cortex. Data presented as mean ± SEM. p**** < 0.0001

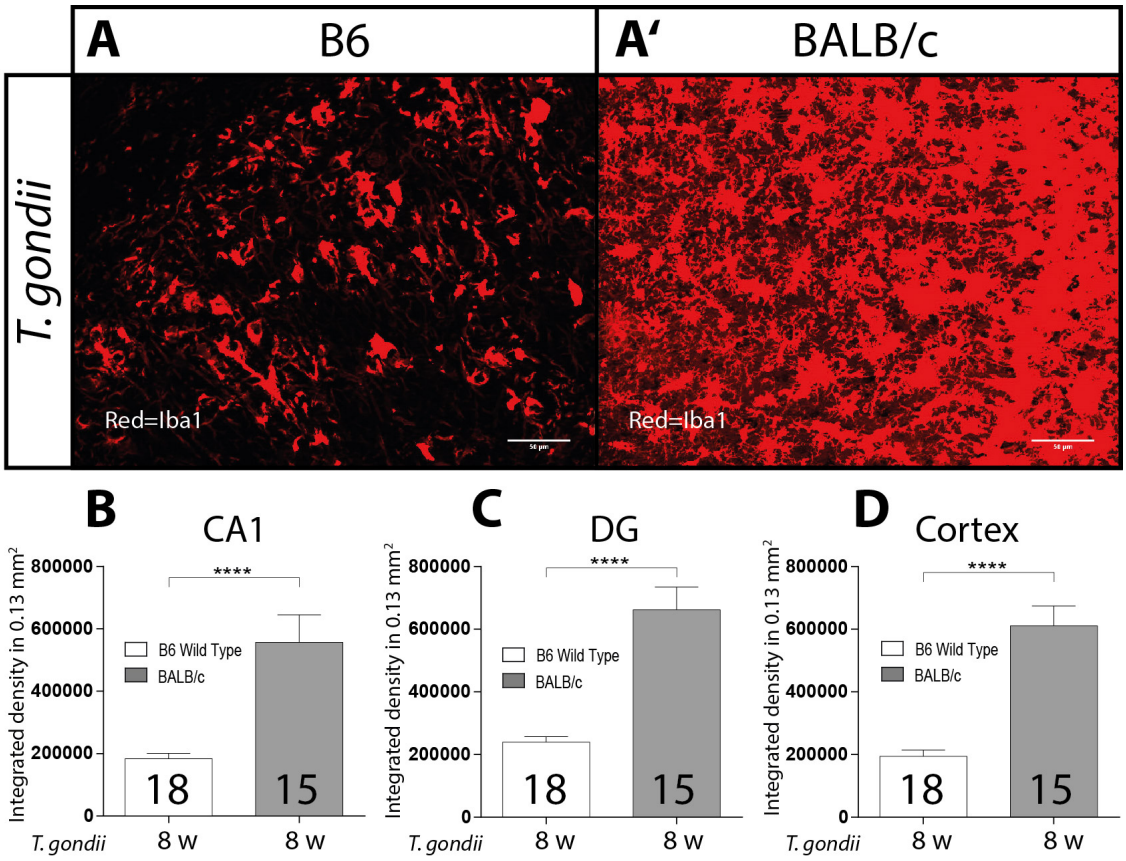

Figure 3.28: Influence of a chronic *Toxoplasma gondii* infection on Iba1 immunoreactivity in BALB/c and B6 wild type mice - (A, A') Exemplified intensity measurements (100 ms exposure) for 8 w *T. gondii* BALB/c and B6 wt mice. Scale bar is 50 µm. Pictures were taken within the cortex. **(B, C, D,)** Integrated density of BALB/c and B6 wt mice in hippocampal *stratum pyramidale*, dentate gyrus and the entorhinal cortex, control and 8 w *T. gondii* infected. Data presented as mean ± SEM. p**** < 0.0001

Table 3.23: Descriptive statistics for Iba1 immuno reactivity in B6 wt and BALB/c wt mice upon *T. gondii* infection (fig. 3.28).

Genotype	CNS area	*T. gondii*	Mean±SEM
B6 wt	Cortex	8 w	194656±19571 ID per 0.13 mm^3
B6 wt	CA1	8 w	183406±17616 ID per 0.13 mm^3
B6 wt	DG	8 w	239470±17309 ID per 0.13 mm^3
BALB/c wt	Cortex	8 w	611254±62942 ID per 0.13 mm^3
BALB/c wt	CA1	8 w	557094±88116 ID per 0.13 mm^3
BALB/c wt	DG	8 w	662142±73075 ID per 0.13 mm^3

3.3 Neurotrophin receptor translation is effected by *T. gondii* infection

As deleting the p75^{NTR} exon IV effects neuronal architecture in the hippocampus and the cortex (section 3.1) of *T. gondii* infected B6 mice differently than the wt control, p75^{NTR} protein levels in B6 and BALB/c (section 3.3.2) control animals were quantified as well as in mice, which have been chronically infected with *T. gondii* for 8 w.

Figure 3.29 shows the effect of 8 w chronic *T. gondii* infection on p75^{NTR} protein levels in the cortex of B6 wt mice. Figure 3.29 A shows representative protein bands from Western blots. While the internal standard (GAPDH) is equally distributed in B6 wt controls and 8 w *T. gondii* infected B6 wt mice, p75^{NTR} levels are reduced in *T. gondii* infected B6 wt mice. Figure 3.29 B shows a significant reduction in p75^{NTR} protein levels in 8 w *T. gondii* infected B6 wt mice compared to the control. Descriptive statistic of fig. 3.29 are listed in table 3.24.

Table 3.24: Descriptive statistics for p75^{NTR} protein level in *T. gondii* infected B6 wt mice (fig. 3.29)

Genotype	CNS area	*T. gondii*	Mean±SEM
B6 wt	Cortex	-	normalized to 1
B6 wt	Cortex	8 w	0,4610±0,01614 of B6 wt control

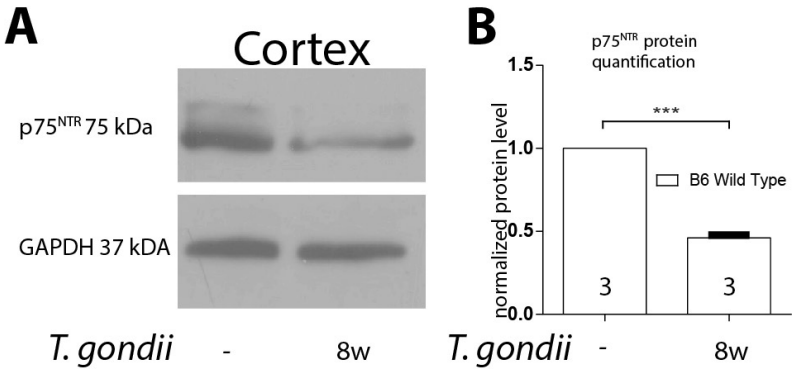

Figure 3.29: Quantification of p75^{NTR} in cortical brain tissue of B6 wt controls and in 8 w *T. gondii* infected B6 wt mice (A) Exemplified Western blots. The antibodies used were anti-p75^{NTR} (rabbit, polyclonal,abcam ab38335, 1:1000) and anti-GAPDH (rabbit polyclonal, Acris AP21839PUN, 1:3000) **(B)** To control mice normalized amount of p75^{NTR} in cortical brain tissue of 8 w *T. gondii* infected B6. Data presented as mean ± SEM, p*<0.05; p**<0.01; p***<0.001; p****<0.0001.

3.3.1 Both isoforms of TrkB are effected by chronic *T. gondii* infection in B6 wt and B6-p75^{NTR} ko mice

P75^{NTR} exerts its functions by interacting with other receptors. Heterodimers consisting of Trk receptors and p75^{NTR} promote growth and pro-survival signaling while increasing the affinity of major neurotrophins to the respective Trk receptor 100-fold compared to the Trk homodimer (Hempstead 1991; Bibel 1999). Importantly TrkB, activated by BDNF, promotes neuronal differentiation, growth and survival. To gain further insight chronically *Toxoplasma gondii* infected B6 wt, B6-p75^{NTR} ko and BALB/c (section 3.3.2) wt were analyzed for the protein level of TrkB.

Table 3.25: Descriptive statistics for TrkB protein level in *T. gondii* infected B6 wt and B6-p75^{NTR} ko mice (fig. 3.30)

Genotype	CNS area	*T. gondii*	TrkB isoform	Mean±SEM
B6 wt	Cortex	-	FL	normalized to 1
B6 wt	Cortex	-	T1	normalized to 1
B6 wt	Cortex	4 w	FL	0,5900±0,04922
B6 wt	Cortex	4 w	T1	0,4151±0,03131
B6 wt	Cortex	8 w	FL	0,3458±0,05218
B6 wt	Cortex	8 w	T1	0,6342±0,02947
B6-p75^{NTR} ko	Cortex	-	FL	1,573±0,2389
B6-p75^{NTR} ko	Cortex	-	T1	1,186±0,1449
B6-p75^{NTR} ko	Cortex	4 w	FL	0,5099±0,1883
B6-p75^{NTR} ko	Cortex	4 w	T1	0,3404±0,01200
B6-p75^{NTR} ko	Cortex	8 w	FL	0,3744±0,01482
B6-p75^{NTR} ko	Cortex	8 w	T1	0,4783±0,04024

Figure 3.30 shows the effect of 4 w and 8 w chronic *T. gondii* infection on TrkB protein levels (both isoforms, full length and T1) in cortical tissue of B6 wt and B6-p75^{NTR} ko mice. Figure 3.30 A shows representative protein bands from Western blots. While the internal standard (Tubulin) is equally distributed, TrkB protein levels are visibly reduced in B6 wt and B6-p75^{NTR} ko mice upon *T. gondii* infection. Figure 3.30 B shows that there is no significant difference in the truncated TrkB isoform (T1) in B6 wt controls compared to the B6-p75^{NTR} ko mice. Figure 3.30 C and D show significant decrease in truncated TrkB levels upon *T. gondii* infection in B6 wt and B6-p75^{NTR} ko mice. Figure 3.30 B' shows a significant increase in full length TrkB in B6-p75^{NTR} ko mice compared to the B6 wt controls. Figure 3.30 C'

and D' show significant decrease in full length TrkB levels upon *T. gondii* infection in B6 wt and B6-p75^{NTR} ko mice. Descriptive statistic of fig. 3.30 are listed in table 3.25.

Table 3.26: Descriptive statistics for TrkB protein level in *T. gondii* infected B6 wt and B6-p75^{NTR} ko mice (fig. 3.31)

Genotype	CNS area	*T. gondii*	TrkB isoform	Mean±SEM
B6 wt	Hippocampus	-	FL	normalized to 1
B6 wt	Hippocampus	-	T1	normalized to 1
B6 wt	Hippocampus	4 w	FL	0,9329±0,2271
B6 wt	Hippocampus	4 w	T1	0,5615±0,1218
B6 wt	Hippocampus	8 w	FL	0,5172±0,09620
B6 wt	Hippocampus	8 w	T1	0,3192±0,06385
B6-p75^{NTR} ko	Hippocampus	-	FL	0,8947±0,08983
B6-p75^{NTR} ko	Hippocampus	-	T1	0,9212±0,1323
B6-p75^{NTR} ko	Hippocampus	4 w	FL	0,8266±0,07342
B6-p75^{NTR} ko	Hippocampus	4 w	T1	0,6681±0,1647
B6-p75^{NTR} ko	Hippocampus	8 w	FL	0,5202±0,2386
B6-p75^{NTR} ko	Hippocampus	8 w	T1	0,4873±0,04127

Figure 3.31 shows the effect of 4 w and 8 w chronic *T. gondii* infection on TrkB protein levels (both isoforms, full length and T1) in hippocampal tissue of B6 wt and B6-p75^{NTR} ko mice. Figure 3.31 A shows representative protein bands from Western blots. Differences in the single panels are observed with a trend of reduced TrkB isoforms in *T. gondii* infected mice in both genotypes. Figure 3.31 B shows that there is no significant difference in the truncated TrkB isoform (T1) in B6 wt controls compared to the B6-p75^{NTR} ko mice. Figure 3.31 C shows a significant decrease in truncated TrkB levels upon *T. gondii* infection in B6 wt mice. Figure 3.31 D shows no significant decrease in truncated TrkB levels upon *T. gondii* infection in B6-p75^{NTR} ko mice. Figure 3.31 B' shows no significant increase in full length TrkB in B6-p75^{NTR} ko mice compared to the B6 wt controls. Figure 3.30 C' and D' show no significant differences in full length TrkB levels upon *T. gondii* infection in B6 wt and B6-p75^{NTR} ko mice. Descriptive statistic of fig. 3.31 are listed in table 3.26.

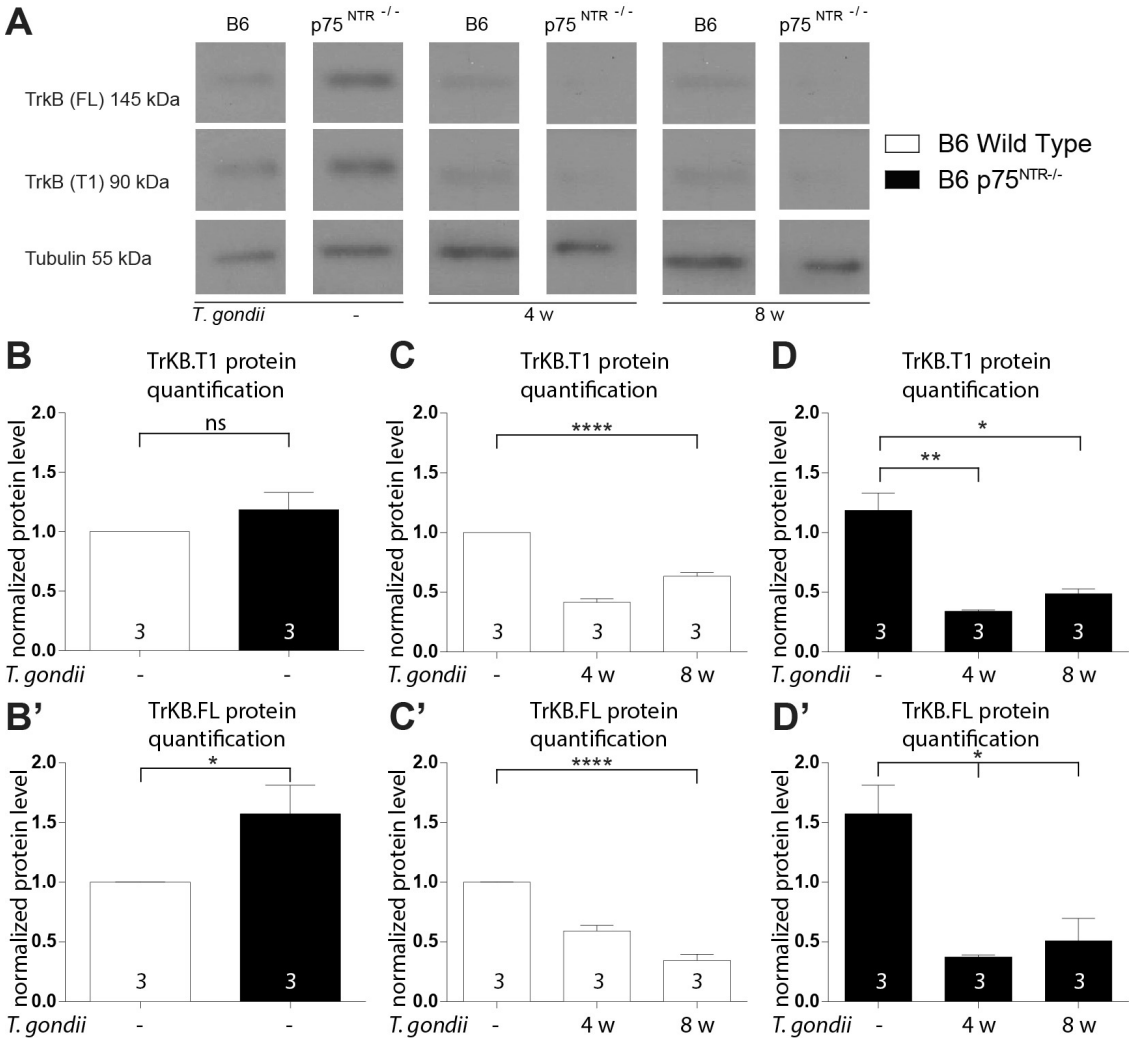

Figure 3.30: Quantification of TrkB (T1 and full length) in cortical brain tissue of B6 wt and B6-p75^{NTR} ko controls and in 4 w and 8 w *T. gondii* infected mice (A) Exemplified Western blots. The antibodies used were anti-TrkB (rabbit, polyclonal, Milipore 07-225, 1:2000) and anti-Tubulin (mouse monoclonal, Sigma-Aldrich, ® T9026, 1:10000) **(B, B')** To B6 control mice normalized amount of TrkB (T1 and full length) in p75$^{NTR-/-}$ mice in brain tissue. **(C, C')** To B6 control mice normalized amount of TrkB (T1 and full length) in 4 w and 8 w *T. gondii* infected B6 mice. **(D, D')** To B6 control mice normalized amount of TrkB (T1 and full length) in control, 4 w and 8 w *T. gondii* infected p75$^{NTR-/-}$ mice. Data presented as mean ± SEM, p*<0.05; p**<0.01; p***<0.001; p****<0.0001.

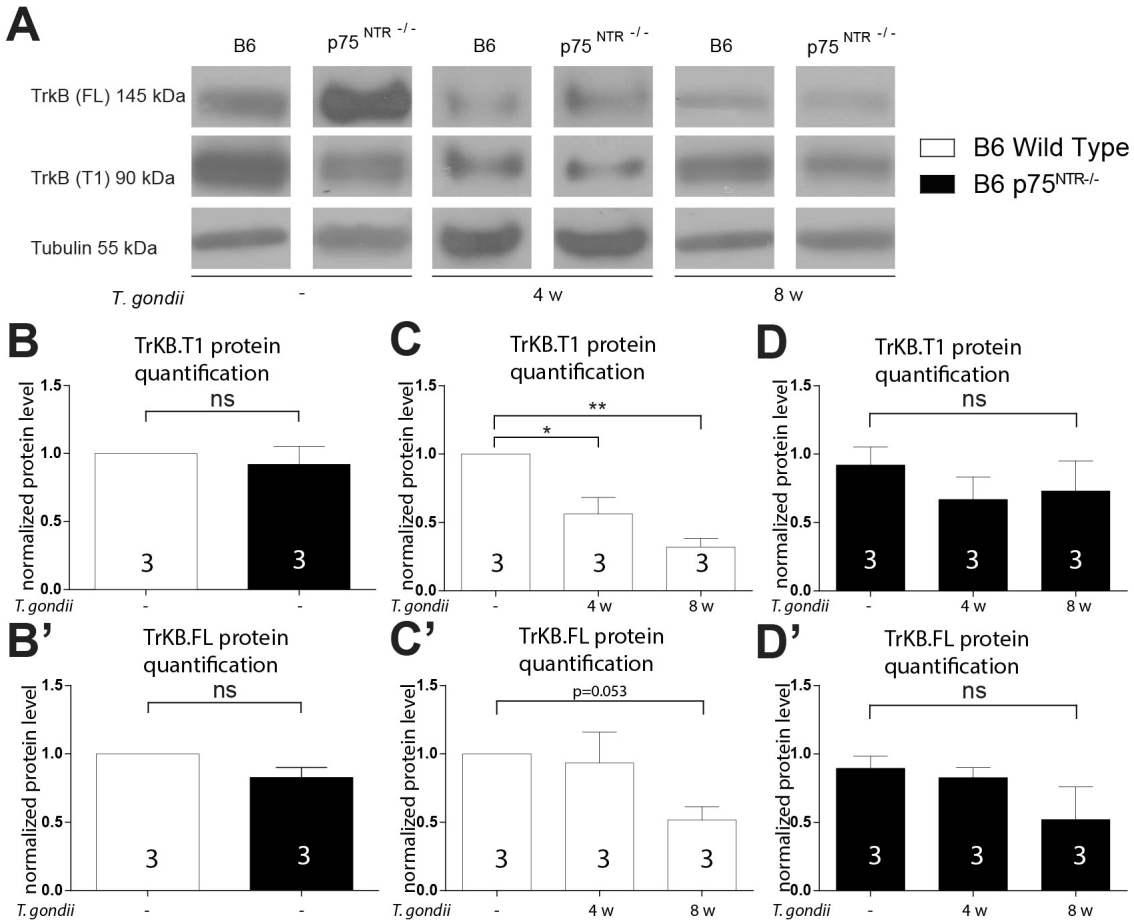

Figure 3.31: Quantification of TrkB (T1 and full length) in hippocampal brain tissue of B6 wt and B6-p75^{NTR} ko controls and in 4 w and 8 w *T. gondii* infected mice (A) Exemplified Western blots. The antibodies used were anti-TrkB (rabbit, polyclonal, Milipore 07-225, 1:2000) and anti-Tubulin (mouse monoclonal, Sigma-Aldrich, ® T9026, 1:10000) **(B, B')** To B6 control mice normalized amount of TrkB (T1 and full length) in p75$^{NTR-/-}$ mice in brain tissue. **(C, C')** To B6 control mice normalized amount of TrkB (T1 and full length) in 4 w and 8 w *T. gondii* infected B6 mice. **(D, D')** To B6 control mice normalized amount of TrkB (T1 and full length) in control, 4 w and 8 w *T. gondii* infected p75$^{NTR-/-}$ mice. Data presented as mean ± SEM, p*<0.05; p**<0.01; p***<0.001; p****<0.0001.

Table 3.27: Descriptive statistics for $p75^{NTR}$ protein level in *T. gondii* infected BALB/c wt mice (fig. 3.32)

Genotype	CNS area	*T. gondii*	Mean±SEM
BALB/c wt	Cortex	-	normalized to 1
BALB/c wt	Cortex	8 w	0,3570±0,06751 of control

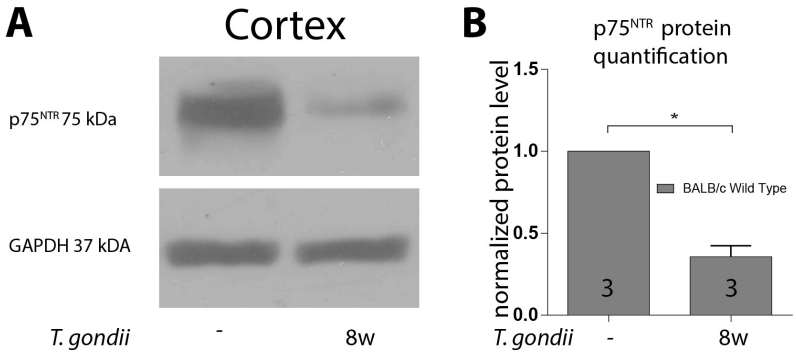

Figure 3.32: Quantification of $p75^{NTR}$ in cortical brain tissue of BALB/c wt controls and in 8 w *T. gondii* infected B6 wt mice (A, B) Exemplified Western blots. The antibodies used were anti-$p75^{NTR}$ (rabbit, polyclonal,abcam ab38335, 1:1000) and anti-GAPDH (rabbit polyclonal, Acris AP21839PUN, 1:3000) **(A', B')** To control mice normalized amount of $p75^{NTR}$ in cortical brain tissue of 8 w *T. gondii* infected BALB/c wt mice. Data presented as mean ± SEM, p*<0.05; p**<0.01; p***<0.001; p****<0.0001.

3.3.2 $p75^{NTR}$ and both isoforms of TrkB are reduced by chronic *T. gondii* infection in BALB/c wt mice

To elucidate whether the effect on neurotrophin receptor levels upon *T. gondii* infection is mouse strain specific BALB/c wt mice were also analyzed for their $p75^{NTR}$ and TrkB levels.

Figure 3.32 shows the effect of 8 w chronic *T. gondii* infection on $p75^{NTR}$ protein levels in the cortex of BALB/c wt mice. Figure 3.32 A shows representative protein bands from Western blots. While the internal standard (GAPDH) is equally distributed in BALB/c wt controls and 8 w *T. gondii* infected BALB/c wt mice, $p75^{NTR}$ levels are reduced in *T. gondii* infected BALB/c wt mice. Figure 3.29 B shows a significant reduction in $p75^{NTR}$ protein levels in 8 w *T. gondii* infected BALB/c wt mice compared to the control. Descriptive statistic of fig. 3.32 are listed in table 3.27.

Figure 3.33 shows the effect of 4 w and 8 w chronic *T. gondii* infection on TrkB protein levels (both isoforms, full length and T1) in hippocampal and cortical tissue

Table 3.28: Descriptive statistics for TrkB protein level in *T. gondii* infected B6 wt and B6-p75^{NTR} ko mice (fig. 3.33)

Genotype	CNS area	*T. gondii*	TrkB isoform	Mean±SEM
BALB/c wt	Hippocampus	-	FL	normalized to 1
BALB/c wt	Hippocampus	-	T1	normalized to 1
BALB/c wt	Hippocampus	8 w	FL	0,8361±0,08320
BALB/c wt	Hippocampus	8 w	T1	1,048±0,1798
BALB/c wt	Cortex	-	FL	normalized to 1
BALB/c wt	Cortex	-	T1	normalized to 1
BALB/c wt	Cortex	8 w	FL	0,5413±0,06206
BALB/c wt	Cortex	8 w	T1	0,4783±0,04024

of BALB/c wt mice. Figure 3.33 A shows representative protein bands from Western blots from hippocampal tissue. Differences in the single panels are observed with a trend of reduced full length TrkB in 8 w *T. gondii* infected BALB/c wt mice. Figure 3.33 B and B' show that there is no significant difference in both TrkB isoforms in BALB/c wt controls compared to the 8 w *T. gondii* infected BALB/c wt mice in hippocampal tissue. Figure 3.33 C shows representative protein bands from Western blots from cortical tissue. Differences in the single panels are observed with a trend of reduced full length TrkB and truncated TrkB in 8 w *T. gondii* infected BALB/c wt mice. Figure 3.33 D and D' show significant decrease in both TrkB isoform levels upon *T. gondii* infection in BALB/c wt mice. Descriptive statistic of fig. 3.33 are listed in table 3.28.

3.3.2.1 Transgenic mice overexpress TrkB isoforms

The results showing that *T. gondii* infection decreases TrkB in B6 an BALB/c mice promted to follow this information up by infecting mice overexpressing TrkB to elucidate the effect neuronal architecture and microglial activation. To validate existing transgenic mouse lines indeed overexpress TrkB isoforms, Western blot analyzes was performed.

Figure 3.34 shows the effect on TrkB protein levels in TrkB.T1+ and TrkB.TK+ compared to B6 wt controls. Figure 3.34 A shows representative protein bands from Western blots. While the internal standard (Tubulin) is equally distributed in the B6 wt control and TrkB.T1+ mouse, the truncated TrkB isoform (TrkB.T1) is clearly increased in the TrkB.T1+ mouse while the full length isoform is not visibly altered. Figure 3.34 A' shows a significant increase in truncated TrkB (TrkB.T1)

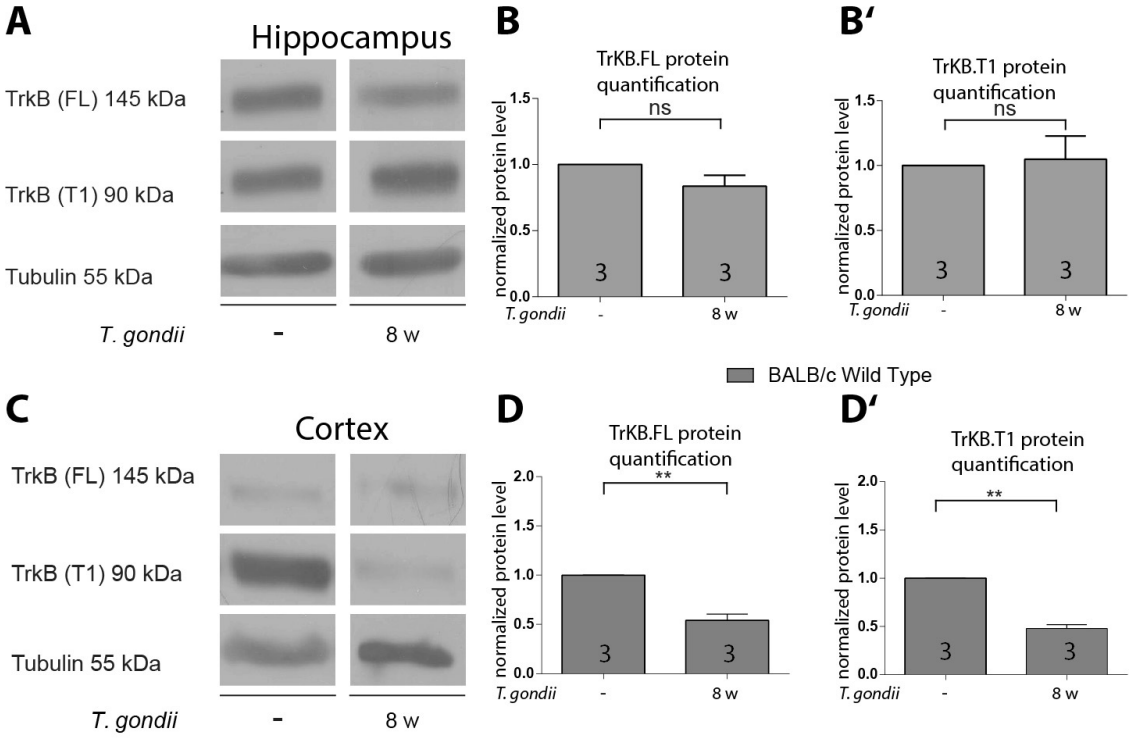

Figure 3.33: Quantification of TrkB (T1 and full length) in cortical and hippocampal brain tissue of BALB/c wt controls and in 8 w *T. gondii* infected BALB/c wt mice (A, C) Exemplified Western blots. The antibodies used were anti-TrkB (rabbit, polyclonal, Milipore 07-225, 1:2000) and anti-Tubulin (mouse monoclonal, Sigma-Aldrich, ® T9026, 1:10000) **(B, B', D, D')** To BALB/c wt control mice normalized amount of TrkB (T1 and full length) in 8 w *T. gondii* infected BALB/c wt mice in brain tissue. Data presented as mean ± SEM, p*<0.05; p**<0.01; p***<0.001; p****<0.0001.

in the TrkB.T1+ mouse compared to the B6 wt control. Figure 3.34 A" shows no significant differences in full length TrkB between the TrkB.T1+ mouse and the B6 wt control. Figure 3.34 B shows representative protein bands from Western blots. While the internal standard (Tubulin) is equally distributed in the B6 wt control and TrkB.TK+ mouse, the full length TrkB isoform shows a bigger band in the TrkB.TK+ mouse compared to the B6 wt control. The truncated isoform band in contrast slightly thinner in the TrkB.TK+ mouse compared to the B6 wt control. Figure 3.34 B' shows a significant decrease in truncated TrkB in the TrkB.TK+ mouse compared to the B6 wt control. Figure 3.34 B" shows a significant increase in full length TrkB in the TrkB.TK+ mouse compared to the B6 wt control. Descriptive statistics for fig. 3.34 are listed in table 3.29.

Table 3.29: Descriptive statistics for TrkB protein level in TrkB.T1+ and TrkB.TK+ mice compared to B6 wt controls (fig. 3.34). he brain tissue was a complete brain homogenate.

Genotype	TrkB isoform	Mean±SEM
B6 wt	FL	normalized to 1
B6 wt	T1	normalized to 1
TrkB.T1+	FL	1,698±0,2022
TrkB.T1+	T1	3,439±0,6720
TrkB.TK+	FL	5,470±1,011
TrkB.TK+	T1	0,5201±0,02452

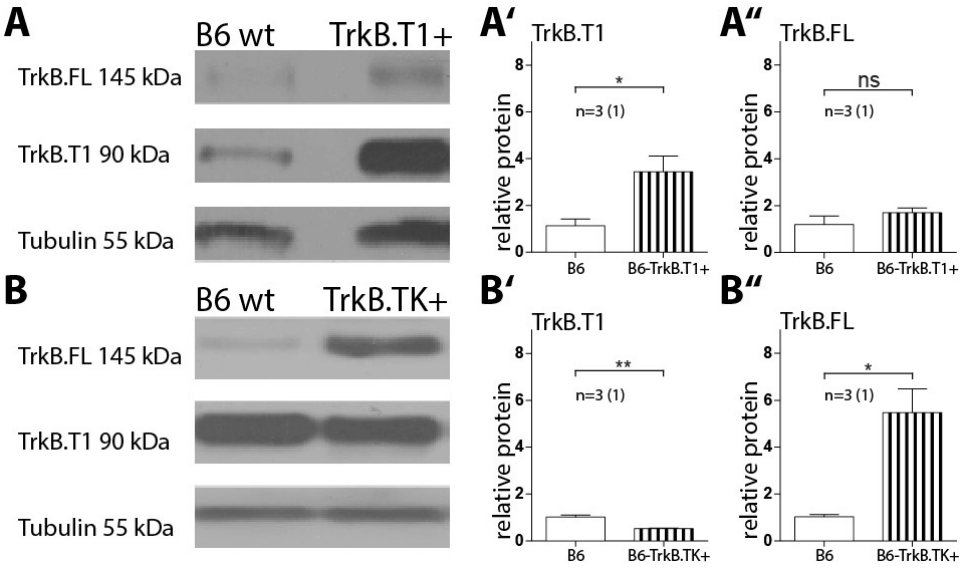

Figure 3.34: Quantification of TrkB (T1 and full length) in brain tissue of TrkB.T1+, TrkB.TK+ and B6 wt control mice (A, B) Exemplified Western blots. The antibodies used were anti-TrkB (rabbit, polyclonal, Milipore 07-225, 1:2000) and anti-Tubulin (mouse monoclonal, Sigma-Aldrich, ® T9026, 1:10000). **A', A", B', B"** To B6 wt control mice normalized amount of TrkB (T1 and full length) in brain tissue of TrkB.T1+ and TrkB.TK+ mice. Data presented as mean ± SEM. * = $p < 0.05$, **= $p < 0.01$, student's *t*-test.

4 Discussion

Neuroinflammation is thought to be one major risk factor from which the parthenogenesis of various neurodegenerative diseases originates. The factors contributing to the difficulties understanding neuroinflammation are diverse. One of the most intriguing properties is the CNS' inherent immune system. CNS has long been described as being immune privileged with the BBB restricting access to the neuronal structures and with the microglia, representing the CNS' immune system. In order to understand neuroinflammation the interaction of the different cell populations of the CNS needs to be understood. The neurotrophic system has been studied for its role in neuronal maintenance for the last decades. Neurotrophins, secreted growth factors, signal through neurotrophin receptors and mediate neuronal survival, differentiation, growth and are crucial for hippocampal learning mechanisms. The past decade brought to attention that neurotrophins are not exclusively expressed and acting in neurons and astrocytes, but in microglia and other cell populations of the immune system (Meeker & Williams, 2014).

As a model for neuroinflammation, chronic CNS infection by *Toxoplasma gondii* was chosen. After initial infection, this parasite takes up permanent residence in the CNS to protect itself from the adaptive immune system of the host. The transmission of *T. gondii* is facilitated by its ability to modify its host's behavior. A specific manipulation of the intermediate host's behavior is typical for certain parasites for their own selective benefit. Classic examples for this manipulation hypothesis concern transmission through the food chain: an immature parasite resides in an intermediate host, that must be eaten by a predatory definitive host before the parasite can reach maturity and complete its sexual life cycle. By altering the intermediate host's behavior, the parasite increases the exposure of that very host to the definite host. *T. gondii* provides a convincing example of such a manipulatory parasite. Its definitive hosts are all members of the cat family (Felidae). This is in accordance with the observation that *T. gondii* infected mice lose their natural fear of the odor of cats and become instead attracted to cat urine (Berdoy

et al., 2000). Additionally, it was shown that *T. gondii* infection affected learning and memory in rats during Morris water maze experiments (Daniels *et al.*, 2014).

In this work the effect of chronic murine neuroinflammation on the dendritic architecture of B6 WT controls, the B6-p75$^{NTR-/-}$ mutant, and a more immunologically robust mouse strain to *T. gondii* infection (BALB/c), was investigated. As the immune response in the CNS is mainly mediated by microglia, additional experiments were aimed to gain, especially morphological, insights on the microglial response on prolonged neuroinflammation. Furthermore, it was investigated whether neurotrophin receptor levels were altered upon *T. gondii* infection.

4.1 Effects of p75^{NTR} on dendritic architecture in chronically *T. gondii* infected mice

A previous publication by Parlog *et al.* (2014) showed a significant loss in spine density in cortical pyramidal neurons in chronically *T. gondii* infected B6 mice and the decrease in dendritic complexity.

In accordance with these results, this work shows that in chronically *T. gondii* infected B6 control mice hippocampal CA1 neurons are significantly less complex compared to the untreated B6 control mice. The results also indicate that this phenotype develops over time during the infection as 4 w *T. gondii* infected B6 control mice show milder changes than the 8 w *T. gondii* infected B6 mice (fig. 3.1). Also, the dendritic spine density decreases upon *T. gondii* infection in cortical and hippocampal pyramidal neurons in B6 control animals compared to untreated controls. The data again indicates that the spine density decreases over time with 8 w infected B6 control mice showing the lowest dendritic spine density and the 4 w infected B6 control mice showing an intermediate phenotype between the B6 controls and the 8 w *T. gondii* infected B6 mice (section 3.1.3).

In contrast to the B6 WT animals, the B6-p75$^{NTR-/-}$ mice show no significant reduction in dendritic complexity on pyramidal CA1 neurons upon *T. gondii* infection (fig. 3.2) at all observed time point. However, a trend towards a decrease can be observed without statistical significance. Intriguingly also the dendritic spine density is not significantly altered 4 w infected with *T. gondii* in the hippocampal CA1 neurons and the basal tuft of cortical LV/VI pyramidal neurons. 8 w into *T. gondii* infection the dendritic decreased significantly in B6-p75$^{NTR-/-}$ mice, indicating that whatever mechanism slows the progression earlier during incubation is less

effective at the later time point.

In a direct comparison between the B6 WT and B6-p75$^{NTR-/-}$ mice show that similar to the results of Zagrebelsky *et al.* (2005) no significant difference in the dendritic architecture of hippocampal CA1 neurons can be observed. Additionally, the dendritic spine density is significantly increased in the basal tuft of CA1 neuron in the B6-p75$^{NTR-/-}$ mice compared to the B6 controls as well on apical dendrites of cortical LV/VI pyramidal neurons. Differences between these results and those of the publication from Zagrebelsky *et al.* in 2005 could be explained by the methods: The 2005 publication utilized mainly *in vitro* experiments and this work *ex vivo* tissue.

The results indicate that some of the effects chronic toxoplasmosis has on dendritic architecture in the cortex, and the hippocampus could be mediated via the p75^{NTR}. Indeed, parasites have shown to mimic neurotrophic factors to prevent for example caspase activation and thereby death of dopaminergic cells (Chuenkova and Pereira, 2003). In their study, a neuraminidase/*trans*-sialidase has been identified to mediate the observed effect, which they named parasite derived neurotrophic factor (PDNF). Although not identified to this date it is possible that *T. gondii* also secretes a protein which has a double function and effectively acts as a PDNF to manipulate host behavior via p75^{NTR}.

Another explanation derives from the concept that neurotrophin signaling operates on a finely tuned scale of receptor distribution. Any imbalance can have a great effect on neurons, e.g., imbalance of neurotrophin receptor isoforms TrkB.FL and TrkB.T1 induces neuronal death (Vidaurre *et al.*, 2012). Furthermore, it is well established that p75^{NTR} and TrkB act as counterparts in their modulation of neuronal plasticity (Chao, 2003). Any receptor dysregulation by the parasite includes the potential to drastically influence neuronal maintenance. Neurotrophin receptor levels are discussed below.

According to the motto form follows function these results indicate that by altering the form, the architecture of the neurons, their function could be changed too. The neuronal arborization and the spine density are defining for the capability of a neuron to participate in the communication. The dendritic spines represent the post-synapse, and reduced overall spines therefor represent a reduced connectivity for incoming signals of other neurons.

4.2 B6 mice and BALB/c mice illustrate substantially different progression of toxoplasmosis - chronic *vs* latent

Silva *et al.* showed in 2010 that B6 mice are more sensitive to *T. gondii* infection than BALB/c mice. The body weight of BALB/c mice indeed is not significantly decreased 4 and 8 weeks after *T. gondii* infection (fig. 3.10). In contrast, B6 mice (WT and $p75^{NTR-/-}$) lose body weight significantly upon *T. gondii* infection. During the experiments it was observed that the B6 mice showed reduced vitality: they did not struggle or fight handling by the experimenter. On the contrary, the BALB/c mice appeared more robust, tried to escape the experimenter and were more active in their cages. Intriguingly also the effect of prolonged *T. gondii* infection on neuronal architecture is less pronounced in BALB/c mice than in B6 mice. While a trend for a decrease in dendritic spine density was observed in hippocampal CA1 pyramidal neurons and cortical LV/VI pyramidal neurons it was only found to be significantly decreased in the basal tuft of CA1 neurons 8 w post infection. This is in strong contrast to what has been observed in the *T. gondii* infected B6 WT mice, where the decrease is significant in both neuron types, basally and apically, 4 w into the infection and even more pronounced 8 w into the infection. As later discussed also the microglial morphology upon *T. gondii* infection differs in these mouse strains (section 4.3).

These results indicate that toxoplasmosis in BALB/c mice indeed represents the latent state of the infection, in a way similar to that observed in immunocompetent humans (Welter *et al.*, 2007), while toxoplasmosis in B6 mice could be described as a chronic state of the infection (confusingly these terms are both used in the literature to describe the former, latent state), a situation in which the acute infection never switches to the latent phase. In the case of B6 mice it maybe best compared to human patients, which are immune deficient. In this patients, the parasite cannot be controlled by the immune system. Most prominently in patients suffering from the late stage of HIV infection (AIDS) or in patients receiving a donor organ, where the immune system is supressed to prevent rejection (Robert-Gangneux & Dardé, 2012; Da Silva Meira *et al.*, 2015; El Lakkis *et al.*, 2015). This leads to dangerous, in many cases life threatening encephalitis (Zhang *et al.*, 2014).

Interestingly Welter *et al.* could show in 2007 that BALB/c mice, which were

previously exposed to *Myocoptes musculinus* (small mites), became very sensitive to *T. gondii* infection similar to the B6 phenotype. This suggests that some immunological priming could possibly weaken the resistance to the parasite. They show that spleen cells had increased the levels of IL-4 in these double-infected mice. This alteration was associated with severe encephalitis. Another

As a result of the strong immunological challenge to B6 mice, it was not possible to perform any behavioral or electrophysiological experiments. This has been particularly underwhelming since the $p75^{NTRExonIV-/-}$ mutant crossbred with the *Thy1*-eGFP transgene is currently only available in B6 but not in BALB/c mice. Correlating morphological findings in the B6-$p75^{NTR-/-}$ mutant with behavioral experiments like the elevated plus maze or the Morris water maze are therefore currently not possible. Electrophysiological recordings, to estimate LTP and LTD for example, were also impossible by the need to rest the animals for at least 24 h in their final location before sacrificing and recording immediately after.

Another observation contributes to this issue: the virulence of the *T. gondii* strain ME49 type II has increased without any indication of the cause. The infections for this thesis were achieved by injecting 2 tissue cysts intraperitoneally. In consultation with Dr. Dunay on this issue, it was explained that when she started working with this strain, she used to inject up to 10 cysts and reduced the number over the years because of an inexplicable increase in virulence.

4.3 Microglial response to *T. gondii* infection depends on mouse strain

It has been established that acute toxoplasmosis initiates microglial response and activation (Chao, 1993; Schlüter 1995; Lüder, 1999, Fischer & Reichmann, 2001). Immunological response in *T. gondii* infected mice is commonly analyzed and characterized by FACS analysis to differentiate monocyte populations (Dunay & Sibley, 2010; Biswas *et al.*, 2015).

The previously underserved morphological analysis of the Iba1+ cells in B6 and BALB/c mice yields some intriguing results. In the B6 wild type and the BALB/c wild type control mice the microglia show the morphological phenotype associated with resting or surveillance in a CNS environment, which has not recently been insulted or infected: a small cell body and long, wavy processes and low levels of Iba1 immunoreactivity (Kettenmann *et al.*, 2011).

In contrast in *T. gondii* infected B6 and BALB/c mice Iba1+ cells alter their morphological phenotype substantially. In B6 mice (WT and $p75^{NTR-/-}$) the Iba1 staining depicts cells which do not resemble typical textbook microglia, activated or resting. The overlay of the Iba1 staining and the *Thy1*-eGFP shows that the microglia are wrapping the neurons in the *T. gondii* infected B6 mice. They extend to cover the cell soma of CA1 neurons and the primary apical dendrite. This association of Iba1+ cells with neuronal structures is so apparent that it can be perceived without the GFP overlay. Additionally, the Iba1 associates with what seems to be blood vessels. Microglial wrapping of neuronal cell bodies is also part of the phenotype observed after peripheral nerve axotomy (Moran & Greaber, 2004). This phenomenon has also been reported in hippocampal organotypic cultures after an ischemic insult and in the cerebral cortex during either acute focal inflammation (Trapp *et al.*, 2007) or following LPS injection (Chen *et al.*, 2012). Microglial wrapping (and synaptic stripping) is usually considered to be a neuroprotective process (Kreutzberg, 1996). Whether this wrapping is always neuroprotective is still not completely understood and discussed controversially (Yamada *et al.*, 2011; Chen *et al.*, 2014).

Iba1+ cells in BALB/c mice also alter their morphology upon *T. gondii* infection. In contrast to the B6 mice, manually counting Iba1+ cells is reliably precise in *T. gondii* infected BALB/c mice with DAPI co-staining. These cells resemble what has been described as activated microglia in the literature. The enlarged cell soma is typical. Also, the processes are less wavy and shorter and can best be described as being spiky. Also, no association with blood vessel was observed during experiments and analysis.

The Iba1 immunoreactivity increases manifold in B6 and BALB/c mice upon *T. gondii* infection compared to the controls, which is another indicator of microglial activation.

Although Silva *et al.* described in 2010 that B6 mice are more sensitive to *T. gondii* infection than BALB/c mice it has, to my best knowledge, never been shown that the microglia in these mice strains react completely different morphologically to the very same parasite infection, in their association with neurons and blood vessels. This raises the question whether it is valid to transfer microglial findings in mice, where they obviously depend on the genetic background, to any other species *T. gondii* can infect, including humans.

The analysis to estimate the concentration of Iba1+ cells in *T. gondii* infected B6

mice (WT and p75$^{NTR-/-}$)is not very precise, as the cells overlap and lose their individual shape. The DAPI co-staining, which makes manual counting in not-infected control mice reliably precise, is not sufficient to separate Iba1+ cells dependable in *T. gondii* infected B6 mice. Therefore the values estimated for Iba1+ cell concentration in *T. gondii* infected B6 mice could yield some inaccuracy and bias from manual counting. With the applied method of analysis, the Iba1+ cells in *T. gondii* infected B6 WT, and B6-p75$^{NTR-/-}$ can not be distinguished. It is nevertheless likely that the microglial concentration increases significantly in B6 and BALB/c mice upon *T. gondii* infection.

The results indicate that the effect of *T. gondii* infection on microglia activation is not mediated primarily by p75^{NTR} and that microglia in B6 and BALB/c mice react differently to the parasite. It has been shown before that the severity of *T. gondii* induced encephalitis in B6 mice is associated with increased VCAM-1 and ALCAM expression in the CNS and higher BBB permeability (Silva *et al.*, 2010).

In contrast to FACS analysis, which utilizes a variety of different markers to differentiate between monocyte populations, the morphological analysis of Iba1+ cells lacks a precise distinction. A co-staining with a anti-F4/80 antibody revealed the same finding as for the Iba1 staining. This means that the observed morphology in *T. gondii* infected mice is not derived of a cross-reaction with the anti-Iba1 antibody. F4/80 is another microglia marker. A differentiation between CNS native microglia and invading macrophages is not possible with Iba1 or F4/80.

4.4 Microglial concentration in B6-p75$^{NTRExonIV-/-}$ mice is increased compared to the wild type

Additionally to the effect of *T. gondii* infection on microglial concentration in B6 and BALB/c mice the microglial concentration in B6-p75$^{NTR-/-}$ controls was compared to B6 WT controls. Although not reaching the levels of *T. gondii* infected mice B6-p75$^{NTR-/-}$ control have significantly higher microglia concentration compared to the B6 WT control. Also, the higher immunoreactivity of Iba1 is significant compared to the B6 WT control (and the BALB/c). To the author's knowledge, microglial density in p75$^{NTR-/-}$ has never been analyzed. The p75^{NTR} is expressed on microglia and macrophages (Nakajima *et al.*, 1998, 2001; Dowling *et al.*, 1999). A mechanism or signaling pathway which indicates the lack of p75^{NTR} increases microglial proliferation is yet to be found. It is known that microglia promote

learning-dependent synapse formation through BDNF mediated synaptic pruning (Parkhurst *et al.*, 2013), whether $p75^{NTR}$ plays a role in this context is also unclear.

4.5 Decreased neurotrophin receptor protein levels in *T. gondii* infected mice

To gain further insight into the participation of neurotrophin signaling in *T. gondii* elicited neuroinflammation the amount of TrkB and $p75^{NTR}$ was measured using Western blot. Both neurotrophin receptors work in tandem and are thought to work in opposing manner. Both the receptors also form heterodimers, which alters their affinity to BDNF and NT-4.

B6 and BALB/c mice both show reduced $p75^{NTR}$ protein levels upon *T. gondii* infection in the cortex and both TrkB isoforms are also significantly reduced in the cortex, also in the B6-$p75^{NTR\text{-}/\text{-}}$ mutant. In the hippocampus, the amount of full-length TrkB is not significantly altered upon infection, but the *T. gondii* infected B6 WT mice show a decrease in trend. Solely in the *T. gondii* infected B6 WT mice the truncated TrkB isoform is significantly decreased upon *T. gondii* infection. The B6-$p75^{NTR\text{-}/\text{-}}$ is not affected, as well as the BALB/c strain. Interestingly the amount of full-length TrkB is higher in the cortex of B6-$p75^{NTR\text{-}/\text{-}}$ control mice compared to their B6 WT counterparts.

BDNF and NT-4, the neurotrophins activating TrkB, are predominantly expressed in the dentate gyrus and the CA3 region of the hippocampus but also less profound throughout the whole CNS (Conner *et al.*, 1997). A reduction in TrkB could possibly indicate reduced BNDF signaling. BDNF signaling is crucial for the maintenance of the neuronal network as it supports the survival of existing neurons and encourages the growth and differentiation of new neurons and synaptic connections. It has been shown that it is crucial for forming memories in the hippocampus (Korte *et al.*, 1995). On the other side of the scale, BNDF also activates $p75^{NTR}$, which is thought to counteract the BDNF-TrkB signaling. By also reducing *T. gondii* might be manipulatively numbing the host's neurotrophic system by down-regulating its receptors.

In preparation for future experiments, two additional B6 mutants were analyzed for their TrkB levels. The B6-TrkB.T1 mutant shows significantly higher TrkB.T1 when compared to the B6 WT while the full-length isoform is not altered. The B6-TrkB.TK+ mutant shows significantly less amount of TrkB.T1 when compared

to the B6 WT while the full-length isoform levels are significantly higher. These results confirm that the mutants overexpress one isoform each.

The third TrkB isoform, the T2, as well as TrkA and TrkC, were not analyzed in this work.

4.6 Inconsistencies in p75^{NTR} literature

One issue, which needs to be addressed, is that existing knowledge about the p75^{NTR} is mainly derived from two different genetic mutants. Lee *et al.* showed in 1992 that a targeted mutation in the exon III of the p75^{NTR} gene leads to deficits in the peripheral sensory nervous system (the p75^{NTR} gene contains six exons in total). Since then different groups used this model to study p75^{NTR} knock out in their research focus. Nearly a decade later von Schack *et al.* (2001) identified an isoform of the p75^{NTR} protein that derived from alternate splicing of the exon III in the p75^{NTR} gene locus. This isoform is also functionally intact in the mutant mouse line lacking the exon III by Lee *et al.* For this reason, von Schack *et al.* generated another mutant line, lacking the exon IV. The publication shows that mice with p75$^{NTR\text{-}ExonIV\text{-}/\text{-}}$ present drastic nervous system defects. In contrast to the mutant lacking the exon III it also reveals a previously unknown role of p75^{NTR} in the formation of blood vessels. Von Schack *et al.* show that the mutant lacking the exon III transcripts into the short s-p75^{NTR} transcript, which differs from the full-length p75^{NTR} (FL-p75^{NTR}) protein. In contrast to the FL-p75^{NTR}, the s-p75^{NTR} lacks three of the four cysteine-rich domains. They furthermore show that the s-p75^{NTR} is coexpressed with the FL-p75^{NTR} in human, rat, and mouse thereby seemingly highly conserved across the species. The p75^{NTR} exonIV lacking mutant in contrast to the 75^{NTR} exonIII lacking mutant lacks a discrete 62 KDa protein in Schwann cells. The lack of both p75^{NTR} proteins leads to a severe phenotype, e.g., partial perinatal lethality and additional defects in the vascular system that have not been observed in the exonIII lacking p75^{NTR} mutants.

Despite these insights the p75$^{NTR\text{-}ExonIII}$ null mutant continuous to be used in the field (Bui *et al.*, 2002; Barrett *et al.*, 2010). Its s-p75^{NTR} isoform is seldom discussed in the publications (Greferath *et al.*, 2000). Following that also review papers referring to this publication fail to explain the problematic nature of this mutant line. The p75$^{NTR\text{-}ExonIII}$ null mouse is simply called a null or p75^{NTR} knock out mouse (Greferath *et al.*, 2000; Barrett *et al.*, 2010). Also, the p75$^{NTR\text{-}ExonIV}$

null mutant is not undisputed. In 2004 Paul *et al.* published that a pro-apoptotic fragment of the $p75^{NTR}$ is expressed in this mutant mouse line. In accordance with von Schack *et al.* they show a lack of the 62 kDa transcript but an additional 26 kDa transcript, which is absent in the $p75^{NTR\text{-}ExonIII\text{-}/\text{-}}$ mutant. This fragment of the $p75^{NTR}$ protein contains a portion of the ECD (extracellular domain) and the transmembrane and intracellular domains. Overexpression of this 26 KDa protein fragment in heterologous cells, in the 2004 study, resulted in an activation of Jun kinase and also induces pro-caspase-3 cleavage. This indicates that the fragment activates $p75^{NTR}$ signaling cascades in the $p75^{NTR\text{-}ExonIV\text{-}/\text{-}}$ mutant. Paul *et al.* conclude that the $p75^{NTR\text{-}ExonIV\text{-}/\text{-}}$ phenotype as seen by von Schack *et al.* in 2001 could reflect a gain-of-function mutation rather than loss of $p75^{NTR}$ function. In 2011 Bogenmann *et al.* introduced a mutant line with floxed exons IV-VI. It has been studied, for example, by Baeza-Raja *et al.* in 2016 and directly been compared to the exon III null mutant, described as $p75^{NTR}$KO in their publication, again without discussing ramifications.

This further questions existing understanding of the $p75^{NTR}$. Its complex signaling pathways and multiple interaction partners are already complicating the research. Studies have for example shown that neuron type specific signaling by the $p75^{NTR}$ death receptor is regulated by differential proteolytic cleavage (Vicario *et al.*, 2015). This work utilized the $p75^{NTR\text{-}ExonIV}$ null mutant without reassessing the 26 KDa fragment described by Paul *et al.* in 2004. Optimally another mutant mouse line would be generated, lacking the complete $p75^{NTR}$ gene. A floxed $p75^{NTR}$ would open up even more possibilities to study the impact of $p75^{NTR}$ during development and in mature mice. Consequently, some crucial experiments and results, which emerged in the last 25 years, need to be repeated and compared between established mutant mouse lines.

4.7 Conclusions and outlook

On the one hand, the results indicate that *T. gondii* infection in B6 mice does not reflect the latent phase of toxoplasmosis but a chronic inflammation caused by the parasite, similarly observed in immune deficient humans. Consequently, the results are not adequate to explain any of the subtle behavior changes upon *T. gondii* infection observed in mouse strains which develop latent toxoplasmosis. The contribution of $p75^{NTR}$ to the *T. gondii* inflicted regression of neuronal struc-

tures is therefore possibly less specific to the parasite manipulating the host than to prolonged CNS inflammation or even encephalitis. The results indicate that in B6-(p75$^{\text{NTRExonIV-/-}}$) mice the decrease in dendritic spine density and dendritic complexity of excitatory pyramidal neurons in the hippocampus and the cortex is slowed in its progression compared to the B6 WT control. This is especially noticeably 4 w into the *T. gondii* infection. However, 8 w into the infection the spine density is effectively as much decreased in the mutant as in the B6 WT mice. Solely the dendritic complexity proves to be more robust 8 w into the infection in the mutant. Shortly after the B6 mice succumb to the infection. Intriguingly the hippocampal amount of TrkB is significantly reduced in the B6 WT mice and not significantly altered in the B6-p75$^{\text{NTRExonIV-/-}}$ upon the infection. This shows that to some extend the degenerative effect of *T. gondii* infection in B6 mice could be mediated or amplified by p75$^{\text{NTR}}$ and TrkB signaling, both of which are activated by BDNF.

On the other hand *T. gondii* infection in BALB/c mice could constitute latent toxoplasmosis, as described in immune competent humans. While in accordance with the generally stronger resistance to *T. gondii* also the neurons are less affected by its infection. Nevertheless, the total amount of p75$^{\text{NTR}}$ and TrkB is reduced in the cortex, indicating a possible manipulation of the parasite within the CNS via the neurotrophic system.

While the microglia (Iba1+ cells) were clearly activated upon *T. gondii* infection in the B6 (mutant and WT) and the BALB/c mice, conclusive statements about differences in the total number of Iba1+ cells are unreasonable at this point with the aforementioned uncertainties in the distinction of single cells in the B6 mice because of the extensive morphological changes. It is still noteworthy to point out the vivid difference in microglial morphology upon *T. gondii* infection between the B6 and the BALB/c mice. A connection between microglial response to the parasite and resistance to its effects on the host is yet unclear.

The amount of Iba1+ cells is significantly higher in the B6-p75$^{\text{NTRExonIV-/-}}$ mutant than in the B6 controls. While p75$^{\text{NTR}}$ is normally expressed on microglia, it is not clear how it could affect proliferation.

As for the outlook, the results have shown that in B6 as well as in BALB/c mice TrkB protein levels are reduced upon *T. gondii* infection. There are two B6 mutant mouse lines available, each overexpressing one of the two TrkB isoforms. Analyzing these would currently be the easiest and fastest way to generate more

data on neurotrophin receptor involvement in *T. gondii* inflicted neuroinflammation. From a methodological viewpoint, it could be beneficial to refrain from the Western blot and instead perform qPCR and ELISA experiments for a better comparability between the different categories and a higher data throughput with a simpler workflow.

To gain a more comprehensive understanding of $p75^{NTR}$ involvement in CNS immunity, a conditional full knockout mutant should be generated and bred into the different mouse strains. Firstly to disentangle the results from any translated $p75^{NTR}$ fragments which are present in the $p75^{NTRExonIII-/-}$ mutant and could be present in the $p75^{NTRExonIV-/-}$, secondly to differentiate the results, depending on the cell type expressing or lacking the receptor. Optimally some of the most crucial insights into $p75^{NTR}$ signaling, which were generated by the present mutant lines, would be experimentally verified. Conflicting results could possibly indicate signaling roles by the aforementioned protein fragments.

While the B6 mouse strain is not suitable to study latent toxoplasmosis, it could be used to examine chronic neuroinflammation with an active pathogen in contrast to the more *in vitro* like approach with LPS treatments mimicking CNS infections or insults. Additionally, microglial neuron wrapping could be studied with this model to gain further insights into the pending question whether it is neuroprotective or neurotoxic by infecting B6 mice with the wide array of available transgenes for this strain.

The BALB/c mouse strain, however, reflects the latent toxoplasmosis and could be used to study the more subtle CNS changes promoted by the parasite to alter the behavior. It is, therefore, necessary to breed the genetic tools (*Thy1*-eGFP, neurotrophin receptor mutants) into the BALB/c background. That would open up the possibility to correlate behavioral and electrophysiological data to the morphological results of neurons and microglia reaction to *T. gondii* infection presented in this work.

5 Literature

Abbott NJ, Rönnbäck L, Hansson E (2006) Astrocyte–endothelial interactions at the blood–brain barrier. Nat Rev Neurosci 7:41–53.

Akiyama H et al. (2000) Inflammation and Alzheimer's disease. Neurobiol Aging 21:383–421.

Allan LE, Petit GH, Brundin P (2010) Cell transplantation in Parkinson's disease: problems and perspectives. Curr Opin Neurol 23:426–432.

Aloisi F (1999) The role of microglia and astrocytes in CNS immune surveillance and immunopathology. Adv Exp Med Biol 468:123–133.

Amor S, Puentes F, Baker D, van der Valk P (2010) Inflammation in neurodegenerative diseases. Immunology 129:154–169.

Ankeny DP, Popovich PG (2009) Mechanisms and implications of adaptive immune responses after traumatic spinal cord injury. Neuroscience 158:1112–1121.

Aprile-Garcia F, Antunica-Noguerol M, Budziñski ML, Liberman AC, Arzt E (2014) Novel insights into the neuroendocrine control of inflammation: the role of GR and PARP1. Endocr Connect 3:R1–R12.

Asami T, Ito T, Fukumitsu H, Nomoto H, Furukawa Y, Furukawa S (2006) Autocrine activation of cultured macrophages by brain-derived neurotrophic factor. Biochem Biophys Res Commun 344:941–947.

Atmaca HT, Kul O, Karakuş E, Terzi OS, Canpolat S, Anteplioğlu T (2014) Astrocytes, microglia/macrophages, and neurons expressing Toll-like receptor 11 contribute to innate immunity against encephalitic Toxoplasma gondii infection. Neuroscience 269:184–191.

Baeza-Raja B, Sachs BD, Li P, Christian F, Vagena E, Davalos D, Le Moan N, Ryu

JK, Sikorski SL, Chan JP, Scadeng M, Taylor SS, Houslay MD, Baillie GS, Saltiel AR, Olefsky JM, Akassoglou K (2016) p75 neurotrophin receptor regulates energy balance in obesity. Cell Rep 14:255–268.

Barde YA, Edgar D, Thoenen H (1982) Purification of a new neurotrophic factor from mammalian brain. EMBO J 1:549–553.

Barrett GL, Reid CA, Tsafoulis C, Zhu W, Williams DA, Paolini AG, Trieu J, Murphy M (2010) Enhanced spatial memory and hippocampal long-term potentiation in p75 neurotrophin receptor knockout mice. Hippocampus 20:145–152.

Beattie MS, Harrington AW, Lee R, Kim JY, Boyce SL, Longo FM, Bresnahan JC, Hempstead BL, Yoon SO (2002) ProNGF Induces p75-Mediated Death of Oligodendrocytes following Spinal Cord Injury. Neuron 36:375–386.

Beggs S, Trang T, Salter MW (2012) P2X4R+ microglia drive neuropathic pain. Nat Neurosci 15:1068–1073.

Berdoy M, Webster JP, Macdonald DW (2000) Fatal attraction in rats infected with Toxoplasma gondii. Proc R Soc B Biol Sci 267:1591–1594.

Berkemeier LR, Winslow JW, Kaplan DR, Nikolics K, Goeddel DV, Rosenthal A (1991) Neurotrophin-5: a novel neurotrophic factor that activates trk and trkB. Neuron 7:857–866.

Bibel M, Hoppe E, Barde YA (1999) Biochemical and functional interactions between the neurotrophin receptors trk and p75NTR. EMBO J 18:616–622.

Biswas A, Bruder D, Wolf SA, Jeron A, Mack M, Heimesaat MM, Dunay IR (2015) Ly6Chigh Monocytes Control Cerebral Toxoplasmosis. J Immunol:1402037.

Block ML, Hong J-S (2005) Microglia and inflammation-mediated neurodegeneration: multiple triggers with a common mechanism. Prog Neurobiol 76:77–98.

Bogenmann E, Thomas PS, Li Q, Kim J, Yang L-T, Pierchala B, Kaartinen V (2011) Generation of Mice with a Conditional Allele for the p75NTR Neurotrophin Receptor Gene. Genes N Y N 2000 49:862–869.

Brosseron F, Krauthausen M, Kummer M, Heneka MT (2014) Body fluid cytokine levels in mild cognitive impairment and Alzheimer's disease: a comparative overview. Mol Neurobiol 50:534–544.

Bruno MA, Cuello AC (2006) Activity-dependent release of precursor nerve growth factor, conversion to mature nerve growth factor, and its degradation by a protease cascade. Proc Natl Acad Sci 103:6735–6740.

Bui NT, König H-G, Culmsee C, Bauerbach E, Poppe M, Krieglstein J, Prehn JHM (2002) p75 neurotrophin receptor is required for constitutive and NGF-induced survival signalling in PC12 cells and rat hippocampal neurones. J Neurochem 81:594–605.

Burnette WN (1981) "Western blotting": electrophoretic transfer of proteins from sodium dodecyl sulfate–polyacrylamide gels to unmodified nitrocellulose and radiographic detection with antibody and radioiodinated protein A. Anal Biochem 112:195–203.

Camacho-Arroyo I, López-Griego L, Morales-Montor J (2009) The role of cytokines in the regulation of neurotransmission. Neuroimmunomodulation 16:1–12.

Carruthers VB, Giddings OK, Sibley LD (1999) Secretion of micronemal proteins is associated with toxoplasma invasion of host cells. Cell Microbiol 1:225–235.

Carson MJ, Doose JM, Melchior B, Schmid CD, Ploix CC (2006) CNS immune privilege: hiding in plain sight. Immunol Rev 213:48–65.

Cauller LJ, Connors BW (1994) Synaptic physiology of horizontal afferents to layer I in slices of rat SI neocortex. J Neurosci 14:751–762.

Chao CC, Hu S, Gekker G, Novick WJ, Remington JS, Peterson PK (1993) Effects of cytokines on multiplication of Toxoplasma gondii in microglial cells. J Immunol 150:3404–3410.

Chao MV (1994) The p75 neurotrophin receptor. J Neurobiol 25:1373–1385.

Chao MV, Bothwell MA, Ross AH, Koprowski H, Lanahan AA, Buck CR, Sehgal A (1986) Gene transfer and molecular cloning of the human NGF receptor. Science 232:518–521.

Chen Z, Jalabi W, Hu W, Park H-J, Gale JT, Kidd GJ, Bernatowicz R, Gossman ZC, Chen JT, Dutta R, Trapp BD (2014) Microglial displacement of inhibitory synapses provides neuroprotection in the adult brain. Nat Commun 5.

Chen Z, Jalabi W, Shpargel KB, Farabaugh KT, Dutta R, Yin X, Kidd GJ, Bergmann CC, Stohlman SA, Trapp BD (2012) Lipopolysaccharide-induced microglial activation and neuroprotection against experimental brain injury is independent of hematogenous TLR4. J Neurosci Off J Soc Neurosci 32:11706–11715.

Chuenkova MV, Pereira MA (2003) PDNF, a human parasite-derived mimic of neurotrophic factors, prevents caspase activation, free radical formation, and death of dopaminergic cells exposed to the Parkinsonism-inducing neurotoxin MPP+. Brain Res Mol Brain Res 119:50–61.

Conner JM, Lauterborn JC, Yan Q, Gall CM, Varon S (1997) Distribution of brain-derived neurotrophic factor (BDNF) protein and mRNA in the normal adult rat CNS: evidence for anterograde axonal transport. J Neurosci Off J Soc Neurosci 17:2295–2313.

Coull JAM, Beggs S, Boudreau D, Boivin D, Tsuda M, Inoue K, Gravel C, Salter MW, De Koninck Y (2005) BDNF from microglia causes the shift in neuronal anion gradient underlying neuropathic pain. Nature 438:1017–1021.

Cuartas A, Jorge M (2014) Cognition and inflammation: the role of cytokines in cognitive performance. Int J Psychol Res 7:8–10.

da Silva Meira C, Pereira-Chioccola VL, Vidal JE, Motoie G, da Costa-Silva TA, Gava R, de Sousa Dantas DS, de Andrade Batista TP, Kassab MJO, Bazzi M, Prestes DP, Strelow VL, Massaia AW, Audi D, Lago MM, Moreira CHV (n.d.) Evolution of Cytokine Profile during the treatment of Cerebral Toxoplasmosis in HIV-infected Patients. J Immunol Methods Available at: http://www.sciencedirect.com/science/article/pii/S0022175915300211 [Accessed July 16, 2015].

Damsker JM, Hansen AM, Caspi RR (2010) Th1 and Th17 cells: adversaries and collaborators. Ann N Y Acad Sci 1183:211–221.

Daniels BP, Sestito SR, Rouse ST (n.d.) An expanded task battery in the Morris water maze reveals effects of Toxoplasma gondii infection on learning and memory in rats. Parasitol Int

Davalos D, Grutzendler J, Yang G, Kim JV, Zuo Y, Jung S, Littman DR, Dustin ML, Gan W-B (2005) ATP mediates rapid microglial response to local brain injury in vivo. Nat Neurosci 8:752–758.

David S, Fry EJ, López-Vales R (2008) Novel roles for Nogo receptor in inflammation and disease. Trends Neurosci 31:221–226.

Deinhardt K, Kim T, Spellman DS, Mains RE, Eipper BA, Neubert TA, Chao MV, Hempstead BL (2011) Neuronal growth cone retraction relies on proneurotrophin receptor signaling through Rac. Sci Signal 4:ra82.

del Rey A, Balschun D, Wetzel W, Randolf A, Besedovsky HO (2013) A cytokine network involving brain-borne IL-1β, IL-1ra, IL-18, IL-6, and TNFα operates during long-term potentiation and learning. Brain Behav Immun 33:15–23.

del Río-Hortega J (1932) Microglia. Cytol Cell Pathol Nerv Syst 2:482–534.

Deli MA, Ábrahám CS, Kataoka Y, Niwa M (2005) Permeability Studies on In Vitro Blood–Brain Barrier Models: Physiology, Pathology, and Pharmacology. Cell Mol Neurobiol 25:59–127.

Dohgu S, Takata F, Yamauchi A, Nakagawa S, Egawa T, Naito M, Tsuruo T, Sawada Y, Niwa M, Kataoka Y (2005) Brain pericytes contribute to the induction and up-regulation of blood–brain barrier functions through transforming growth factor-β production. Brain Res 1038:208–215.

Doll DN, Barr TL, Simpkins JW (2014) Cytokines: their role in stroke and potential use as biomarkers and therapeutic targets. Aging Dis 5:294–306.

Domeniconi M, Hempstead BL, Chao MV (2007) Pro-NGF secreted by astrocytes promotes motor neuron cell death. Mol Cell Neurosci 34:271–279.

Dowling P, Ming X, Raval S, Husar W, Casaccia–Bonnefil P, Chao M, Cook S, Blumberg B (1999) Up-regulated p75NTR neurotrophin receptor on glial cells in MS plaques. Neurology 53:1676–1676.

Dowse T, Soldati D (2004) Host cell invasion by the apicomplexans: the significance of microneme protein proteolysis. Curr Opin Microbiol 7:388–396.

Dunay IR, Sibley LD (2010) Monocytes mediate mucosal immunity to Toxoplasma gondii. Curr Opin Immunol 22:461–466.

Eikelenboom P, Bate C, Van Gool WA, Hoozemans JJM, Rozemuller JM, Veerhuis R, Williams A (2002) Neuroinflammation in Alzheimer's disease and prion disease. Glia 40:232–239.

El Lakkis I, Di Pace BS, Cunningham TD, Troy SB (2015) Association between latent toxoplasmosis and psychiatric disorders in HIV-infected subjects. J Acquir Immune Defic Syndr 1999 68:e8-9.

Elkabes S, DiCicco-Bloom EM, Black IB (1996) Brain microglia/macrophages express neurotrophins that selectively regulate microglial proliferation and function. J Neurosci Off J Soc Neurosci 16:2508–2521.

Esposito D, Patel P, Stephens RM, Perez P, Chao MV, Kaplan DR, Hempstead BL (2001) The cytoplasmic and transmembrane domains of the p75 and Trk A receptors regulate high affinity binding to nerve growth factor. J Biol Chem 276:32687–32695.

Fahnestock M, Michalski B, Xu B, Coughlin MD (2001) The Precursor Pro-Nerve Growth Factor Is the Predominant Form of Nerve Growth Factor in Brain and Is Increased in Alzheimer's Disease. Mol Cell Neurosci 18:210–220.

Fan Y-J, Wu LL-Y, Li H-Y, Wang Y-J, Zhou X-F (2008) Differential effects of pro-BDNF on sensory neurons after sciatic nerve transection in neonatal rats. Eur J Neurosci 27:2380–2390.

Feng G, Mellor RH, Bernstein M, Keller-Peck C, Nguyen QT, Wallace M, Nerbonne JM, Lichtman JW, Sanes JR (2000) Imaging Neuronal Subsets in Transgenic Mice Expressing Multiple Spectral Variants of GFP. Neuron 28:41–51.

Ferguson DJ, Hutchison WM, Pettersen E (1989) Tissue cyst rupture in mice chronically infected with Toxoplasma gondii. An immunocytochemical and ultrastructural study. Parasitol Res 75:599–603.

Ferri CC, Moore FA, Bisby MA (1998) Effects of facial nerve injury on mouse motoneurons lacking the p75 low-affinity neurotrophin receptor. J Neurobiol 34:1–9.

Feustel SM, Meissner M, Liesenfeld O (2012) Toxoplasma gondii and the blood-brain barrier. Virulence 3:182–192.

Filardo EJ (2002) Epidermal growth factor receptor (EGFR) transactivation by estrogen via the G-protein-coupled receptor, GPR30: a novel signaling pathway with potential significance for breast cancer. J Steroid Biochem Mol Biol 80:231–238.

Fischer H-G, Bonifas U, Reichmann G (2000) Phenotype and Functions of Brain Dendritic Cells Emerging During Chronic Infection of Mice with Toxoplasma gondii. J Immunol 164:4826–4834.

Fischer HG, Nitzgen B, Reichmann G, Gross U, Hadding U (1997) Host cells of Toxoplasma gondii encystation in infected primary culture from mouse brain. Parasitol Res 83:637–641.

Fischer H-G, Reichmann G (2001) Brain Dendritic Cells and Macrophages/Microglia in Central Nervous System Inflammation. J Immunol 166:2717–2726.

Frade JM, Barde YA (1998) Microglia-derived nerve growth factor causes cell death in the developing retina. Neuron 20:35–41.

Fry EJ, Ho C, David S (2007) A Role for Nogo Receptor in Macrophage Clearance from Injured Peripheral Nerve. Neuron 53:649–662.

Gabbott PL, Somogyi P (1986) Quantitative distribution of GABA-immunoreactive neurons in the visual cortex (area 17) of the cat. Exp Brain Res 61:323–331.

Gehrmann J, Matsumoto Y, Kreutzberg GW (1995) Microglia: intrinsic immuneffector cell of the brain. Brain Res Brain Res Rev 20:269–287.

Ginhoux F, Greter M, Leboeuf M, Nandi S, See P, Gokhan S, Mehler MF, Conway SJ, Ng LG, Stanley ER, Samokhvalov IM, Merad M (2010) Fate mapping analysis reveals that adult microglia derive from primitive macrophages. Science 330:841–845.

Greferath U, Bennie A, Kourakis A, Bartlett PF, Murphy M, Barrett GL (2000) Enlarged cholinergic forebrain neurons and improved spatial learning in p75 knockout mice. Eur J Neurosci 12:885–893.

Griffin WS, Sheng JG, Roberts GW, Mrak RE (1995) Interleukin-1 expression in different plaque types in Alzheimer's disease: significance in plaque evolution. J Neuropathol Exp Neurol 54:276–281.

Hallböök F, Ibáñez CF, Persson H (1991) Evolutionary studies of the nerve growth factor family reveal a novel member abundantly expressed in Xenopus ovary. Neuron 6:845–858.

Halonen SK, Chiu F-C, Weiss LM (1998) Effect of Cytokines on Growth of Toxoplasma gondii in Murine Astrocytes. Infect Immun 66:4989–4993.

Hanisch U-K, Kettenmann H (2007) Microglia: active sensor and versatile effector cells in the normal and pathologic brain. Nat Neurosci 10:1387–1394.

Harrington AW, Leiner B, Blechschmitt C, Arevalo JC, Lee R, Mörl K, Meyer M, Hempstead BL, Yoon SO, Giehl KM (2004) Secreted proNGF is a pathophysiological death-inducing ligand after adult CNS injury. Proc Natl Acad Sci U S A 101:6226–6230.

Hartmann M, Brigadski T, Erdmann KS, Holtmann B, Sendtner M, Narz F, Lessmann V (2004) Truncated TrkB receptor-induced outgrowth of dendritic filopodia involves the p75 neurotrophin receptor. J Cell Sci 117:5803–5814.

Hasan W, Pedchenko T, Krizsan-Agbas D, Baum L, Smith PG (2003) Sympathetic neurons synthesize and secrete pro-nerve growth factor protein. J Neurobiol 57:38–53.

Haseloff RF, Blasig IE, Bauer H-C, Bauer H (2005) In Search of the Astrocytic Factor(s) Modulating Blood–Brain Barrier Functions in Brain Capillary Endothelial Cells In Vitro. Cell Mol Neurobiol 25:25–39.

Heese K, Hock C, Otten U (1998) Inflammatory Signals Induce Neurotrophin Expression in Human Microglial Cells. J Neurochem 70:699–707.

Hempstead BL (2006) Dissecting the diverse actions of pro- and mature neurotrophins. Curr Alzheimer Res 3:19–24.

Hempstead BL, Martin-Zanca D, Kaplan DR, Parada LF, Chao MV (1991) High-affinity NGF binding requires coexpression of the trk proto-oncogene and the low-affinity NGF receptor. Nature 350:678–683.

Heneka MT, O'Banion MK, Terwel D, Kummer MP (2010) Neuroinflammatory processes in Alzheimer's disease. J Neural Transm Vienna Austria 1996 117:919–947.

Henkel JS, Engelhardt JI, Siklós L, Simpson EP, Kim SH, Pan T, Goodman JC, Siddique T, Beers DR, Appel SH (2004) Presence of dendritic cells, MCP-1, and activated microglia/macrophages in amyotrophic lateral sclerosis spinal cord tissue. Ann Neurol 55:221–235.

Hersch SM, White EL (1981) Quantification of synapses formed with apical dendrites of Golgi-impregnated pyramidal cells: variability in thalamocortical inputs, but consistency in the ratios of asymmetrical to symmetrical synapses. Neuroscience 6:1043–1051.

Hohn A, Leibrock J, Bailey K, Barde Y-A (1990) Identification and characterization of a novel member of the nerve growth factor/brain-derived neurotrophic factor family. Nature 344:339–341.

Holmes C, Cunningham C, Zotova E, Woolford J, Dean C, Kerr S, Culliford D, Perry VH (2009) Systemic inflammation and disease progression in Alzheimer disease. Neurology 73:768–774.

Hoozemans JJM, O'Banion MK (2005) The role of COX-1 and COX-2 in Alzheimer's disease pathology and the therapeutic potentials of non-steroidal anti inflammatory drugs. Curr Drug Targets CNS Neurol Disord 4:307–315.

Huang EJ, Reichardt LF (2001) NEUROTROPHINS: Roles in Neuronal Development and Function. Annu Rev Neurosci 24:677–736.

Ibáñez CF, Simi A (2012) p75 neurotrophin receptor signaling in nervous system injury and degeneration: paradox and opportunity. Trends Neurosci 35:431–440.

Ip NY, Ibáñez CF, Nye SH, McClain J, Jones PF, Gies DR, Belluscio L, Le Beau MM, Espinosa R, Squinto SP (1992) Mammalian neurotrophin-4: structure,

chromosomal localization, tissue distribution, and receptor specificity. Proc Natl Acad Sci U S A 89:3060–3064.

Ishizuka N, Weber J, Amaral DG (1990) Organization of intrahippocampal projections originating from CA3 pyramidal cells in the rat. J Comp Neurol 295:580–623.

Jansen P, Giehl K, Nyengaard JR, Teng K, Lioubinski O, Sjoegaard SS, Breiderhoff T, Gotthardt M, Lin F, Eilers A, Petersen CM, Lewin GR, Hempstead BL, Willnow TE, Nykjaer A (2007) Roles for the pro-neurotrophin receptor sortilin in neuronal development, aging and brain injury. Nat Neurosci 10:1449–1457.

Jones KR, Reichardt LF (1990) Molecular cloning of a human gene that is a member of the nerve growth factor family. Proc Natl Acad Sci 87:8060–8064.

Jones TC, Alkan S, Erb P (1986) Spleen and lymph node cell populations, In vitro cell proliferation and interferon-y production during the primary immune response to Toxoplasma gondii. Parasite Immunol 8:619–629.

Kandel ER (2011) Principles of neural science. New York: McGraw-Hill Medical Publishing Division.

Kansas GS (1996) Selectins and their ligands: current concepts and controversies. Blood 88:3259–3287.

Kaplan DR, Hempstead BL, Martin-Zanca D, Chao MV, Parada LF (1991) The trk proto-oncogene product: a signal transducing receptor for nerve growth factor. Science 252:554–558.

Kenchappa RS, Tep C, Korade Z, Urra S, Bronfman FC, Yoon SO, Carter BD (2010) p75 neurotrophin receptor-mediated apoptosis in sympathetic neurons involves a biphasic activation of JNK and up-regulation of tumor necrosis factor-alpha-converting enzyme/ADAM17. J Biol Chem 285:20358–20368.

Kettenmann H, Hanisch U-K, Noda M, Verkhratsky A (2011) Physiology of Microglia. Physiol Rev 91:461–553.

Kim L, Butcher BA, Denkers EY (2004) Toxoplasma gondii Interferes with Lipopolysaccharide Induced Mitogen-Activated Protein Kinase Activation by Mecha-

nisms Distinct from Endotoxin Tolerance. J Immunol 172:3003–3010.

Klein R, Jing SQ, Nanduri V, O'Rourke E, Barbacid M (1991) The trk proto-oncogene encodes a receptor for nerve growth factor. Cell 65:189–197.

Korte M, Carroll P, Wolf E, Brem G, Thoenen H, Bonhoeffer T (1995) Hippocampal long-term potentiation is impaired in mice lacking brain-derived neurotrophic factor. Proc Natl Acad Sci U S A 92:8856–8860.

Kraemer BR, Snow JP, Vollbrecht P, Pathak A, Valentine WM, Deutch AY, Carter BD (2014a) A Role for the p75 Neurotrophin Receptor in Axonal Degeneration and Apoptosis Induced by Oxidative Stress. J Biol Chem 289:21205–21216.

Kraemer BR, Yoon SO, Carter BD (2014b) The Biological Functions and Signaling Mechanisms of the p75 Neurotrophin Receptor. Handb Exp Pharmacol 220: 121–164.

Kreutzberg GW (1996) Microglia: a sensor for pathological events in the CNS. Trends Neurosci 19:312–318.

Kubota Y (2014) Untangling GABAergic wiring in the cortical microcircuit. Curr Opin Neurobiol 26:7–14.

Lachenmaier SM, Deli MA, Meissner M, Liesenfeld O (2011) Intracellular transport of Toxoplasma gondii through the blood–brain barrier. J Neuroimmunol 232:119–130.

Lai AY, Todd KG (2008) Differential regulation of trophic and proinflammatory microglial effectors is dependent on severity of neuronal injury. Glia 56:259–270.

Larkum ME, Senn W, Lüscher H-R (2004) Top-down Dendritic Input Increases the Gain of Layer 5 Pyramidal Neurons. Cereb Cortex 14:1059–1070.

Lebrun-Julien F, Bertrand MJ, De Backer O, Stellwagen D, Morales CR, Di Polo A, Barker PA (2010) ProNGF induces TNFalpha-dependent death of retinal ganglion cells through a p75NTR non-cell-autonomous signaling pathway. Proc Natl Acad Sci U S A 107:3817–3822.

Lee FS, Rajagopal R, Kim AH, Chang PC, Chao MV (2002) Activation of Trk Neurotrophin Receptor Signaling by Pituitary Adenylate Cyclase-activating

Polypeptides. J Biol Chem 277:9096–9102.

Lee K-F, Li E, Huber LJ, Landis SC, Sharpe AH, Chao MV, Jaenisch R (1992) Targeted mutation of the gene encoding the low affinity NGF receptor p75 leads to deficits in the peripheral sensory nervous system. Cell 69:737–749.

Lee R, Kermani P, Teng KK, Hempstead BL (2001) Regulation of cell survival by secreted proneurotrophins. Science 294:1945–1948.

Leng J, Butcher BA, Egan CE, Abdallah DSA, Denkers EY (2009) Toxoplasma gondii Prevents Chromatin Remodeling Initiated by TLR Triggered Macrophage Activation. J Immunol 182:489–497.

LeVay S (1973) Synaptic patterns in the visual cortex of the cat and monkey. Electron microscopy of Golgi Preparations. J Comp Neurol 150:53–85.

Levi-Montalcini R, Angeletti PU (1963) Essential role of the nerve growth factor in the survival and maintenance of dissociated sensory and sympathetic embryonic nerve cells in vitro. Dev Biol 6:653–659.

Ley K, Laudanna C, Cybulsky MI, Nourshargh S (2007) Getting to the site of inflammation: the leukocyte adhesion cascade updated. Nat Rev Immunol 7:678–689.

Li XG, Somogyi P, Ylinen A, Buzsáki G (1994) The hippocampal CA3 network: an in vivo intracellular labeling study. J Comp Neurol 339:181–208.

Liu Y, Zhou L-J, Wang J, Li D, Ren W-J, Peng J, Wei X, Xu T, Xin W-J, Pang R-P, Li Y-Y, Qin Z-H, Murugan M, Mattson MP, Wu L-J, Liu X-G (2017) TNF-α Differentially Regulates Synaptic Plasticity in the Hippocampus and Spinal Cord by Microglia-Dependent Mechanisms after Peripheral Nerve Injury. J Neurosci 37:871–881.

Löscher W, Potschka H (2005) Blood-brain barrier active efflux transporters: ATP-binding cassette gene family. NeuroRX 2:86–98.

Lucin KM, Wyss-Coray T (2009) Immune activation in brain aging and neurodegeneration: too much or too little? Neuron 64:110–122.

Lüder CG, Giraldo-Velásquez M, Sendtner M, Gross U (1999) Toxoplasma gondii in

primary rat CNS cells: differential contribution of neurons, astrocytes, and microglial cells for the intracerebral development and stage differentiation. Exp Parasitol 93:23–32.

Lue LF, Brachova L, Civin WH, Rogers J (1996) Inflammation, A beta deposition, and neurofibrillary tangle formation as correlates of Alzheimer's disease neurodegeneration. J Neuropathol Exp Neurol 55:1083–1088.

Lynch MA (2002) Interleukin-1 beta exerts a myriad of effects in the brain and in particular in the hippocampus: analysis of some of these actions. Vitam Horm 64:185–219.

Magaki S, Mueller C, Dickson C, Kirsch W (2007) Increased production of inflammatory cytokines in mild cognitive impairment. Exp Gerontol 42:233–240.

Maisonpierre PC, Belluscio L, Squinto S, Ip NY, Furth ME, Lindsay RM, Yancopoulos GD (1990) Neurotrophin-3: a neurotrophic factor related to NGF and BDNF. Science 247:1446–1451.

Mallat M, Houlgatte R, Brachet P, Prochiantz A (1989) Lipopolysaccharide stimulated rat brain macrophages release NGF in vitro. Dev Biol 133:309–311.

Mantovani S, Garbelli S, Pasini A, Alimonti D, Perotti C, Melazzini M, Bendotti C, Mora G (2009) Immune system alterations in sporadic amyotrophic lateral sclerosis patients suggest an ongoing neuroinflammatory process. J Neuroimmunol 210:73–79.

McAfoose J, Baune BT (2009) Evidence for a cytokine model of cognitive function. Neurosci Biobehav Rev 33:355–366.

McDonald KK, Aulas A, Destroismaisons L, Pickles S, Beleac E, Camu W, Rouleau GA, Vande Velde C (2011) TAR DNA-binding protein 43 (TDP-43) regulates stress granule dynamics via differential regulation of G3BP and TIA-1. Hum Mol Genet 20:1400–1410.

McGeer PL, Akiyama H, Itagaki S, McGeer EG (1989) Immune system response in Alzheimer's disease. Can J Neurol Sci J Can Sci Neurol 16:516–527.

Meeker R, Williams K (2014) Dynamic Nature of the p75 Neurotrophin Receptor in Response to Injury and Disease. J Neuroimmune Pharmacol:1–14.

Meeker RB, Poulton W, Clary G, Schriver M, Longo FM (2016) Novel p75 neurotrophin receptor ligand stabilizes neuronal calcium, preserves mitochondrial movement and protects against HIV associated neuropathogenesis. Exp Neurol 275, Part 3:182–198.

Meira C da S, Pereira-Chioccola VL, Vidal JE, Motoie G, Costa-Silva TA da, Gava R (2015) Evolution of cytokine profile during the treatment of cerebral toxoplasmosis in HIV-infected patients. J Immunol Methods 426:14–18.

Mi S, Lee X, Shao Z, Thill G, Ji B, Relton J, Levesque M, Allaire N, Perrin S, Sands B, Crowell T, Cate RL, McCoy JM, Pepinsky RB (2004) LINGO-1 is a component of the Nogo-66 receptor/p75 signaling complex. Nat Neurosci 7:221–228.

Michaelsen K, Zagrebelsky M, Berndt-Huch J, Polack M, Buschler A, Sendtner M, Korte M (2010) Neurotrophin receptors TrkB.T1 and p75NTR cooperate in modulating both functional and structural plasticity in mature hippocampal neurons. Eur J Neurosci 32:1854–1865.

Miller G (2005) Neuroscience. The dark side of glia. Science 308:778–781.

Misiak B, Leszek J, Kiejna A (2012) Metabolic syndrome, mild cognitive impairment and Alzheimer's disease–the emerging role of systemic low-grade inflammation and adiposity. Brain Res Bull 89:144–149.

Money KM, Stanwood GD (2013) Developmental origins of brain disorders: roles for dopamine. Front Cell Neurosci 7

Moran LB, Graeber MB (2004) The facial nerve axotomy model. Brain Res Brain Res Rev 44:154–178.

Morisaki JH, Heuser JE, Sibley LD (1995) Invasion of Toxoplasma gondii occurs by active penetration of the host cell. J Cell Sci 108:2457–2464.

Morishima M, Morita K, Kubota Y, Kawaguchi Y (2011) Highly Differentiated Projection-Specific Cortical Subnetworks. J Neurosci 31:10380–10391.

Murray KN, Parry-Jones AR, Allan SM (2015) Interleukin-1 and acute brain injury. Front Cell Neurosci 9

Nagayach A, Patro N, Patro I (2014a) Astrocytic and microglial response in experimentally induced diabetic rat brain. Metab Brain Dis 29:747–761.

Nagayach A, Patro N, Patro I (2014b) Experimentally induced diabetes causes glial activation, glutamate toxicity and cellular damage leading to changes in motor function. Front Cell Neurosci 8:355.

Nagayach A, Patro N, Patro I (2015) Microglia in the Physiology and Pathology of Brain. Proc Natl Acad Sci India Sect B Biol Sci:1–14.

Nakajima K, Kikuchi Y, Ikoma E, Honda S, Ishikawa M, Liu Y, Kohsaka S (1998) Neurotrophins regulate the function of cultured microglia. Glia 24:272–289.

Neumann H, Medana IM, Bauer J, Lassmann H (2002) Cytotoxic T lymphocytes in autoimmune and degenerative CNS diseases. Trends Neurosci 25:313–319.

Nykjaer A, Willnow TE (2012) Sortilin: a receptor to regulate neuronal viability and function. Trends Neurosci 35:261–270.

Osunkalu VO, Akanmu SA, Ofomah NJ, Onyiaorah IV, Adediran AA, Akinde RO, Onwuezobe IA (2011) Seroprevalence of Toxoplasma gondii IgG antibody in HIV-infected patients at the Lagos University Teaching Hospital. HIVAIDS - Res Palliat Care

Paolicelli RC, Bolasco G, Pagani F, Maggi L, Scianni M, Panzanelli P, Giustetto M, Ferreira TA, Guiducci E, Dumas L, Ragozzino D, Gross CT (2011) Synaptic pruning by microglia is necessary for normal brain development. Science 333:1456–1458.

Parkhurst CN, Yang G, Ninan I, Savas JN, Yates JR 3rd, Lafaille JJ, Hempstead BL, Littman DR, Gan W-B (2013) Microglia Promote Learning-Dependent Synapse Formation through Brain-Derived Neurotrophic Factor. Cell 155:1596–1609.

Parlog A, Harsan L-A, Zagrebelsky M, Weller M, Elverfeldt D von, Mawrin C, Korte M, Dunay IR (2014a) Chronic murine toxoplasmosis is defined by subtle changes in neuronal connectivity. Dis Model Mech 7:459–469.

Parlog A, Schlüter D, Dunay IR (2014b) Toxoplasma gondii induced neuronal alterations. Parasite Immunol:n/a-n/a.

Parnavelas JG, Sullivan K, Lieberman AR, Webster KE (1977) Neurons and their synaptic organization in the visual cortex of the rat. Cell Tissue Res 183:499–517.

Parpura V, Heneka MT, Montana V, Oliet SHR, Schousboe A, Haydon PG, Stout RF, Spray DC, Reichenbach A, Pannicke T, Pekny M, Pekna M, Zorec R, Verkhratsky A (2012) Glial cells in (patho)physiology. J Neurochem 121:4–27.

Patro IK, Amit null, Shrivastava M, Bhumika S, Patro N (2010) Poly I:C induced microglial activation impairs motor activity in adult rats. Indian J Exp Biol 48:104–109.

Patro N, Singh K, Patro I (2013) Differential microglial and astrocytic response to bacterial and viral infection in the developing hippocampus of neonatal rats. Indian J Exp Biol 51:606–614.

Paul CE, Vereker E, Dickson KM, Barker PA (2004) A Pro-Apoptotic Fragment of the p75 Neurotrophin Receptor Is Expressed in p75NTRExonIV Null Mice. J Neurosci 24:1917–1923.

Perry VH, Cunningham C, Holmes C (2007) Systemic infections and inflammation affect chronic neurodegeneration. Nat Rev Immunol 7:161–167.

Poo MM (2001) Neurotrophins as synaptic modulators. Nat Rev Neurosci 2:24–32.

Prandovszky E, Gaskell E, Martin H, Dubey JP, Webster JP, McConkey GA (2011) The neurotropic parasite Toxoplasma gondii increases dopamine metabolism. PloS One 6:e23866.

Puehringer D, Orel N, Lüningschrör P, Subramanian N, Herrmann T, Chao MV, Sendtner M (2013) EGF transactivation of Trk receptors regulates the migration of newborn cortical neurons. Nat Neurosci 16:407–415.

Radeke MJ, Misko TP, Hsu C, Herzenberg LA, Shooter EM (1987) Gene transfer and molecular cloning of the rat nerve growth factor receptor. Nature 325:593–597.

Rahman A, Fazal F (2008) Hug Tightly and Say Goodbye: Role of Endothelial ICAM-1 in Leukocyte Transmigration. Antioxid Redox Signal 11:823–839.

Robert-Gangneux F, Dardé M-L (2012) Epidemiology of and Diagnostic Strategies for Toxoplasmosis. Clin Microbiol Rev 25:264–296.

Roberti G, Mantelli F, Macchi I, Massaro-Giordano M, Centofanti M (2014) Nerve growth factor modulation of retinal ganglion cell physiology. J Cell Physiol 229:1130–1133.

Rosenthal A, Goeddel DV, Nguyen T, Lewis M, Shih A, Laramee GR, Nikolics K, Winslow JW (1990) Primary structure and biological activity of a novel human neurotrophic factor. Neuron 4:767–773.

Saxena K, Patro N, Patro I (2007) FK506 protects neurons following peripheral nerve injury via immunosuppression. Cell Mol Neurobiol 27:1049–1057.

Schafer DP, Lehrman EK, Kautzman AG, Koyama R, Mardinly AR, Yamasaki R, Ransohoff RM, Greenberg ME, Barres BA, Stevens B (2012) Microglia sculpt postnatal neural circuits in an activity and complement-dependent manner. Neuron 74:691–705.

Schlüter D, Bertsch D, Frei K, Hübers SB, Wiestler OD, Hof H, Fontana A, Deckert-Schlüter M (1998) Interferon-gamma antagonizes transforming growth factor-beta2-mediated immunosuppression in murine Toxoplasma encephalitis. J Neuroimmunol 81:38–48.

Schlüter D, Deckert M, Hof H, Frei K (2001) Toxoplasma gondii infection of neurons induces neuronal cytokine and chemokine production, but gamma interferon- and tumor necrosis factor-stimulated neurons fail to inhibit the invasion and growth of T. gondii. Infect Immun 69:7889–7893.

Schlüter D, Hein A, Dörries R, Deckert-Schlüter M (1995) Different subsets of T cells in conjunction with natural killer cells, macrophages, and activated microglia participate in the intracerebral immune response to Toxoplasma gondii in athymic nude and immunocompetent rats. Am J Pathol 146:999–1007.

Schlüter D, Kaefer N, Hof H, Wiestler OD, Deckert-Schlüter M (1997) Expression pattern and cellular origin of cytokines in the normal and Toxoplasma gondii-infected murine brain. Am J Pathol 150:1021–1035.

Sholl DA (1953) Dendritic organization in the neurons of the visual and motor cortices of the cat. J Anat 87:387–406.1.

Silva NM, Manzan RM, Carneiro WP, Milanezi CM, Silva JS, Ferro EAV, Mineo JR (2010) Toxoplasma gondii: The severity of toxoplasmic encephalitis in C57BL/6 mice is associated with increased ALCAM and VCAM-1 expression in the central nervous system and higher blood–brain barrier permeability. Exp Parasitol 126:167–177.

Soldati D, Meissner M (2004) Toxoplasma as a novel system for motility. Curr Opin Cell Biol 16:32–40.

Spruston N (2008) Pyramidal neurons: dendritic structure and synaptic integration. Nat Rev Neurosci 9:206–221.

Srinivasan B, Roque CH, Hempstead BL, Al-Ubaidi MR, Roque RS (2004) Microglia-derived Pronerve Growth Factor Promotes Photoreceptor Cell Death via p75 Neurotrophin Receptor. J Biol Chem 279:41839–41845.

Stich O, Andres TA, Gross CM, Gerber SI, Rauer S, Langosch JM (2015) An observational study of inflammation in the central nervous system in patients with bipolar disorder. Bipolar Disord 17:291–302.

Streit WJ, Walter SA, Pennell NA (1999) Reactive microgliosis. Prog Neurobiol 57:563–581.

Suzuki Y, Yang Q, Remington JS (1995) Genetic Resistance against Acute Toxoplasmosis Depends on the Strain of Toxoplasma gondii. J Parasitol 81: 1032– 1034.

Swardfager W, Lanctôt K, Rothenburg L, Wong A, Cappell J, Herrmann N (2010) A Meta-Analysis of Cytokines in Alzheimer's Disease. Biol Psychiatry 68:930–941.

Syroid DE, Maycox PJ, Soilu-Hänninen M, Petratos S, Bucci T, Burrola P, Murray S, Cheema S, Lee KF, Lemke G, Kilpatrick TJ (2000) Induction of postnatal schwann cell death by the low-affinity neurotrophin receptor in vitro and after axotomy. J Neurosci Off J Soc Neurosci 20:5741–5747.

Tandon PN (2007) Brain cells–recently unveiled secrets: their clinical significance.

Neurol India 55:322–327.

Teismann P, Tieu K, Cohen O, Choi D-K, Wu DC, Marks D, Vila M, Jackson-Lewis V, Przedborski S (2003) Pathogenic role of glial cells in Parkinson's disease. Mov Disord Off J Mov Disord Soc 18:121–129.

Teng HK (2005) ProBDNF Induces Neuronal Apoptosis via Activation of a Receptor Complex of p75NTR and Sortilin. J Neurosci 25:5455–5463.

Thomson AM, Deuchars J (1997) Synaptic interactions in neocortical local circuits: dual intracellular recordings in vitro. Cereb Cortex N Y N 1991 7:510–522.

Tian L, Rauvala H, Gahmberg CG (2009) Neuronal regulation of immune responses in the central nervous system. Trends Immunol 30:91–99.

Towbin H, Staehelin T, Gordon J (1979) Electrophoretic transfer of proteins from polyacrylamide gels to nitrocellulose sheets: procedure and some applications. Proc Natl Acad Sci U S A 76:4350–4354.

Trang T, Beggs S, Salter MW (2011) Brain-derived neurotrophic factor from microglia: a molecular substrate for neuropathic pain. Neuron Glia Biol 7:99–108.

Trapp BD, Wujek JR, Criste GA, Jalabi W, Yin X, Kidd GJ, Stohlman S, Ransohoff R (2007) Evidence for synaptic stripping by cortical microglia. Glia 55:360–368.

Tremblay M-È, Lowery RL, Majewska AK (2010) Microglial interactions with synapses are modulated by visual experience. PLoS Biol 8:e1000527.

Ulmann L, Hatcher JP, Hughes JP, Chaumont S, Green PJ, Conquet F, Buell GN, Reeve AJ, Chessell IP, Rassendren F (2008) Up-regulation of P2X4 receptors in spinal microglia after peripheral nerve injury mediates BDNF release and neuropathic pain. J Neurosci Off J Soc Neurosci 28:11263–11268.

Vaegter CB, Jansen P, Fjorback AW, Glerup S, Skeldal S, Kjolby M, Richner M, Erdmann B, Nyengaard JR, Tessarollo L, Lewin GR, Willnow TE, Chao MV, Nykjaer A (2011) Sortilin associates with Trk receptors to enhance anterograde transport and neurotrophin signaling. Nat Neurosci 14:54–61.

Vallochi A (2008) Molecular markers of susceptibility to ocular toxoplasmosis, host and guest behaving badly. Clin Ophthalmol

Vehmas AK, Kawas CH, Stewart WF, Troncoso JC (2003) Immune reactive cells in senile plaques and cognitive decline in Alzheimer's disease. Neurobiol Aging 24:321–331.

Venero JL, Burguillos MA, Brundin P, Joseph B (2011) The executioners sing a new song: killer caspases activate microglia. Cell Death Differ 18:1679–1691.

Verkhratsky A, Parpura V, Pekna M, Pekny M, Sofroniew M (2014) Glia in the pathogenesis of neurodegenerative diseases. Biochem Soc Trans 42:1291–1301.

Vicario A, Kisiswa L, Tann JY, Kelly CE, Ibáñez CF (2015) Neuron-type-specific signaling by the p75NTR death receptor regulated by differential proteolytic cleavage. J Cell Sci:jcs.161745.

Vidaurre OG, Gascón S, Deogracias R, Sobrado M, Cuadrado E, Montaner J, Rodríguez-Peña A, Díaz-Guerra M (2012) Imbalance of neurotrophin receptor isoforms TrkB-FL/TrkB-T1 induces neuronal death in excitotoxicity. Cell Death Dis 3:e256.

Villeda SA et al. (2011) The aging systemic milieu negatively regulates neurogenesis and cognitive function. Nature 477:90–94.

Volosin M, Trotter C, Cragnolini A, Kenchappa RS, Light M, Hempstead BL, Carter BD, Friedman WJ (2008) Induction of proneurotrophins and activation of p75NTR-mediated apoptosis via neurotrophin receptor-interacting factor in hippocampal neurons after seizures. J Neurosci Off J Soc Neurosci 28:9870–9879.

von Schack D, Casademunt E, Schweigreiter R, Meyer M, Bibel M, Dechant G (2001) Complete ablation of the neurotrophin receptor p75NTR causes defects both in the nervous and the vascular system. Nat Neurosci 4:977–978.

Wang B, Wu N, Liang F, Zhang S, Ni W, Cao Y, Xia D, Xi H (2013) 7,8-dihydroxyflavone, a small-molecule tropomyosin-related kinase B (TrkB) agonist, attenuates cerebral ischemia and reperfusion injury in rats. J Mol Histol 45:129–140.

Welter Á, Mineo JR, De Oliveira Silva DA, Lourenço EV, Vieira Ferro EA, Roque-Barreira MC, Maria da Silva N (2007) BALB/c mice resistant to Toxoplasma gondii infection proved to be highly susceptible when previously infected with Myocoptes musculinus fur mites. Int J Exp Pathol 88:325–335.

Wetzel DM, Håkansson S, Hu K, Roos D, Sibley LD (2003) Actin Filament Polymerization Regulates Gliding Motility by Apicomplexan Parasites. Mol Biol Cell 14:396–406.

Yamada J, Nakanishi H, Jinno S (2011) Differential involvement of perineuronal astrocytes and microglia in synaptic stripping after hypoglossal axotomy. Neuroscience 182:1–10.

Yamashita T, Tucker KL, Barde Y-A (1999) Neurotrophin Binding to the p75 Receptor Modulates Rho Activity and Axonal Outgrowth. Neuron 24:585–593.

Yan J, Zhou X, Guo J-J, Mao L, Wang Y-J, Sun J, Sun L-X, Zhang L-Y, Zhou X-F, Liao H (2012) Nogo-66 inhibits adhesion and migration of microglia via GTPase Rho pathway in vitro. J Neurochem 120:721–731.

Yang F, Je H-S, Ji Y, Nagappan G, Hempstead B, Lu B (2009a) Pro-BDNF-induced synaptic depression and retraction at developing neuromuscular synapses. J Cell Biol 185:727–741.

Yang J, Siao C-J, Nagappan G, Marinic T, Jing D, McGrath K, Chen Z-Y, Mark W, Tessarollo L, Lee FS, Lu B, Hempstead BL (2009b) Neuronal release of proBDNF. Nat Neurosci 12:113–115.

Yuste R (2011) Dendritic Spines and Distributed Circuits. Neuron 71:772–781.

Zagrebelsky M, Holz A, Dechant G, Barde Y-A, Bonhoeffer T, Korte M (2005) The p75 neurotrophin receptor negatively modulates dendrite complexity and spine density in hippocampal neurons. J Neurosci Off J Soc Neurosci 25:9989–9999.

Zarbock A, Müller H, Kuwano Y, Ley K (2009) PSGL-1-dependent myeloid leukocyte activation. J Leukoc Biol 86:1119–1124.

Zhang Y, Chen H, Chen Y, Wang L, Cai Y, Li M, Wen H, Du J, An R, Luo Q, Wang X, Lun Z-R, Xu Y, Shen J (2014) Activated microglia contribute to

neuronal apoptosis in Toxoplasmic encephalitis. Parasit Vectors 7:372.

6 Danksagung

An dieser Stelle möchte ich allen Menschen danken, die mich auf dem Weg zur Dissertation begleitet und unterstützt haben:

Als erstes geht ein besonderer Dank an meinen Doktorvater Prof. Dr. Martin Korte für das große Interesse und die Förderung während meiner Doktorarbeit und für die einmalige Gelegenheit diese Doktorarbeit an der Schnittstelle von immunologischer und neurobiologischer Forschung anfertigen zu dürfen.

Prof. Dr. Reinhard Köster danke ich für die Übernahme des Koreferates, sowie Prof. Dr. Robert Hänsch für die Leitung der Promotionskommission.

Frau Dr. Marta Zagrebelsky möchte ich danken für ihre vielseitige, geduldige und umfangreiche Hilfe vorallem während der Tiefen dieser Dissertation.

Weiterer Dank gilt meinen Kooperationspartnern aus Magdeburg, namentlich Frau Prof. Dr. Ildiko Rita Dunay und Dr. Alexandru Parlog. Ich möchte mich für die Kooperation im Bereich der Infektionen mit *Toxoplasma gondii* bedanken.

Außerdem danke ich der gesamten AG zelluläre Neurobiologie. Ich habe mich zu jedem Zeitpunkt wertgeschätzt und unterstützt gefühlt: Eine so angenehme Arbeitsatmosphäre ist wirklich etwas ganz Besonderes. Daher danke den Postdocs: Frau Dr. Kristin Michaelsen, Herr Dr. Martin Rothkegel, Herr Dr. Andreas Holz, Frau Anita Remus und Frau Dr. Gayane Grigoryan; den technischen Assistenten und dem Sekretariat: Frau Sybille Bläsche, Frau Ilona Demesvary-Steller, Herr Reinhard Huwe, Frau Heike Kessler, Frau Tania Meßerschmidt, Frau Diane Mundil, Frau Bettina Sandner, Frau Eva Saxinger und Frau Carmen Wucherpfennig.

Natürlich gilt dieser Dank umso mehr meinen direkten Weggefährten, die teils bereits promoviert sind oder sich auf dem besten Wege dahin befinden: Steffi, Manna, Franzi, Yves, Susi, Lotti, Niklas, Jonas, Steffen, Max, Abi, Shirin, Leoni, Ulrike, Qin, Cristina, Nina und Claudia. Es war eine unvergessliche Zeit!

Einen ganz besonderen Dank hat meine wundervolle Familie verdient. Danke, dass Ihr mich immer unterstützt habt! Außerdem danke ich meinen Freunden und Frau Berg.

Mein größter Dank gilt jederzeit Ann-Katrin.